FORSCHUNGSZENTRUM KARLSRUHE
Technik und Umwelt

Wissenschaftliche Berichte
FZKA 6285

Corrosion Evaluation of Metallic Materials for Long-Lived HLW/Spent Fuel Disposal Containers

Final Report 1996-1998

E. Smailos, A. Martínez-Esparza[1)], B. Kursten[2)], G. Marx[3)], I. Azkarate[4)]

Institut für Nukleare Entsorgungstechnik

[1)] ENRESA, Madrid (E), [2)] SCK.CEN, Mol (B),
[3)] FU Berlin (D), [4)] INASMET, San Sebastian (E)

EC-Contract No. FI4W-CT95-0002

Forschungszentrum Karlsruhe GmbH, Karlsruhe
1999

ABSTRACT

Extended corrosion studies were performed on preselected HLW/Spent Fuel container materials (carbon steel, stainless steels, Ti99.8-Pd, Hastelloy C4) under simulated disposal conditions in rock salt, granite and clay environments. The objectives of the studies were: to evaluate the effect of essential parameters on corrosion, to gain an improved understanding of corrosion mechanisms, and to provide more accurate data for a materials degradation model that can be used to predict the lifetime of containers. The investigations included long-term immersion tests, electrochemical studies, and stress corrosion cracking studies. Parameters investigated in salt environment were: pH, composition of brines, chemical species present in brines, gamma radiation, welding and slow strain rates at 25°C-170°C. In granitic water, the effect of slow strain rates on the stress corrosion cracking resistance of steels was examined at 90°C. Finally, in oxidizing clay water (aerobic conditions), the influence of temperature (16°C, 90°C), and content of Cl^-, SO_4^{2-} and $S_2O_3^{2-}$ on corrosion was investigated.

The results obtained confirm previous findings that the alloy Ti99.8-Pd is the strongest candidate for the realization of the **corrosion-resistant container concept** in the three geological formations rock salt, granite and clay. This alloy is under all test conditions resistant to pitting corrosion and stress corrosion cracking, and its general corrosion is negligible low. The nickel base alloy Hastelloy C4 resists also pitting corrosion up to 90°C in oxidizing clay water. Therefore, this alloy is a further promising container material for disposal in clay. The stainless steels suffer from pitting corrosion in clay water at elevated Cl^- concentrations. Also in granitic environment, pitting was observed on the stainless steel AISI 316L. Therefore, the use of stainless steels as container material could lead to long-term pitting corrosion problems. The TStE355 carbon steel is an actively corroding material in salt brines and clay water, and its corrosion rate is significantly higher than that of corrosion resistant materials such as Ti99.8-Pd or Hastelloy C4. However, the corrosion rates of this steel imply corrosion allowances acceptable for thick-walled containers. In granitic environment (90°C) some pits were detected on the carbon steel. Therefore, the kinetics of the pitting corrosion in this environment should be examined by long-term corrosion tests. Further investigations on steels, Hastelloy C4 and Ti99.8-Pd are in progress.

Bewertung der Korrosionsbeständigkeit von metallischen Werkstoffen für langzeitbeständige HAW-Endlagerbehälter

KURZFASSUNG

Es wurden umfangreiche Korrosionsuntersuchungen an ausgewählten Behälterwerkstoffen (unlegierter Stahl, Cr-Ni-Stähle, Hastelloy C4 und Ti99,8-Pd) unter simulierten Endlagerbedingungen in Steinsalz, Granit und Ton durchgeführt. Die Ziele der Untersuchungen waren: Bewertung des Einflusses wichtiger Parameter auf das Korrosionsverhalten der Werkstoffe, Verbesserung der Kenntnisse über die Korrosionsmechanismen und die Gewinnung von sicheren Daten für ein Korrosionsmodell mit dem die Standzeit der Behälter unter Endlagerbedingungen prognostiziert werden kann. Die Untersuchungen umfaßten Langzeit-Immersionstests, elektrochemische Untersuchungen und Spannungsrißkorrosionsuntersuchungen. Untersuchte Parameter für die Endlagerung in Steinsalz waren: pH, Zusammensetzung der Salzlösungen, ausgewählte chemische Spezies in Salzlösungen, Gammastrahlung, Schweißen, langsame Dehnungsraten und Temperatur. In Granitwasser wurde der Effekt von langsamen Dehnungsraten auf die Beständigkeit von Stählen gegenüber Spannungsrißkorrosion bei 90°C untersucht. In Tonwasser wurde der Einfluß der Temperatur und der Konzentration von Cl^-, SO_4^{2-} und $S_2O_3^{2-}$ auf die Korrosion geprüft.

Die Ergebnisse bestätigen frühere Untersuchungen, daß die Legierung Ti99,8-Pd der aussichtsreichste Werkstoff für die Realisierung des **korrosionsresistenten Behälterkonzeptes** in den drei geologischen Formationen Steinsalz, Granit und Ton ist. Diese Legierung ist unter allen Prüfbedingungen beständig gegenüber Loch- und Spannungsrißkorrosion und ihre Flächenkorrosion ist vernachlässigbar klein (<1µm/a). Die Nickelbasislegierung Hastelloy C4 ist ebenfalls beständig gegenüber Lochkorrosion in oxidierendem Tonwasser und damit ein aussichtsreicher Behälterwerkstoff. Die Cr-Ni-Stähle sind anfällig gegenüber Lochkorrosion in Tonwasser bei höherer Cl^--Konzentration. Auch in Granitwasser zeigt der Cr-Ni-Stahl AISI 316 L eine Anfälligkeit gegenüber Lochkorrosion. Damit könnten Endlagerbehälter aus Cr-Ni-Stahl ihre Langzeit-Barrierenfunktion im Endlager durch Lochkorrosion verlieren. Der unlegierte Stahl TStE355 ist ein aktiv korrodierendes Material in Salzlösungen und Tonwasser und damit ist seine Korrosionsrate wesentlich höher als diejenige der korrosionsresistenten Werkstoffe Hastelloy C4 und Ti99,8-Pd. Allerdings führen die ermittelten Korrosionsraten des untersuchten unlegierten Stahls zu akzeptablen Korrosionszuschlägen für einen dickwandigen Behälter. In Granitwasser (90°C) wurde eine Anfälligkeit des Stahls gegenüber Lochkorrosion festgestellt. Daher sind Langzeituntersuchungen zur Bestimmung der Kinetik der Lochkorrosion notwendig. Weitere Korrosionsuntersuchungen an Stählen, Hastelloy C4 und Ti99,8-Pd sind im Gange.

TABLE OF CONTENTS

EXECUTIVE SUMMARY

I. Background and Objectives

The waste container as a part of the multibarrier system contributes to the safety disposal of HLW/Spent Fuel in geological formations by protecting the waste forms against a radionuclide mobilization by attack of salt brines or groundwater. The main requirement on the container materials is long-term corrosion resistance under normal operating and accident conditions in the repository.

In the present work, in-depth corrosion studies were performed on preselected container materials in rock salt, granite and clay environments. The work was undertaken as a joint project by FZK.INE (project coordinator), FU-Berlin, ENRESA/INASMET and SCK.CEN. Work at FZK.INE and FU-Berlin has concentrated on disposal in rock salt, ENRESA/INASMET considered disposal both in rock salt and granite, and SCK.CEN covered disposal in clay.

The objectives of the studies were: to evaluate the effect of essential parameters on corrosion, to gain an improved understanding of corrosion mechanisms, and to provide more accurate data for material degradation models that can be used to predict the lifetime of containers.

Following preselected container materials were investigated:

- Carbon steel as the most promising material for the **corrosion-allowance container design** in rock salt, granite and clay.

- The alloy Ti99.8-Pd and stainless steels as the strongest candidates for the **corrosion-resistant container design** in rock salt and in granite/clay, respectively. In case of disposal in clay, some investigations were performed also on the nickel base alloy Hastelloy C4 and on Ti99.8-Pd.

The investigations included long-term immersion tests, electrochemical-radiochemical studies and stress corrosion cracking studies in the three geological media rock salt, granite and clay. The influence of important parameters on the corrosion behaviour of the various materials was examined. These parameters were:

- In salt brines: pH, composition of brines, chemical species present in brines, gamma radiation, welding and slow strain rates at temperatures of 90°C-170°C.

- In granitic water: slow strain rates at 90°C.

- In clay water: temperature, content of Cl^-, SO_4^{2-} and $S_2O_3^{2-}$ of the medium.

II. Investigations and Results

II.1 Salt environments

II.1.1 Long-term immersion tests on TStE355 steel and Ti99.8-Pd in salt brines.

The influence of important parameters on the long-term corrosion behaviour of TStE355 carbon steel and Ti99.8-Pd in NaCl-rich and $MgCl_2$-rich brines was examined up to 20 months at temperatures of 90°C-170°C. These parameters are:

For TStE355 steel: initial pH (1-10) of the brines, selected chemical species present in brines ($B(OH)^-_4$, Fe^{3+}, H_2O_2, ClO^-) in concentrations of 10^{-1}-10^{-3} mol/l, and welding (TIG and EB welding).

For Ti99.8-Pd: gamma radiation of 10 Gy/h, and TIG and EB welding.

The materials were evaluated for general corrosion and local corrosion by using gravimetry, measurements of pit depths, surface profilometry and metallography.

The results obtained in the brines show that the TStE355 carbon steel is resistant to pitting corrosion in the sense of an active-passive corrosion element. The general corrosion rates of the steel in the $MgCl_2$-rich brine (70 µm/a at 90°C and 224 µm/a at 170°C) are significantly higher than in the NaCl-rich brine (5 µm/a at 90°C and 46 µm/a at 170°C). However, such values imply corrosion allowances acceptable for thick-walled containers.

Initial pH values of the NaCl-rich brine between 1 and 5, and of the $MgCl_2$-rich brine between 3 and 7 do not affect significantly the corrosion rate of the steel at 170°C. Chemical species such as $B(OH)^-_4$, Fe^{3+}, H_2O_2 and ClO^- increase the corrosion rate of the steel at 90°C in NaCl-rich brine from 5 µm/a to 236 µm/a, and in the $MgCl_2$ – rich brine from 70 µm/a to about 120 µm/a. However, at 170°C these chemical species cause no significantly increase in corrosion rate over the value in the pure brine.

Tungsten Inert Gas (TIG) welding and Electron Beam (EB) welding as potential container closure techniques clearly decrease the corrosion resistance of the steel in $MgCl_2$-rich brine at 150°C. A possible measure to improve the corrosion resistance of the welded steel could be a thermal stress relief treatment of the welds. Corresponding corrosion studies on such thermal treated specimens are planned.

II.1.2 Electrochemical and radiochemical studies on Ti99.8-Pd in salt brines

Combined electrochemical and radiochemical studies were performed on Ti99.8-Pd in salt brines in order to get a detailed insight into the corrosion kinetics, and especially into the potential influence of the radiolytic products H_2O_2 and ClO^- on corrosion. Both unwelded and welded specimens were examined. The studies were performerd in $MgCl_2$-rich brine (Q-brine) and in NaCl brines at temperatures between 25°C and 80°C at Free Corrosion Potential (Rest Potential E_{corr}) and at various applied potentials. The method used was the Radioisotope Method (RIM) which combines classical electrochemical procedures (potentiostatic and potentiodynamic measurements, impedance and photocurrent measurements) with radiochemical

ones, especially neutron activation analysis. Furthermore, microscopic examinations were carried out in order to decide whether pitting corrosion or general corrosion has taken place. For a better understanding of the results obtained from the experiments with H_2O_2, the relevant corrosion of Ti99.8-Pd was studied under the influence of F^-.

The brines used for the experiments were:

Saturated NaCl-brine:	111.6 mol NaCl/1000 mol H_2O.
NaCl-rich brine (brine 3) :	108.65 mol NaCl/1000 mol H_2O.
$MgCl_2$-rich brine (Q-brine):	67.8 - 82.4 mol $MgCl_2$/1000 mol H_2O (depending on the temperature of 25°C-80°C).

Measurements at rest potentials (350 - 450 mV) demonstrate that the corrosion rates are proportional to the H_2O_2 concentration of the brines. In all three brine systems at 25°C and 55°C the corrosion rates are 22 - 28 µm/a for $2.9 \cdot 10^{-2}$ mol/l H_2O_2 (average concentration) and decrease to 0.5 ± 0.3 µm/a for $2.9 \cdot 10^{-5}$ mol/l H_2O_2 (average concentration), the latter being the only one relevant to practical conditions.

At rest potentials, there are no significant differences in the various brines with respect to corrosion. At H_2O_2 concentrations $\leq 10^{-5}$ mol/l, no influence on corrosion of Ti99.8Pd can be detected.

The dependence of the corrosion rate w on the H_2O_2 concentration is given by the following equation:

$$w = \left(k_1' + k_2' \cdot c_{H_2O_2}\right) \cdot \frac{V_{Sol} \cdot M_{Ti}}{A_{El} \cdot \rho_{Ti}}$$

Here k'_1 is the velocity constant of corrosion without peroxide, k'_2 the velocity constant of corrosion in presence of H_2O_2 , V_{sol} the volume of brine, M the molar mass of titanium, A_{El} the area of the electrode, and ρ_{Ti} the density of titanium.

At rest potentials, the investigations of welds demonstrate that in all three brines the corrosion is identical with that of the Ti99.8-Pd metal.

In addition to measurements at rest potentials, measurements at applied potentials in the range from -1000 mV to +1000 mV were performed. Experiments carried out in saturated NaCl brine demonstrate that the Ti99.8-Pd has a marked active range between -400 mV and -100 mV. At a very high average H_2O_2 concentration of $5 \cdot 10^{-2}$ mol/l (not relevant for disposal), the maximum corrosion rates in this range are 1500 µm/a at 25°C and increase up to 2800 µm/a at 80°C. But at the realistic average H_2O_2 concentration of $< 5 \cdot 10^{-4}$ mol/l, no influence of H_2O_2 on Ti99.8Pd corrosion was observed.

Corresponding measurements were carried out in brine 3 and Q-brine at 25°C. In these salt brines at $5 \cdot 10^{-2}$ mol/l H_2O_2, a marked active range was not observed. The maximum corrosion rates are 6 ± 1 µm/a in brine 3 and 3 ± 1 µm/a in Q-brine.

The specific conductivities of the protecting oxide layers, determined electrochemically, show that Mg^{2+} ions in the brines increase the resistance of Ti99.8-Pd to corrosion significantly.

Measurements in presence of F^- were carried out for a better interpretation of the results obtained under the influence of H_2O_2. At rest potential, the corrosion rates increase with increasing F^- concentration because of the formation of TiF_6^{2-}, and the anodic current density increases like in the case of H_2O_2 shifting the potential to more negative values. But in contrast to H_2O_2, which decays in O_2 and H_2O and therefore influences the cathodic current density, the F^- does not decompose. So it does not influence the cathodic current density.

A further product of radiolysis in salt brines is the ClO^-. In order to evaluate whether ClO^- has an influence on the corrosion behaviour of Ti99.8-Pd, potentiostatic measurements were carried out in saturated NaCl brine with a ClO^- content of $8 \cdot 10^{-2}$ mol/l, in the potential range from -1000 mV to +1000 mV at 25°C, 55°C and 80°C. The high ClO^- concentration was used to detect differences between the corrosion in ClO^- free brine and in brine containing ClO^-. In both brines, the corrosion behaviour of Ti99.8-Pd is identical. Furthermore, there is not a dependence on the temperature.

In general, the results obtained from these experiments demonstrate that Ti99.8-Pd is an extremely corrosion resistant material in brines

II.1.3 Stress corrosion cracking studies on TStE355 carbon steel and Ti99.8-Pd in salt brines

The resistance of TStE355 carbon steel and Ti99.8-Pd to Stress Corrosion Cracking (SCC) was investigated in NaCl-rich brine and argon (reference medium) at 170°C and slow strain rates (10^{-4}-$10^{-7}s^{-1}$) by using the Slow Strain Rate Technique (SSRT). Besides specimens of the parent material (base material), welded specimens simulating possible container closure techniques were tested. Following welding procedures were examined:

- EBW (Electron Beam Welding) for steel and Ti99.8-Pd.
- FCAW (Flux Cored Arc Welding) for the steel.
- PAW (Plasma Arc Welding) for the titanium alloy.

After each slow strain rate test, the elongation, reduction of area, energy, yield strength, maximum load, and true stress at fracture were measured to assess the loss of ductility of the studied material. This was complemented by metallographic and fractrographic studies.

TStE355 carbon steel

The results of the slow strain rate tests obtained for the parent material and EB and FCA welded steel specimens in 5M NaCl at 170°C show a clear decrease of the elongation and reduction of area parameters, compared to the values in argon. The drop of these parameters is not significant at the highest strain rate ($10^{-4}s^{-1}$) but it is important at the other lower strain rates used in the tests. The values of the yield strength and maximum load parameters do not show important differences in the two media, for both parent and welded specimens. The loss of ductility of the specimens

tested in the salt brine is mainly manifested in the reduction of area in the fracture zone.

The loss of ductility, which occurred by the steel when tested in the salt brine is explained by the embrittling effect of the hydrogen produced on the specimen surface during the test. Due to general corrosion, hydrogen is produced and penetrates into the material, mainly through the highly stressed zones of the specimen, and interacts with the microstructure resulting in a deterioration of the mechanical properties.

Metallographic examinations of parent and welded specimens show secondary cracks with a maximum crack depth of 130 μm when tested in NaCl brine at the slowest strain rate. This indicates a slight sensitivity to SCC under the test conditions applied. In all cases, the fracture of welded specimens is located in the base material.

The SEM fracture surface examinations of tested specimens show a change from a fully ductile fracture surface with dimples formation for specimens tested in argon to a more brittle fracture mode when the tests were performed in the salt brine. The brittle nature of the fracture surface becomes greater as the strain rate is slower.

Concerning the welded specimens, there was not observed any effect of the EB and FCA welding procedures on the SCC behaviour of the material.

X-Ray Diffraction (XRD) analysis of the corrosion products formed on the surface of steel specimens tested in NaCl at 170°C shows that the oxide layer mainly consists of magnetite (Fe_3O_4) .

Ti99.8-Pd (TiGr-7 alloy)

The SSRT results obtained on the TiGr-7 alloy and its EB and PA welded joints at 170°C and a strain rate of $10^{-7}s^{-1}$ show that after testing in the brine the mechanical values of the material, both for the parent and the welded specimens, are very close to those in argon.

No secondary cracks were observed in the metallographic examinations of the specimens after testing in the brine, indicating that under the test conditions applied the TiGr-7 alloy is not sensitive to SCC. EB and PA weldings do not affect the behaviour of the material to SCC. The fracture surface of the specimens shows a fully ductile fracture mode for tests performed in argon and in NaCl brine.

II.2 Granite Environment

II.2.1 Stress corrosion cracking studies on TStE355 carbon steel and AISI 316L stainless steel

The resistance of TStE355 carbon steel and AISI 316L stainless steel to Stress Corrosion Cracking (SCC) in granite-bentonite water and argon (reference medium) was investigated at 90°C and strain rates of 10^{-4}-$10^{-7}s^{-1}$. The test method used was the Slow Strain Rate Technique (SSRT). Both welded and unwelded specimens were examined. The welding procedures applied were:

- EBW (Electron Beam Welding) and FCAW (Flux Cored Arc Welding) for the carbon steel.
- GTAW (Gas Tungsten Arc Welding) for the stainless steel.

After each slow strain rate test, the elongation, reduction of area, energy, yield strength, maximum load, and true stress at fracture were measured to assess the loss of ductility of the studied materials. This was complemented by metallographic and fractographic studies.

TStE355 carbon steel

The SSRT results show that the TStE355 steel suffers a loss of ductility in the granitic environmnet, mainly noticed in the reduction of area and true stress at fracture. The drop of these parameters is not significant at the highest rate ($10^{-4}s^{-1}$) but it is important at any of the other slower strain rates used in the tests, due to the longer exposure to the corrosion medium. There are no important changes in the yield strength and maximum load parameters in granitic water.

The loss of ductility observed by the carbon steel when tested in bentonite-granitic water is explained by the embrittling effect of the hydrogen produced during the slow strain rate test. In all cases, the fracture of welded specimens was located in the base metal.

In the metallographic studies carried out on the parent and welded TStE355 steel specimens, no clear signs of sensitivity to SCC in granitic water were found. Areas of localized corrosion are present on the lateral surface of TStE355 specimens when tested at the slowest strain rate of $10^{-7}s^{-1}$. However, these areas, deeper in the case of welded specimens, have a crack length/crack width ratio relation near 1, indicating rather a localized corrosion due to the local and repetitive breaking of the oxide layer than secondary cracking. The crack length / crack width ratio parameter gives an idea of the sharpness of the crack and is useful to quantify and compare the resistance of the tested materials to SCC. It is important to mention that the term crack is used in a wide sense including both secondary cracks and localized corrosion due to the breaking of the oxide layer.

AISI 316L stainless steel

The values of elongation, reduction of area, maximum load and yield strength in the granitic environment are very close to those obtained in argon, thus indicating no loss of ductility. The fracture of the welded specimens was always located in the base material. Secondary cracks typical for stress corrosion cracking have not been observed under any of the test conditions. Several AISI 316L steel specimens tested in the granitic water at the slowest strain rate of $10^{-7}s^{-1}$ show isolated pits near the fracture zone.

The SEM examinations show a fully ductile fracture surface with dimples formation for the specimens tested in the granitic environment. EB and GTA weldings do not affect the resistance of the AISI 316 stainless steel to SCC.

II.3 Clay Environment

The investigations in clay environment aimed at studying systematically the corrosion behaviour of nine preselected materials under representative disposal conditions. These materials were: carbon steel TStE355, stainless steels AISI 316L, AISI 316L hMo, AISI 316Ti and AISI 309S, higher alloyed stainless steels UHB 904L and Cronifer 1925hMo, nickel alloy Hastelloy C4, and titanium alloy Ti/0.2Pd. An important advantage of laboratory experiments compared to in-situ experiments is that they allow to study separate the various phases of the disposal, e.g. the aerobic and anaerobic phases. The various relevant environmental parameters (temperature, concentration of anions that influence localized corrosion) were varied according to the results of prior studies and according to the relevant disposal concepts. As most of the studied materials were corrosion resistant materials that can suffer mainly from localized corrosion, the research effort focused on pitting corrosion.

The susceptibility of the candidate container materials to pitting corrosion was evaluated by performing cyclic potentiodynamic polarization measurements and determining the following characteristic potentials from the obtained polarization curves:

- the free corrosion potential, E_{corr}: this is the potential of the metal under open circuit conditions in the studied environment,

- the critical potential for pit nucleation, E_{np}: this is the potential above which pits nucleate and develop, and

- the protection potential, E_{pp}: this is the potential below which no pitting occurs and above which pits already nucleated can grow.

Furthermore, the actual corrosion potential, i.e. the open circuit potential of the metal in the studied environment under realistic conditions, is determined from E_{corr} (t) curves. Indeed, the corrosion potential increases with oxygen content and with time before reaching a stable value. This value, which was almost independent from alloy composition and electrolyte composition, was used for the interpretation of the polarization curves.

The tests were conducted in synthetic oxidizing Boom clay water at 90°C and 16°C. The influence of chloride, sulphate and thiosulphate was evaluated. Chloride is an anion known to induce pitting. In pits and crevices, high chloride concentrations can occur. During the oxidation of pyrite in Boom clay, e.g. under the influence of a thermal and gamma radiation field, sulphate is formed, with thiosulphate as an intermediate product. In general, sulphate inhibits pitting corrosion, but in the presence of thiosulphate, the occurence of pitting has sometimes been noticed.

At 90°C, the nickel alloy Hastelloy C4 and the titanium alloy Ti/0.2 Pd (Ti99.8-Pd) do not show any signs of pitting attack in all tested brines (synthetic oxidizing Boom clay water with chloride contents up to 10000 ppm and thiosulphate contents up to 100 ppm). The carbon steel TStE355 shows the characteristic electrochemical behaviour for a corrosion-allowance material, i.e., the corrosion rate increases exponentially with overpotential. The stainless steels AISI 316L, AISI 316L hMo, AISI 316Ti, AISI

309S, and the higher alloyed stainless steels Cronifer 1925 hMo and UHB 904L suffer from pitting corrosion but the pitting potentials remain high, even at the highest investigated chloride concentrations. The value of the protection potential, however, is almost as low as, and in some cases even lower than the actual corrosion potential. This means that the use of these alloys, and in particular of the alloys AISI 316L, AISI 316L hMo, AISI 316 Ti, and AISI 309S in oxidizing Boom clay water does include the risk of pitting corrosion.

Sulphate inhibits pitting corrosion in the absence of thiosulphate, as confirmed by our tests. The influence of thiosulphate was found to be significant for the alloys AISI 316L hMo, AISI 316Ti, AISI 309S, and UHB 904L. The pitting potential decreases only slightly with increasing thiosulphate concentration, but the protection potential drops as much as 300 to 400 mV when 100 ppm thiosulphate is added to synthetic oxidizing Boom clay water, and the effect is already significant at 50 ppm. Bearing in mind that thiosulphate concentrations up to 17 ppm have been found in interstitial clay water under the influence of a gamma radiation field, these findings indicate that in contact with Boom clay water that is oxidized under the influence of a thermal and radiation field, the alloys AISI 316L hMo, AISI 316Ti, AISI 309S, and UHB 904L, could suffer from pitting corrosion, depending of course on the *in situ* value of the corrosion potentials of these alloys in the Boom clay host rock formation.

At 16°C, the susceptibility to pitting corrosion is generally lower. None of the investigated alloys show pitting attack in synthetic oxidizing clay water containing 100 ppm chloride. The alloys UHB 904L, Cronifer 1925 hMo, Hastelloy C4, and Ti/0.2 Pd (Ti99.8-Pd) do not suffer from pitting corrosion at all in any of the investigated solutions. Sulphate even decreases the alloys' susceptibility to pitting corrosion. The increase of the thiosulphate concentration has a small effect on the characteristic pitting potentials but these remain above the actual corrosion potential. Summarizing, all investigated alloys, except carbon steel TStE355, resist pitting in synthetic oxidizing clay water under realistic conditions (100 ppm Cl^-) at 16°C.

A database with experimental results was constructed. For each of the alloys, a data sheet was written, containing the values of the pitting and protection potentials for each of the test solutions. These data sheets give valuable information on the pitting behaviour of the investigated alloys, and can serve as a basis for future modelling. In addition, the database contains all the polarization curves. To use this database at its full potential, however, it is necessary to know the values of the *in situ* corrosion potentials of the investigated candidate container materials in the Boom clay formation.

III. Conclusions and Recommendations

- The alloy Ti99.8-Pd is the strongest candidate for the realization of the **corrosion-resistant container concept** in the three geological formations rock salt, granite and clay. A such **corrosion-resistant container concept** could consist of a carbon steel container as mechanical support provided with a corrosion protection layer made of Ti99.8-Pd. For this concept, the contact corrosion between Ti99.8-Pd and steel must be investigated. In addition, electrochemical studies on the stability of this material pair at high temperature (about 150°C) are needed.

- The nickel base alloy Hastelloy C4 seems to be a promising material for corrosion resistant containers in clay. However, more investigations are required. These should include above all the examination of the resistance of the material to crevice corrosion, and in the presence of strong oxidants as they are formed under gamma radiation (e.g. H_2O_2).

- The stainless steels AISI 316L, AISI 316LhMo, AISI 316LTi, AISI 309S, and the higher alloyed stainless steels Cronifer 1925hMo and UHB 904L suffer from pitting corrosion under certain conditions in oxidizing clay environment. Therefore, for the reliable assessment of these steels as container materials in clay, studies at realistic corrosion potentials are necessary. Stress corrosion cracking problems for the AISI 316L in granitic environments are not expected but pitting corrosion could occur.

- The TStE355 carbon steel continues to be considered as a promising container material for the realization of the **corrosion-allowance concept** in rock salt. However, a welding technique for the manufacture of a corrosion resistant closing of carbon steel containers must be qualified. The slight sensitivity to stress corrosion cracking and the loss of ductility (hydrogen embrittlement) in NaCl brine at 170°C observed in the slow strain tests are significant only at very low strain rates. In granitic environments and 90°C, the steel is resistant to stress corrosion cracking, but as in the NaCl brine, a loss of ductility occured at very low strain rates. Finally, in oxidizing clay environment, a strong non-uniform corrosion of the actively corroding carbon steel is expected.

A benefit of the use of carbon steel containers is the establishment of reducing conditions in the near field of the repository by corroded iron, and, therefore, the expected high retardation of radionuclides by iron corrosion products (e.g. Fe_3O_4, Fe_2O_3, $Fe(OH)_2$). Corresponding sorption experiments are planned. An important question which still needs to be clarified with a view to the use of the corrosion-allowance carbon steels is namely, whether the amount of hydrogen generated by the corrosion of iron or by the radiolysis of brines can be tolerated in the repository. In future corrosion studies, besides the materials investigated in this study, the suitability of copper-base materials (Cu-Ni alloys) as alternative to the steels will be examined. Furthermore, corrosion models must be developed in order to predict the lifetime of waste containers under disposal conditions.

1. INTRODUCTION

In present concepts for the disposal of spent fuel or vitrified high-level waste (HLW) in geological formations such as rock salt, granite and clay, the waste container (overpack) is one of several barriers for the immobilization of radionuclides. Its function is to isolate the waste from the disposal environment for as long as practicable. This barrier function is important above all during the elevated-temperature phase in the repository which lasts a few hundred years (300-500 years). The main threat to container integrity is corrosion through contact with groundwater or salt brines which may be present in the disposal area under certain conditions. Accordingly, extended studies on various metallic materials have been undertaken in the authors´ laboratories aimed at identifying corrosion resistant materials for long-lived containers.

In previous studies[1,2,3,4], two approaches were identified for the manufacture of long-lived containers for disposal in rock salt, granite and clay. These are: the **corrosion-allowance concept** and the **corrosion-resistant concept**. The first envisages metals of lower resistance (actively corroding materials) that can be used economically in sufficient thickness to allow corrosion for a desired lifetime. For this concept, carbon steels are the most promising material for all three rock formations. The second concept is based on the use of highly corrosion-resistant metals. Such materials degrade at a very low corrosion rate by forming a passive surface layer. For this concept, the strongest candidates are the alloy Ti99.8-Pd (Ti/0.2Pd,TiGr-7) for rock salt, and stainless steels for granite and clay.

In the present research programme, further in-depth corrosion studies have been performed on the above mentioned materials at FZK.INE, FU-Berlin, ENRESA/INASMET and SCK.CEN in the frame of a joint programme. The objectives of the studies in rock salt, granite and clay environments were:

- to evaluate the effect of essential parameters on corrosion.
- to gain a better understanding of corrosion mechanisms.
- to provide more accurate data for a material degradation model that can be used to predict the lifetime of such containers.

Work at FZK.INE and FU-Berlin has concentrated on disposal in rock salt, ENRESA/INASMET considered both rock salt and granite, and SCK.CEN covered disposal in clay. The whole programme was coordinated by FZK.INE. The studies included long-term immersion experiments, electrochemical/radiochemical studies and slow strain rate tests.

In the present final report, the progress achieved in the research programme from January 1996 to December 1998 shall be described.

2. WORK PROGRAMME

The work programme consisted of three tasks:

- Corrosion studies in salt environments (FZK.INE, FU-Berlin, ENRESA/INASMET)

Long-term immersion tests on the preselected TStE355 carbon steel and the alloy Ti99.8-Pd. Determination of the effect of initial pH, selected chemical species, gamma radiation and welding on the corrosion in salt brines (FZK.INE).

Combined electrochemical and radiochemical studies on Ti99.8-Pd in salt brines. Examination of the effect of the gamma radiolytic products H_2O_2 and ClO^- on the electrochemical corrosion behaviour (FU-Berlin).

Stress corrosion cracking (SCC) studies on TStE355 steel and Ti99.8-Pd in NaCl brine by means of the slow strain rate technique (ENRESA/INASMET).

- Corrosion studies in granite environments (ENRESA/INASMET)

Stress corrosion cracking studies on TStE355 carbon steel and AISI316L stainless steel in bentonite buffered granitic groundwater.

- Corrosion studies in clay environments (SCK.CEN)

Electrochemical corrosion studies on various container materials. Evaluation of the influence of temperature and content of Cl^-, SO_4^{2-} and $S_2O_3^{2-}$ of the medium on corrosion. The investigations focused on carbon steel and stainless steels. Nevertheless, some investigations were performed also on the nickel base alloy Hastelloy C4 and the alloy Ti99.8-Pd.

3. LONG-TERM IMMERSION TESTS ON TStE355 STEEL AND Ti99.8-Pd IN SALT BRINES

The influence of important parameters as initial pH, selected chemical species, gamma radiation and welding on the corrosion behaviour of TStE355 steel and Ti99.8-Pd in NaCl-rich and $MgCl_2$-rich brines was investigated. The experiments lasted up to 20 months and were performed at realistic disposal temperatures of 90°C-170°C. Such investigations are important because:

- The pH of brines can influence significantly the corrosion behaviour of metals by forming or dissolving protective oxide layers on the metal surface.

- Chemical species which intrude into the brines, e.g. as salt impurities or be generated by gamma radiolysis of the brine can affect the corrosion behaviour of metals by various processes, e.g. change of redox potential, formation of complexes.

- The interaction of gamma radiation with salt brine produces reducing/oxidizing reactive particles and stable products (e.g. H_2, $Cl_2^{\bullet-}$, H_2O_2, ClO^-) which may change the rate and mechanism of corrosion. Furthermore, the absorption of gamma

radiation in the semi-conducting protective oxide layers of metals such as Ti99.8-Pd will induce photoradiation effects, which may change the corrosion rate.

- Welds can have a different corrosion behaviour than the parent material because welding causes changes in the material structure and generates tensile stresses in the weld region and in the Heat Affected Zone (HAZ).

3.1 Experimental

3.1.1 Materials, test brines and specimens

The materials TStE355 steel and Ti99.8-Pd were investigated in the hot-rolled and annealed condition and had the following compositions in wt%:

TStE355 steel: 0.17 C; 0.44 Si; 1.49 Mn; bal Fe.
Ti99.8-Pd: 0.18 Pd; 0.05 Fe; 0.01 C; 0.04 O_2; bal Ti.

The brines had following compositions (wt%):

$MgCl_2$-rich “Q-brine” (brine 1):
26.8 $MgCl_2$; 4.7 KCl; 1.4 NaCl; 1.4 $MgSO_4$; 65.7 H_2O; (pH(25°C)=4.6).
NaCl-rich brine (brine 3):
25.9 NaCl; 0.23 K_2SO_4; 0.21 $CaSO_4$; 0.16$MgSO_4$; 73.5 H_2O; (pH(25°C)=6.5).

For the investigations plane specimens having the dimensions 40mmx20mmx4mm were used. Besides the parent materials (unwelded specimens), Tungsten-Inert-Gas (TIG) welded and Electron Beam (EB) welded specimens were examined in order to evaluate the suitability of these welding procedures as potential container closure techniques.

3.1.2 Test conditions and experimental setups

For the investigations into the influence of pH on steel corrosion, the initial pH of the Q-brine was variied between 3 and 7, and that of the NaCl-rich brine between 1 and 10. The various pH values were adjusted by addition of HCl or NaOH to the brines. The test temperature was 170°C and the maximum test duration 1 year.

The influence of selected chemical species on the steel corrosion was examined up to 520 days in both abovementioned brines at 90°C and 170°C. The specimens added to the brines and their concentrations are given in Table 3.1. Following species were examined: the salt impurity $B(OH)_4^-$, the main gamma radiolytic products of the brines H_2O_2 and ClO^-, and Fe^{3+}. The latter can be generated by oxidation of the container corrosion product Fe^{2+} as a result of radiolysis or ingress of oxygen into the disposal area. Both the individual and the synergistic effect of the chemical species on corrosion was investigated. For this, the species were added to the brine single or all simultaneously. The concentration of the various species in the brines varied between 10^{-1} mol/l and 10^{-3} mol/l. For comparison, investigations were performed in the brines also without additions of chemical species (“pure brines”).

The irradiation-corrosion studies on Ti99.8-Pd were conducted in Q-brine at 150°C and a gamma dose rate of 10 Gy/h (10^3 rad/h) which is relevant for the thick-walled

container discussed (steel container with Ti99.8-Pd corrosion protection). For comparison, experiments without radiation have been conducted in the brine. The experiments lasted up to 1 year.

The experimental setups used for the experiments are described in previous work[5]. Shortly, for the experiments without irradiation, stainless steel pressure vessels provided with corrosion resistant insert vessels made of PTFE were used to avoid evaporation of the brines (boiling point: about 115°C). The experiments under gamma irradiation were performed in the spent fuel storage pool of KFA Jülich. For these experiments, autoclaves made of Ti99.8-Pd were used. With these experimental equipments used, the initial test conditions were oxidizing. The total amount of oxygen available in the systems was about 15 mg, corresponding to 0.19 mg O_2/cm^2 specimen. This oxygen amount was consumed very fast by reactions with Fe so that after few days reducing conditions were established. Evaluation of the specimens regarding general and local corrosion was carried out by gravimetry, measurements of pit depth, surface profilometry and metallography. The integral corrosion rate of the specimens was calculated from the experimental determined weight losses and the material density.

TABLE 3.1 Chemical species examined in the corrosion studies on TStE355 steel in salt brines

Species	Added to the brine as	Concentration Mol/l
$B(OH)^-_4$	H_3BO_3	$1.4 \cdot 10^{-1}$
Fe^{3+}	$FeCl_3 \cdot 6H_2O$	$3.5 \cdot 10^{-2}$
H_2O_2	15% H_2O_2-solution	10^{-3}; 10^{-2}
ClO^-	15% NaClO- solution	10^{-3}

3.2 Results

3.2.1 Influence of pH on steel corrosion in brines

In both brines and at all pH values the steel is resistant to pitting corrosion in the sense of an active-passive corrosion element. Under the test conditions, a non-uniform general corrosion is observed, and the thickness reduction of the specimens increases linearly with the corrosion time. Figures 3.1 and 3.2 show by way of example the linear time-dependence of the thickness reduction of the steel specimens in the two brines at 170°C and pH=5. The integral corrosion rates of the steel in dependence of the initial pH values of the brines are shown in Figures 3.3 and 3.4. The values are calculated from the weight losses and the material density.

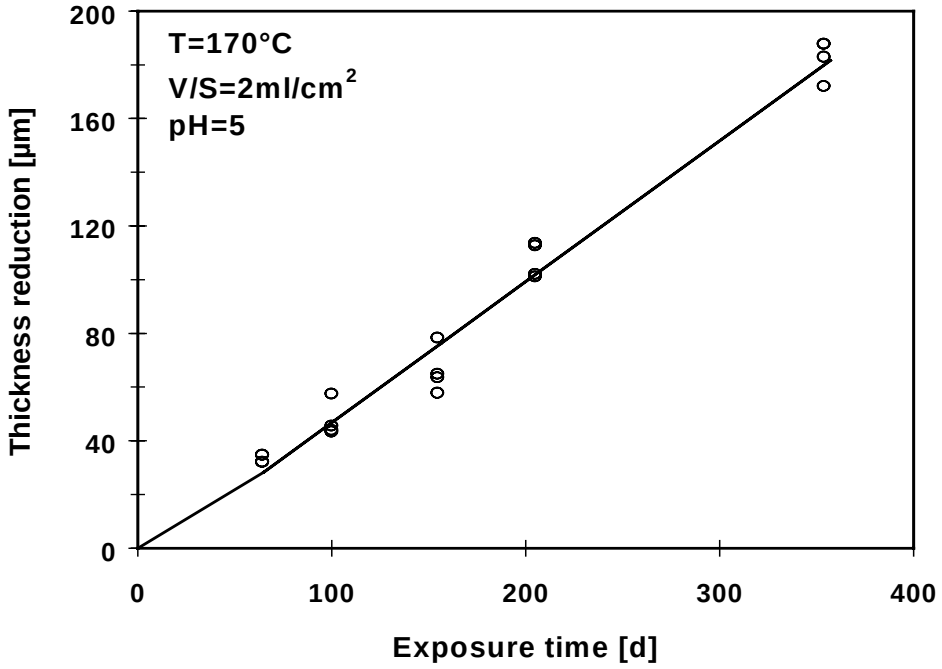

FIGURE 3.1 Time-dependence of the thickness reduction of the TStE355 steel in the $MgCl_2$-rich Q-brine at 170°C and pH=5

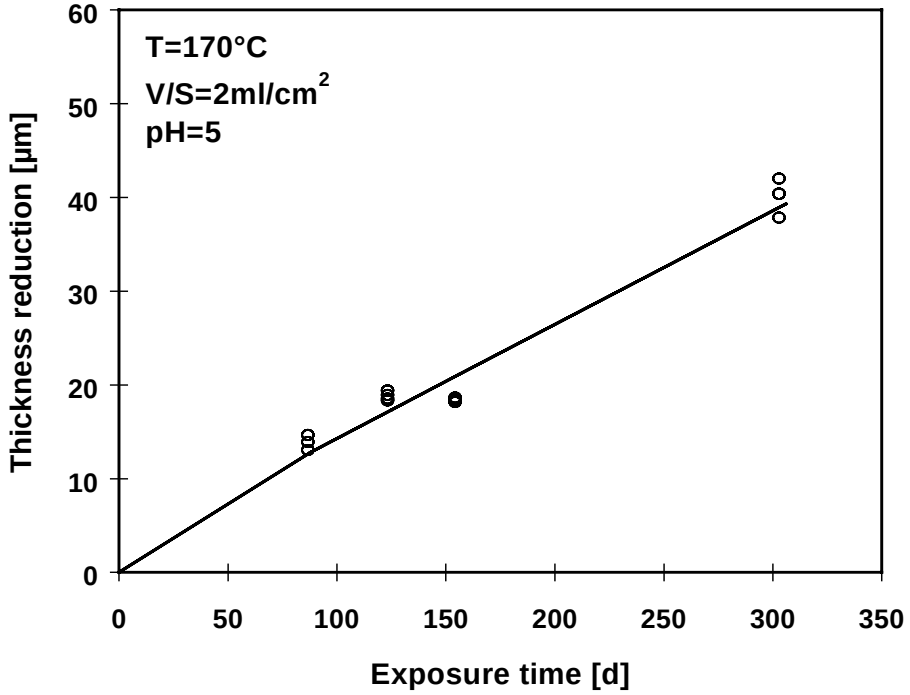

FIGURE 3.2 Time-dependence of the thickness reduction of the TStE355 steel in NaCl-rich brine at 170°C and pH=5

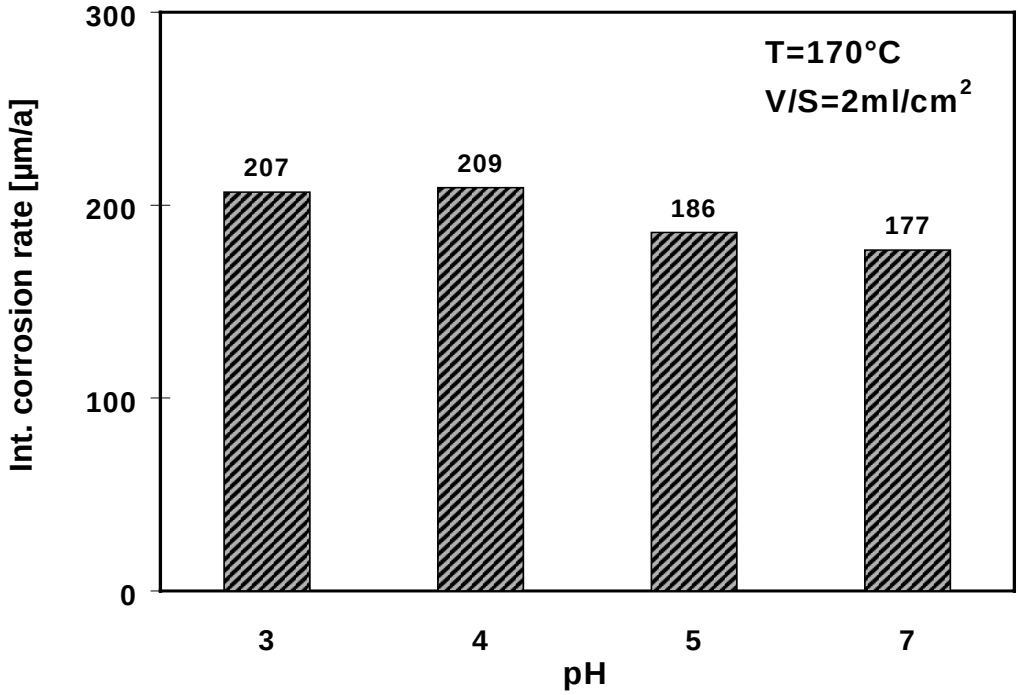

FIGURE 3.3 Corrosion rate of the TStE355 steel as a function of pH in Q-brine at 170°C

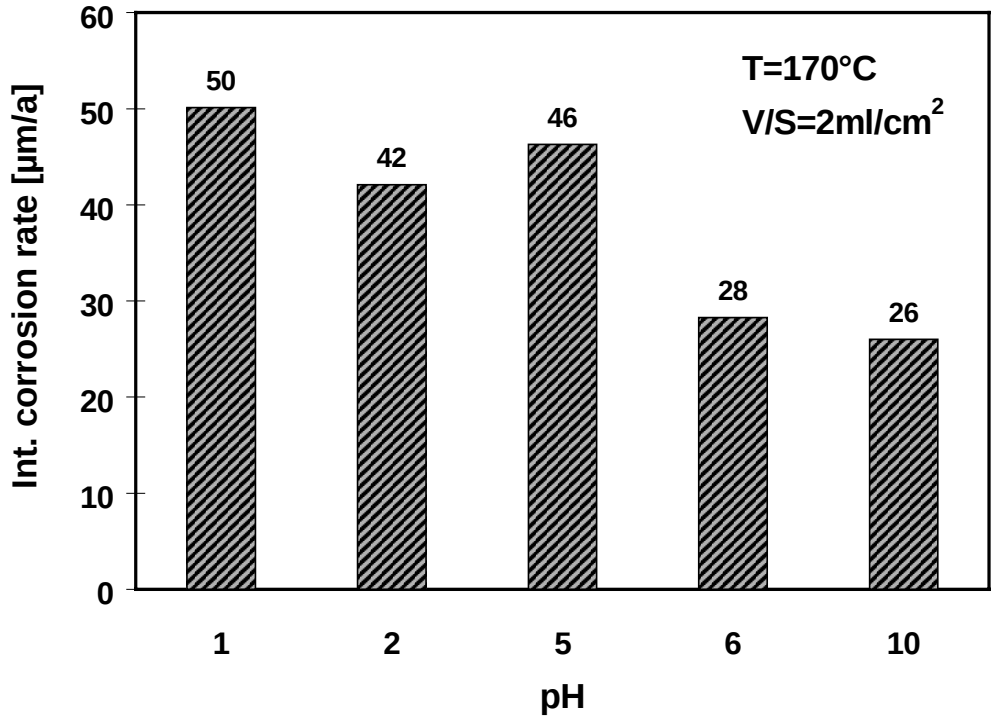

FIGURE 3.4 Corrosion rate of the TStE355 steel as a function of pH in NaCl-rich brine at 170°C

In the ranges between 3 and 7 in Q-brine (Fig.3.3) and 1 and 5 in NaCl-rich brine (Fig. 3.4), the pH has no significant influence on the corrosion rate of the steel. In these ranges, the values (177 µm/a-209 µm/a in Q-brine, and 42 µm/a-50 µm/a in NaCl-rich brine) differ among one another only about 20% at the maximum which is within the statistical variations of the measured values. It is important to mention that after termination of the specimens exposure to the brines, nearly the same pH value of 4.5-4.8 in Q-brine and 5.4-5.7 in NaCl-rich brine, respectively, was measured in all brines independent of their initial pH. It appears that the pH of the brines will be buffered by the reaction of the corrosion products with the brine constituents so that in the above-mentioned ranges the initial pH does not affect significantly the corrosion behaviour of the steel. However, at higher pH values of the NaCl-rich brine than 5 (pH=6-10), the corrosion rates of the steel clearly decrease to 26 µm/a-28 µm/a. This fact may be explained by the formation of a very dense corrosion protection layer on the metal surface, which was observed in the metallographic examinations.

The comparison of the corrosion rates of the steel in the two brines (Figures 3.3 and 3.4) shows that the values in the $MgCl_2$-rich "Q-brine" are significantly higher than in the NaCl-rich brine. The higher corrosivity of the $MgCl_2$-rich brine is attributed to its higher HCl concentration. This could be explained by the higher Cl^--concentration and the hydrolysis of Mg^{2+}. The acceleration of the steel corrosion in brines containing high amounts of $MgCl_2$ is in line with the results reported by Westermann et. al. [6].

3.2.2 Influence of chemical species on steel corrosion in brines

The results obtained in Q-brine with and without additions of chemical species indicate that the thickness reduction of the steel specimens (general corrosion) increases linearly with the exposure time. The integral corrosion rates of the steel over a test period of up to 1 year in the various brines at 90°C and 170°C are shown in Fig. 3.5. At 90°C the values in the brines containing chemical species amount 90 µm/a –123 µm/a and are therefore a factor of about 1.3-1.8 higher than in the pure brine (70 µm/a). In all brines at 90°C the corrosion attack was non-uniform. Pitting corrosion in the sense of an active-passive corrosion element was not observed.

The increase in temperature from 90°C to 170°C increases the corrosion rates of the steel in all brines, especially in the pure brine (224 µm/a at 170°C compared to 70 µm/a at 90°C). The comparison of the corrosion rates at 170°C indicates that the addition of the chemical species to the brine does not noticeably increase the corrosion rate of the steel (224 µm/a in the pure brine compared to 254 µm/a in the presence of all species). In fact, in the brines containing $B(OH)_4^-$ or Fe^{3+}, the corrosion rates at 170°C (115 µm/a and 155 µm/a, respectively) are clearly lower then in the pure brine. This is attributed to the formation of very dense corrosion protection layers on the specimens. However, after long exposure times to the brines containing chemical species, local corrosion attacks were observed on the steel specimens. The maximum depth of these pits after 1 year exposure time to the brines amounted up to 500 µm which is clearly higher than the non-uniform corrosion of the specimens in the pure brine at 170°C (about 200 µm after 1 year). Due to the local corrosion attacks of the steel specimens, the values for the general corrosion rates at 170°C given in Fig. 3.5 represent average corrosion rates.

As in Q-brine, the thickness reduction of the steel specimens in NaCl-rich brine increases linearly with the exposure time. The integral corrosion rates of the steel over a test period of up to 520 days in the various brines at 90°C and 170°C are shown in Fig.3.6. At 90°C the corrosion rate in the pure NaCl-rich brine is very small (5 µm/a). The addition of the chemical species to the brine (single or all species simultaneously) clearly increases the corrosion rate of the steel. The highest rates occur in the brines containing $B(OH)^-_4$ (102 µm/a) and all species simultaneously (236 µm/a). The latter indicates a synergistic effect.

At 170°C the corrosion rate in the pure brine (46 µm/a) is clearly higher than at 90°C (5 µm/a). However, the addition of the chemical species to the brine does not significantly increase the corrosion rate of the steel over the value in the pure brine. The maximum corrosion rates at 170°C occur in the brines containing $B(OH)^-_4$ (58 µm/a), Fe^{3+} (59 µm/a) and all species simultaneously (73 µm/a). These values are only a factor 1.3-1.6 higher than those in the pure brine.

The comparison of the results obtained at the two test temperatures shows that the increase of temperature from 90°C to 170°C accelerates the corrosion rates of the steel only in the pure brine, and to a certain extent in the ClO^--containing brine. In fact, in the brines containing $B(OH)^-_4$, Fe^{3+} and all species, respectively, the corrosion rates at 170°C are lower than at 90°C. This is attributed to the formation of a very dense corrosion protection layer at 170°C which was observed in the metallographic examinations. However, after long exposure times, the corrosion layer formed in the brine containing all species broke down locally, and a non-uniform corrosion with a maximum penetration depth of 130 µm was observed after 1 year exposure time. In all other brines and at both test temperatures, the corrosion of the steel was nearly uniform.

The comparison of the steel corrosion rates in the two brines shows that the values in Q-brine are clearly higher than in NaCl-rich brine. This is attributed to the higher HCl concentration of the Q-brine, as discussed before.

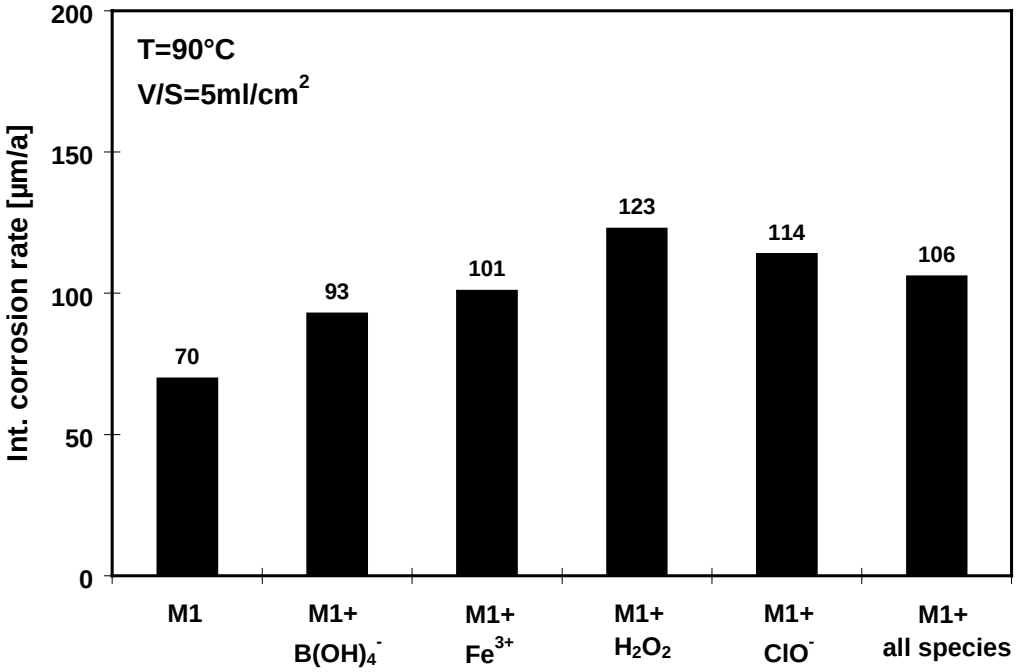

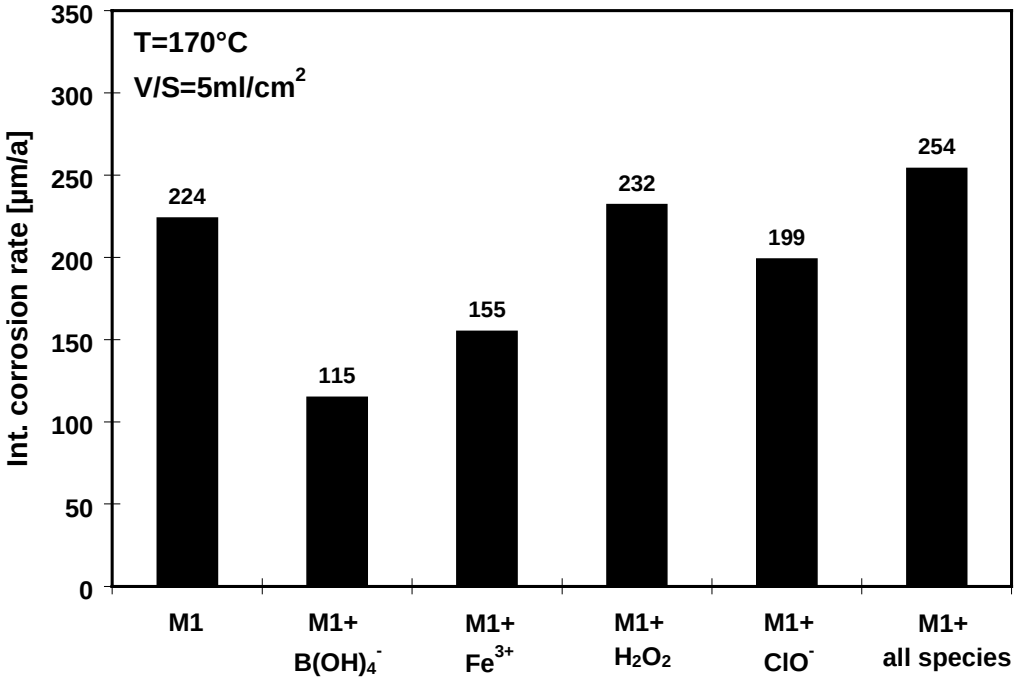

FIGURE 3.5 Corrosion rates of TStE355 steel in Q-brine with and without chemical species at 90°C and 170°C

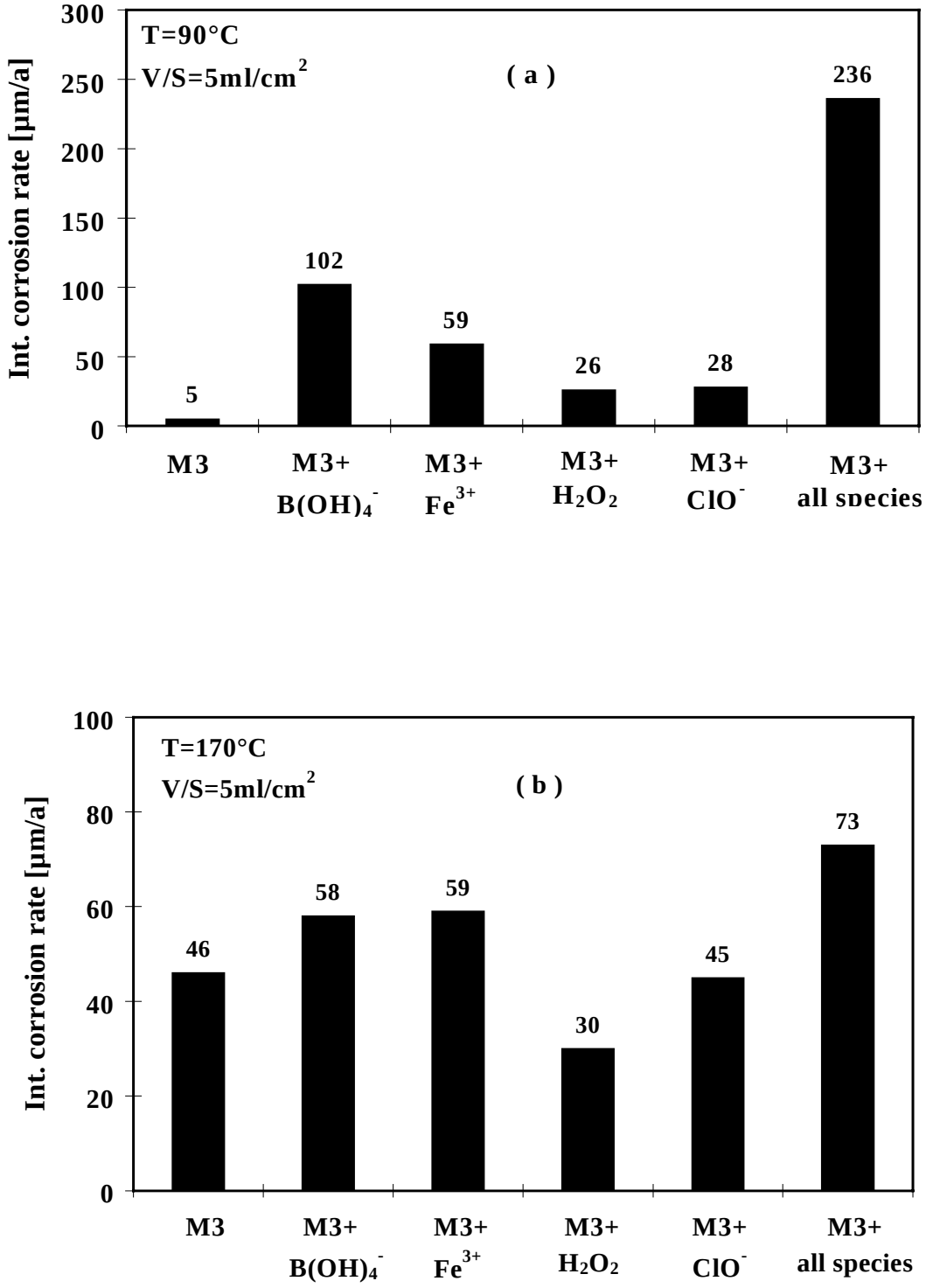

FIGURE 3.6 Corrosion rates of TStE355 steel at 90°C and 170°C in NaCl brine with and without additions of chemical species

3.2.3 Influence of gamma radiation on the corrosion of Ti99.8-Pd in Q-brine

The corrosion results obtained for Ti99.8-Pd in the $MgCl_2$-rich Q-brine at 150°C are given in Table 3.2. The general corrosion of this alloy in the brine is negligible low (< 1 µm/a). The imposition of a 10 Gy/h gamma radiation field on the 150°C brine environment does not increase the corrosion of the material. Surface profiles and metallographic examinations (see micrographs Figures 3.7 and 3.8) show that Ti99.8-Pd is resistant to pitting corrosion both with and without irradiation. Under the test conditions, a completely uniform corrosion was observed. Detailed results are published elsewhere[7].

TABLE 3.2 Corrosion of Ti99.8-Pd in Q-brine at 150°C with and without gamma radiation field

Exposure time (d)	Weight loss*) (mg)	Dose rate (Gy/h)	Corrosion rate*) (µm/a)
63	0	0.10 ± 0.04	0.09 ± 0.040
125		0.06 ± 0.06	0.02 ± 0.020
191		3.50 ± 0.02	0.73 ± 0.004
268		0.10 ± 0.04	0.02 ± 0.008
63	10	0.10 ± 0.10	0.06 ± 0.060
174		0.62 ± 0.09	0.14 ± 0.020
244		3.79 ± 0.06	0.62 ± 0.010
356		1.49 ± 0.14	0.21 ± 0.020

*) average value of three specimens

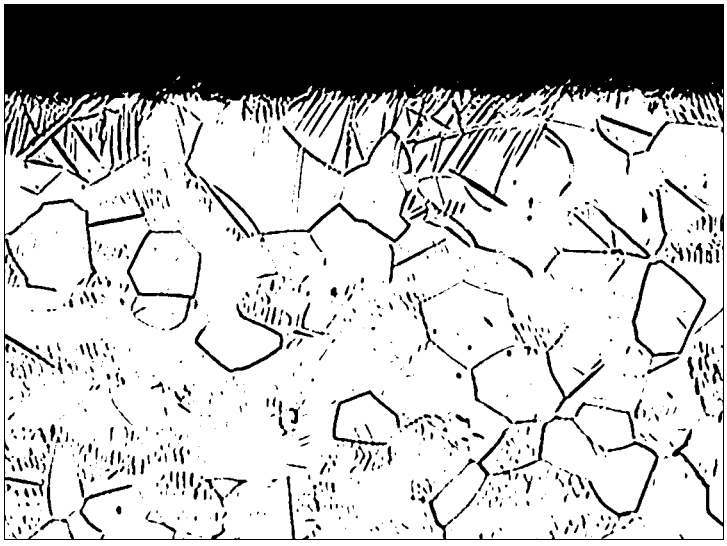

FIGURE 3.7 Optical micrograph of Ti99.8-Pd after 340 days exposure to Q-brine at 150°C (X200)

FIGURE 3.8 Optical micrograph of Ti99.8-Pd after 340 days exposure to Q-brine at 150°C and 10Gy/h (X200)

3.2.4 Influence of welding on the corrosion of the TStE355 steel and Ti99.8-Pd

The influence of Tungsten-Inert-Gas (TIG) welding and Electron Beam (EB) welding on the corrosion of TStE355 steel and Ti99.8-Pd was investigated up to 20 months in Q-brine at 150°C. For comparison, unwelded specimens (parent material) were also investigated.

The time dependence of the thickness reduction of welded and unwelded steel specimens in the brine is shown in Fig. 3.9. The general corrosion rates and the local corrosion results obtained for the specimens are compiled in Table 3.3. In the investigated time intervall between 100 and 585 days the thickness reduction of the unwelded specimens increases linearly with the exposure time. A non-uniform general corrosion was observed and the corrosion rate amounts 55 µm/a. The general corrosion rate of the TIG and EB welded specimens (173 µm/a) is a factor of about 3 higher than that of the unwelded specimens. Furthermore, the welded specimens suffered from severe local corrosion attacks in the welds and the Heat Affected Zone (HAZ). The maximum depth of such local attacks reached after 306 days values up to 500-600 µm. In general, it can be stated that TIG and EB welded specimens show a very similar corrosion behaviour, and that these welding techniques clearly decrease the corrosion resistance of the steel in the test brine.

In case of the alloy Ti99.8-Pd, the TIG and EB welding do not reduce the high corrosion resistance of this material in the Q-brine. As the unwelded specimens, the TIG and EB welded specimens show a negligible general corrosion (<1 µm/a), and a high resistance to local corrosion.

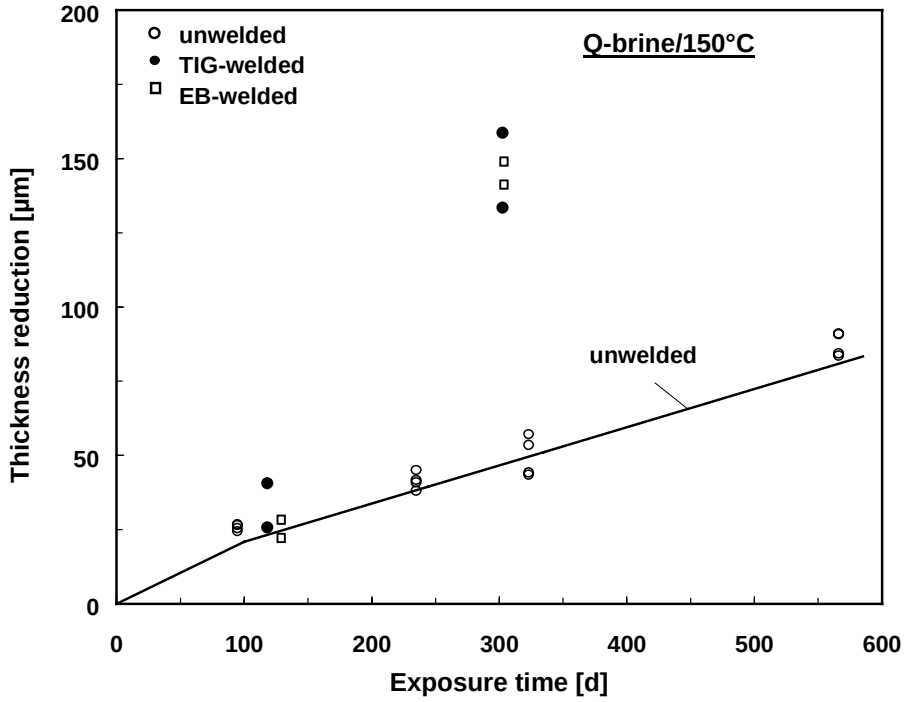

FIGURE 3.9 Time dependence of general corrosion of welded and unwelded TStE355 steel at 150°C in Q-brine

TABLE 3.3 Corrosion of welded and unwelded TStE355 steel in Q-brine at 150°C

Material condition	Test Time (d)	Integral corrosion rate (µm/a)	Max. depth of local corrosion (µm)		
			Base material	Weld	HAZ
unwelded	585	55.1 ± 6.0	60	–	–
TIG-welded	306	173.0 ± 16.0	80	300	500
EB-welded	306	171.8 ± 5.0	30	740	650

4. ELECTROCHEMICAL AND RADIOCHEMICAL STUDIES ON Ti99.8-Pd IN SALT BRINES

Combined electrochemical and radiochemical studies were performed on Ti99.8-Pd in salt brines in order to get a detailed insight into the corrosion kinetics and especially into the potential influence of the radiolytic products H_2O_2 and ClO^- on corrosion. Both unwelded and welded specimens were examined. The studies were performed in $MgCl_2$-rich brine (Q-brine) and in NaCl brines at temperatures between 25°C and 80°C at Free Corrosion Potential (Rest Potential E_{corr}) and at various applied potentials. The method used was the Radioisotope Method (RIM)[8] which combines classical electrochemical procedures (potentiostatic and potentiodynamic measurements, impedance and photocurrent measurements) with radiochemical

ones, especially neutron activation analysis. Furthermore, microscopic examinations were carried out in order to decide whether pit corrosion or general corrosion has taken place. For a better understanding of the results obtained from the experiments with H_2O_2, the corrosion of Ti99.8-Pd was studied under the influence of F^-.

4.1 Corrosion studies at rest potential

4.1.1 Experimental

The influence of H_2O_2 on the corrosion of Ti99.8-Pd was investigated in three brines, namely saturated NaCl-brine, NaCl-rich brine and $MgCl_2$-rich "Q-brine" at 25°C, 55°C and 80°C (Table 4.1). The concentration of dissolved titanium in the brines was continuously measured for about 250 hours by means of γ-spectroscopy. The experiments were performed under conservative conditions, namely at very high initial H_2O_2 concentrations in the brines between $7 \cdot 10^{-5}$ mol/l and $3.5 \cdot 10^{-2}$ mol/l. The average H_2O_2 concentration in the brines ranged between $3 \cdot 10^{-5}$ mol/l and $1.5 \cdot 10^{-2}$ mol/l. Under realistic disposal conditions, an H_2O_2 concentration in the brines of only 10^{-6}-10^{-7} mol/l is expected.

TABLE 4.1 Composition of salt brines (in mol salt / 1000 mol H_2O)

	NaCl	KCl	$MgCl_2$	$MgSO_4$	$CaSO_4$	K_2SO_4
Saturated NaCl brine	111.6	--	--	--	--	--
Brine 3 (NaCl-rich)	108.65	--	--	0.33	0.38	0.33
Q-brine ($MgCl_2$-rich) 25°C	8.9	11.6	67.8	5.2	--	--
Q-brine ($MgCl_2$-rich) 55°C	6.8	17.4	77.3	3.2	--	--
Q-brine ($MgCl_2$-rich) 80°C	9.8	21.8	82.4	3.0	--	--

Besides studies in presence of H_2O_2, the corrosion of Ti99.8-Pd was studied at 25°C in saturated NaCl brine containing F^- (0.03 mol/l - 0.66 mol/l) and also in presence of 0.08 mol/l ClO^- at 25°C, 55°C and 80°C. This high ClO^- concentration is not relevant to practical conditions, but only to basic research.

Before starting the investigations, the oxide layers on the electrodes were removed with an etching solution containing 1 part 30% HF, 4 parts 69% HNO_3 and 5 parts H_2O. Then, the electrodes were exposed to the corrosion medium. In order to determine the rest potential, the curves potential vs. time were measured.

4.1.2 Results in H_2O_2 containing brines

Rest potentials of Ti99.8-Pd

All rest potentials of Ti99.8-Pd in the brines containing H_2O_2 are in the passive range (Table 4.2). The values refer to the standard hydrogen electrode. Attention should be paid to the fact that although the corrosion rates increase with increasing H_2O_2 concentration, the function rest potential vs. H_2O_2 concentration passes a minimum (Figure 4.1).

This is due to different H_2O_2 influences on the anodic and cathodic partial current densities. The anodic current density is increased by TiO_2^{2+} formation, shifting the rest potential to the negative range. The O_2 formation by H_2O_2 decomposition on the other hand increases the cathodic current density, shifting the rest potential to more positive values. As a model this can be demonstrated by Figure 4.2

TABLE 4.2: Rest potentials of Ti99.8-Pd in presence of H_2O_2 in salt brines

Brine	Initial H_2O_2 concentration mol/l	Average H_2O_2 concentration mol/l	Rest potential (25°C) mV	Rest potential (55°C) mV	Rest potential (80°C) mV
sat. NaCl	$7.0\cdot10^{-5}$	$3\cdot10^{-5}$	487	379	201
	$7.0\cdot10^{-4}$	$3\cdot10^{-4}$	450	389	24
	$3.5\cdot10^{-3}$	$1.5\cdot10^{-3}$	421	606	42
	$7.0\cdot10^{-3}$	$3\cdot10^{-3}$	368	648	116
	$3.5\cdot10^{-2}$	$1.5\cdot10^{-2}$	441	433	238
	$7.0\cdot10^{-2}$	$3\cdot10^{-2}$	461	483	271
Brine 3	$7.0\cdot10^{-5}$	$3\cdot10^{-5}$	478	378	258
	$7.0\cdot10^{-4}$	$3\cdot10^{-4}$	461	380	115
	$3.5\cdot10^{-3}$	$1.5\cdot10^{-3}$	413	570	272
	$7.0\cdot10^{-3}$	$3\cdot10^{-3}$	361	412	260
	$3.5\cdot10^{-2}$	$1.5\cdot10^{-2}$	422	456	470
	$7.0\cdot10^{-2}$	$3\cdot10^{-2}$	424	512	272
Q-brine	$7.0\cdot10^{-5}$	$3\cdot10^{-5}$	474	501	317
	$7.0\cdot10^{-4}$	$3\cdot10^{-4}$	404	583	354
	$3.5\cdot10^{-3}$	$1.5\cdot10^{-3}$	388	312	525
	$7.0\cdot10^{-3}$	$3\cdot10^{-3}$	410	360	405
	$3.5\cdot10^{-2}$	$1.5\cdot10^{-2}$	402	675	700
	$7.0\cdot10^{-2}$	$3\cdot10^{-2}$	414	575	478

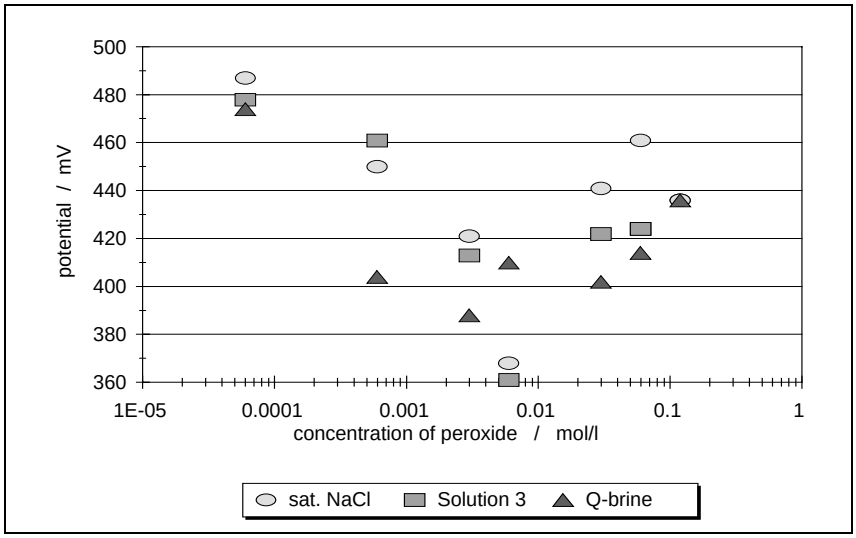

FIGURE 4.1 Rest potentials of Ti99.8-Pd in presence of H_2O_2 in salt brines at 25°C

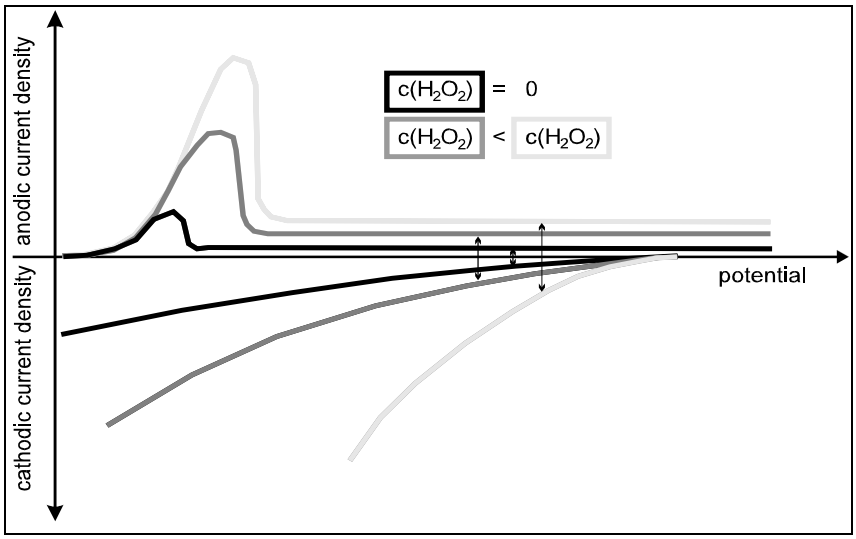

FIGURE 4.2 Shift of the rest potential (model)

Mass loss of Ti99.8-Pd

The mass loss of Ti99.8-Pd in H_2O_2 containing brines was continuously measured for 200 - 250 hours. Figure 4.3 shows the time-dependence of the mass loss at 25°C in saturated NaCl brine containing different concentrations of peroxide. From the slope of the straight line, the linear corrosion rate can be determined. From Figure 4.3 two corrosion ranges can be seen. Within the first 50 hours the corrosion of Ti99.8-Pd is relative high and depends on the H_2O_2 content in the brine. In the second range starting at 60 - 65 hours, the corrosion is very low and independent from the H_2O_2 content.

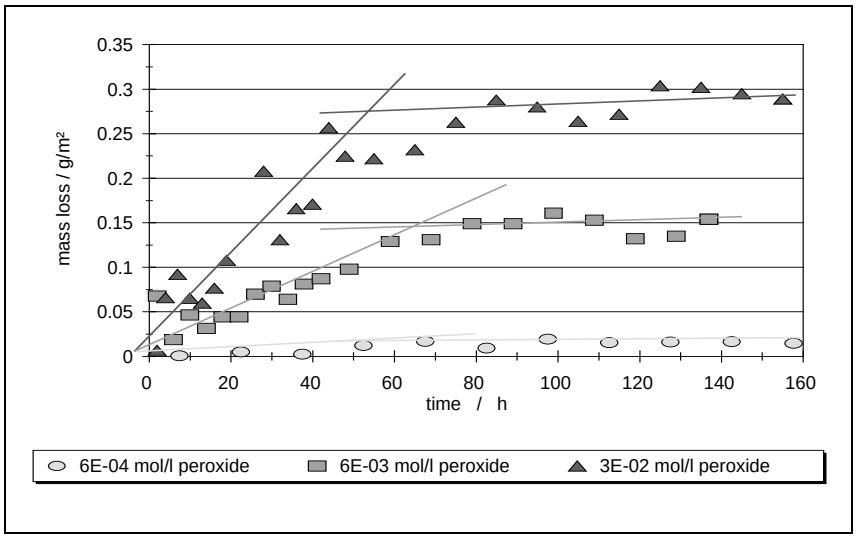

FIGURE 4.3 Time dependence of the mass loss of Ti99.8-Pd at rest potential in saturated NaCl brine containing H_2O_2 (25°C)

This behaviour can be explained as follows:

In the first range the titanium dissolves in accordance with the following equations:

$$Ti + 2\,H_2O \longrightarrow TiO_2 + 4\,H^+ + 4\,e^- \quad (1)$$

$$TiO_2 + H_2O_2 + 2\,H^+ \longrightarrow TiO_2^{2+} + 2\,H_2O \quad (2)$$

The corrosion depends on the peroxide concentration, but H_2O_2 decays into water and oxygen corresponding to the equation:

$$2\,H_2O_2 \longrightarrow 2\,H_2O + O_2 \quad (3)$$

Because of equations (2) and (3), the peroxide concentration of the brine decreases with time. After 60 - 65 hours there is not any H_2O_2 in the brine any more and the corrosion is definitely lower. By means of UV-Vis-spectroscopy, H_2O_2 was not detected in these brines, only TiO_2^{2+} was present.

In the second range, the corrosion of Ti99.8-Pd corresponds to the corrosion in saturated NaCl brine, which is free from peroxide.

Measured corrosion rates of Ti99.8-Pd

The corrosion rates are listed up in Table 4.3. The corrosion rates of Ti99.8-Pd measured in saturated NaCl brine, brine 3 and Q-brine at 25°C do not show any significant differences within the error limit. In all three systems a linear relationship exists between the corrosion rates and the H_2O_2 concentration. In brines with an average H_2O_2 concentration of $2.9 \cdot 10^{-2}$ mol/l, the corrosion rates are in the range from 12 to 22 µm/a. This specific H_2O_2 concentration is definitely higher than that one expected under practical conditions, and therefore it is only relevant with respect to basic research. At a more realistic H_2O_2 concentration of $2.9 \cdot 10^{-5}$ mol/l, the corrosion rates are only 0.6 ± 0.3 µm/a. These specific corrosion rates are only by a factor of 1.5 - 2.0 higher than those obtained in H_2O_2 free brines. At even smaller H_2O_2 concentrations ($\leq 10^{-5}$ mol/l), no influence of peroxide on Ti99.8-Pd corrosion can be detected at all.

From earlier investigations[8] in brines without H_2O_2, it can be concluded that, the corrosion is not influenced by higher temperatures up to 80°C. The corrosion rates are 0.4 ± 0.2 µm/a. Also in brines containing peroxide any increase of the corrosion was obtained at 55°C and 80°C. However, the rapid decay of H_2O_2 at 80°C increases the statistical error significantly.

TABLE 4.3 Corrosion rates of Ti99.8-Pd at rest potentials in brines containing H_2O_2

Brine	Initial H_2O_2 concentration mol/l	Average H_2O_2 concentration mol/l	Corrosion rates (25°C) µm/a	Corrosion rates (55°C) µm/a	Corrosion rates (80°C) µm/a
sat. NaCl	0	0	0.3 ± 0.2	0.3 ± 0.2	
	$7.0 \cdot 10^{-5}$	$2.9 \cdot 10^{-5}$	0.6 ± 0.3	0.6 ± 0.2	0.7 ± 0.3
	$7.0 \cdot 10^{-4}$	$2.9 \cdot 10^{-4}$	0.5 ± 0.3	0.7 ± 0.3	0.9 ± 0.2
	$3.5 \cdot 10^{-3}$	$1.5 \cdot 10^{-3}$	0.8 ± 0.3	0.9 ± 0.7	0.2 ± 0.2
	$7.0 \cdot 10^{-3}$	$2.9 \cdot 10^{-3}$	2.1 ± 0.5	3.9 ± 0.7	1.7 ± 1.7
	$3.5 \cdot 10^{-2}$	$1.5 \cdot 10^{-2}$	9 ± 2	5 ± 1	3.7 ± 0.3
	$7.0 \cdot 10^{-2}$	$2.9 \cdot 10^{-2}$	18 ± 2	21 ± 2	20 ± 3
Brine 3	0	0	0.4 ± 0.2	0.3 ± 0.2	
	$7.0 \cdot 10^{-5}$	$2.9 \cdot 10^{-5}$	0.9 ± 0.2	0.2 ± 0.2	0.2 ± 0.2
	$7.0 \cdot 10^{-4}$	$2.9 \cdot 10^{-4}$	0.5 ± 0.1	0.5 ± 0.1	0.2 ± 0.2
	$3.5 \cdot 10^{-3}$	$1.5 \cdot 10^{-3}$	0.9 ± 0.1	0.5 ± 0.2	0.6 ± 0.3
	$7.0 \cdot 10^{-3}$	$2.9 \cdot 10^{-3}$	4 ± 2	0.4 ± 0.1	0.7 ± 0.1
	$3.5 \cdot 10^{-2}$	$1.5 \cdot 10^{-2}$	4.0 ± 0.5	2.6 ± 0.8	5 ± 1
	$7.0 \cdot 10^{-2}$	$2.9 \cdot 10^{-2}$	17 ± 4	14 ± 3	12 ± 2
Q-brine	0	0	0.4 ± 0.2	0.4 ± 0.3	
	$7.0 \cdot 10^{-5}$	$2.9 \cdot 10^{-5}$	0.6 ± 0.2	0.1 ± 0.1	0.5 ± 0.3
	$7.0 \cdot 10^{-4}$	$2.9 \cdot 10^{-4}$	0.3 ± 0.1	0.3 ± 0.1	0.9 ± 0.8
	$3.5 \cdot 10^{-3}$	$1.5 \cdot 10^{-3}$	0.6 ± 0.1	0.3 ± 0.1	1.9 ± 1.5
	$7.0 \cdot 10^{-3}$	$2.9 \cdot 10^{-3}$	0.7 ± 0.1	1.1 ± 1.0	2.6 ± 2.0
	$3.5 \cdot 10^{-2}$	$1.5 \cdot 10^{-2}$	3.7 ± 0.8	3.1 ± 1.2	9.7 ± 2.2
	$7.0 \cdot 10^{-2}$	$2.9 \cdot 10^{-2}$	21 ± 4	22 ± 5	14 ± 4

4.1.3 Kinetics of Titanium corrosion under the influence of H_2O_2

General remarks

The corrosion of Titanium can be described with the following three reactions:

1. Reaction of Ti with H_2O:

$$Ti + H_2O \xrightarrow{k_1} TiO^{2+} + 2H^+ + 4e^- \qquad (4)$$

2. Reaction of Ti with H_2O_2:

$$Ti + H_2O_2 \xrightarrow{k_2} TiO_2^{2+} + 2H^+ + 4e^- \qquad (5)$$

3. Decay of H_2O_2:

$$H_2O_2 \xrightarrow{k_3} H_2O + \tfrac{1}{2}O_2 \qquad (6)$$

k_1, k_2 and k_3 are the velocity constants.

Decay of H_2O_2

The decay of H_2O_2 was determined by use of jodometric titration. Figure 4.4 shows the dependence of H_2O_2 concentration on time.

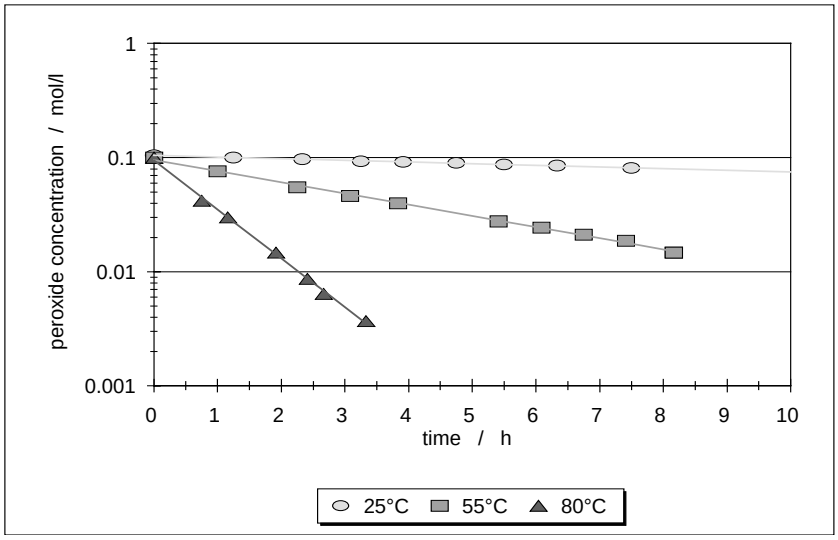

FIGURE 4.4 Decay of H_2O_2 at various temperatures

The following logarithmic relationship was found between peroxide concentration c_{H2O2} and time t:

$$c_{H_2O_2} = c^{o}_{H_2O_2} \cdot e^{-k_3 \cdot t} \qquad (7)$$

Here c^{o}_{H2o2} is the initial concentration and k_3 is the velocity constant of the H_2O_2 decay. Table 4.4 contains the calculated values of k_3 in the various salt brines at 25°C, 55°C and 80°C.

TABLE 4.4 Velocity constants of H_2O_2 decay in salt brines

	k_3 (25°C) h^{-1}	k_3 (55°C) h^{-1}	k_3 (80°C) h^{-1}
sat. NaCl brine	0.032 ± 0.007	0.19 ± 0.03	1.06 ± 0.09
Brine 3	0.032 ± 0.001	0.19 ± 0.01	0.98 ± 0.09
Q-brine	0.035 ± 0.004	0.22 ± 0.02	1.08 ± 0.09

There are no differences of the H_2O_2 decay in the investigated brines. k_3 increases with increasing temperature. By use of the Arrhenius equation

$$k_3 = k_3^0 \cdot e^{-E_A/RT} \qquad (8)$$

the activation energy E_A of this decay can be determined (Figure 4.5). It is k^0_3 = (1.4 ± 0.3)·10^8/h and E_A = (799 ± 34) J/mol.

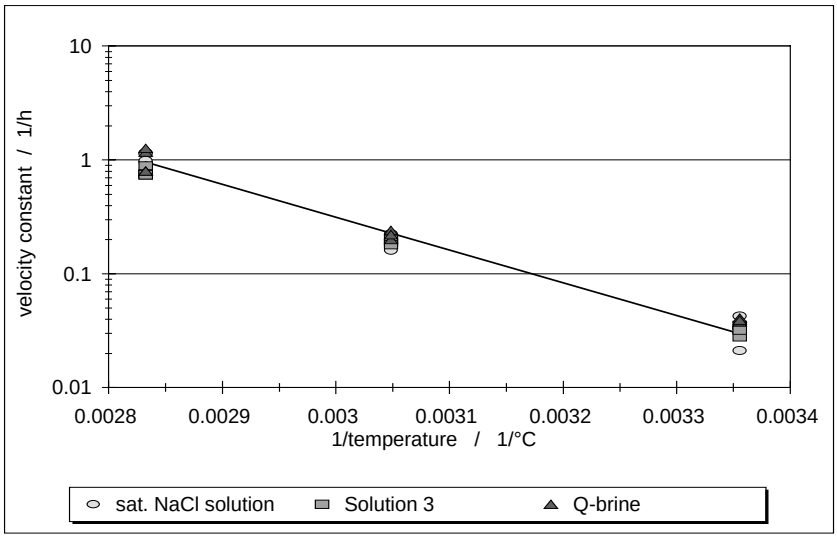

FIGURE 4.5 Determination of activation energy of the H_2O_2 decay in salt brines

Theoretical considerations for the corrosion rate of titanium

The evaluation of the time dependence of the mass loss determined γ-spectroscopically, makes the titanium corrosion under the influence of H_2O_2 be described kinetically.

The change of titanium concentration vs. time is given by equation (9):

$$\left(\frac{dc_{Ti;Sol}}{dt}\right) = k_1' + k_2' \cdot c_{H_2O_2} \qquad (9)$$

Here k_1 is the velocity constant of corrosion in a brine being free of H_2O_2, and k_2' is the velocity constant of corrosion under the influence of H_2O_2.

Under experimental conditions the peroxide concentration c_{H2O2} is not constant and equation (7) must be taken into consideration. In this case, the amount of the dissolved titanium $c_{Ti;sol.}$ can be calculated from equation (10) for each time:

$$c_{Ti;Sol} = k_1' \cdot t + \frac{k_2' \cdot c^o_{H_2O_2}}{k_3} \cdot \left(1 - e^{-k_3 \cdot t}\right) \qquad (10)$$

Figure 4.6 shows the measured and calculated concentrations of Ti99.8-Pd at rest potential in saturated NaCl brine containing H_2O_2.

For a known constant H_2O_2 concentration, the corrosion rate w is given by equation (11):

$$w = \left(\frac{dc_{Ti;Sol}}{dt}\right) \cdot \frac{V_{Sol} \cdot M_{Ti}}{A_{El} \cdot \rho_{Ti}} = \left(k_1' + k_2' \cdot c_{H_2O_2}\right) \cdot \frac{V_{Sol} \cdot M_{Ti}}{A_{El} \cdot \rho_{Ti}} \qquad (11)$$

Here V_{Sol} is the volume of the brine, M_{Ti} the molar mass of titanium, A_{El} the area of the electrode and ρ_{Ti} the density of titanium.

In saturated NaCl brine at 25°C, the velocity constants are: $k_1' = (9 \pm 8) \cdot 10^{-10}$ mol/l·h and $k_2' = (16 \pm 5) \cdot 10^{-7}$/h.

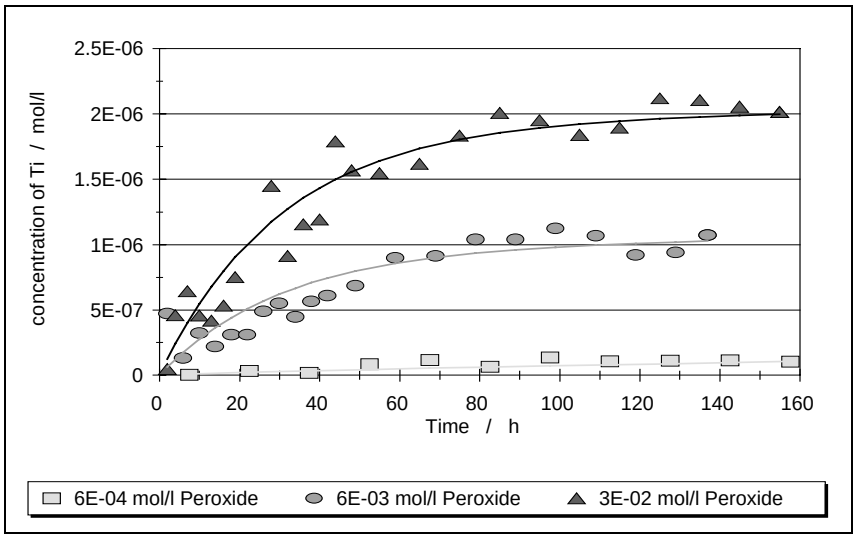

FIGURE 4.6 Measured and calculated concentrations of Ti99.8-Pd at rest potential in saturated NaCl brine containing H_2O_2 (25°C)

Kinetical calculations for practical conditions

Under practical conditions in a waste repository, the H_2O_2 concentration is in equilibrium, that means the rate of radiolytical H_2O_2 production equals the rate of H_2O_2 decay:

$$\left(+\frac{dc_{H_2O_2}}{dt}\right)_{prod.} = \left(-\frac{dc_{H_2O_2}}{dt}\right)_{desint.} = k_3 \cdot c_{H_2O_2;eq} \qquad (12)$$

Taking equation (13) into account[9]

$$G = \frac{c_{H_2O_2} \cdot N_A}{D_a \cdot \rho_{Sol}} \qquad (13)$$

the H_2O_2 concentration can be calculated with the following equation:

$$c_{H_2O_2} = \frac{G \cdot \dot{D}_a^{max} \cdot \rho_{Sol}}{k_3 \cdot N_A} \qquad (14)$$

Here G is 0.70 per 100 eV and the permitted dose rate $\dot{D}_a^{max}$ is 0.2 mGy/h. The density of the relevant salt brine ρ_{Sol} is 1.2 g/cm^3, the velocity constant of peroxide decay is $(3 \pm 1)\cdot 10^{-2}$/h and the Avogadro constant N_A is $6.02\cdot 10^{23}$/mol.
For 1 MeV radiation energy, the relevant H_2O_2 concentration is approximately only 10^{-6} mol/l under given conditions in a waste repository.

4.1.4 Results in F^- containing brines

For a better interpretation of the results in brines containing H_2O_2, the corrosion of Ti99.8-Pd was measured under the influence of F^- at rest potential and 25°C.

If the corrosion of Ti99.8-Pd were increased by a non decomposing reagent like NaF, forming TiF_6^{2-}-ions, the relevant corrosion rates should be increased and the rest potential would be decreased. In this case, F^- should have no influence on the cathodic current density at all.

$$TiO_2 + 6\,F^- + 4\,H^+ \rightarrow TiF_6^{2-} + 2\,H_2O \qquad (15)$$

The corrosion rates listed up in Table 4.5 indicate that the values increase with increasing F^- concentration, being in accordance with the behaviour of H_2O_2 containing brines. But in contrast to H_2O_2 the rest potentials decrease with increasing F^--content of the brine. This behaviour is in accordance with the model aforementioned. A minimum of the rest potential curve was not obtained.

TABLE 4.5 Rest potentials and corrosion rates of Ti99.8-Pd in presence of F^- in saturated NaCl brine at 25°C

Concentration of F^- mol/l	Rest potential mV	Corrosion rates µm/a
0.003	300	0.1 ± 0.1
0.006	453	0.9 ± 0.3
0.03	423	5.3 ± 0.5
0.06	180	11.5 ± 0.5

4.1.5 Results in ClO^- containing brines

Another product of radiolysis in salt brine is hypochlorite ClO^-, which may influence the corrosion behaviour of the Ti99.8-Pd. In order to examine whether there is a difference in the corrosion behaviour of Ti99.8-Pd in brines with and without ClO^-, a very high ClO^- concentration of 0.08 mol/l was used. This value is significantly higher than that expected under relevant disposal conditions.

The results obtained are shown in Table 4.6. At rest potentials, the presence of hypochlorite does not influence the corrosion behaviour of Ti99.8-Pd. For example, at 80°C in saturated NaCl brine being free of ClO^-, the corrosion rate is 0.3 ± 0.2 µm/a and in a brine containing ClO^- the rate is 0.4 ± 0.2 µm/a. Under practical conditions, therefore, hypochlorite can be neglected with respect to its influence on corrosion.

TABLE 4.6 Rest potentials and corrosion rates of Ti99.8-Pd in presence of 0.08 mol/l ClO^- in saturated NaCl brine

Temperature °C	Rest potential mV	Corrosion rates µm/a
25	453	0.3 ± 0.2
55	436	0.2 ± 0.2
80	167	0.4 ± 0.2

4.2 Corrosion studies at applied potentials

4.2.1 Experimental

The Radioisotope Method was applied to determine the corrosion rates of Ti99.8-Pd. The concentration of titanium in the brine was continuously measured for 21 hours in saturated NaCl brine, brine 3 and Q-brine at 25°C, 55°C and 80°C. The effect of H_2O_2 on the corrosion of Ti99.8-Pd was studied between $7 \cdot 10^{-5}$ mol/l and $7 \cdot 10^{-2}$ mol/l in the passive range at 500 mV and in the active range at –250 mV. Furthermore, investigations into corrosion were carried out at various potentials between -1000 mV and +1000 mV. In the same potential range the corrosion of Ti99.8-Pd was investigated in presence of the radiolytic product ClO^- in saturated NaCl brine at 25°C, 55°C and 80°C.

Before starting the experiments the oxide layers on the electrodes were removed with the relevant etching solutions (see 4.1.1). Then, the electrode was polarized at 2000 mV to realize a reproducible surface. The thickness of this oxide layer is 2 - 3 nm and corresponds to the thickness built up in air. After the corrosion experiments, cyclovoltammogrammes between -500 mV and +2000 mV were carried out.

4.2.2 Results in H_2O_2 containing brines

Corrosion in saturated NaCl brine

Investigations into corrosion were performed in saturated NaCl brine at various applied potentials from -1000 mV to +1000 mV. In earlier measurements in saturated NaCl brine at 25°C and an average H_2O_2 concentration at $5 \cdot 10^{-2}$ mol/l, an active range was obtained between -400 mV and -1000 mV with maximum corrosion rates of about 1500 µm/a. The same experiments were carried out at 55°C and 80°C. The results are listed up in Table 4.7. In the active range, the corrosion increases and the maximum corrosion rate at 80°C is 4150 µm/a. However, this value is not relevant for disposal conditions, as the H_2O_2 concentrations used in this experiments are much higher than that expected in the practice ($\leq 10^{-5}$). In the NaCl brine at 25°C containing only an average H_2O_2 content of $5 \cdot 10^{-3}$ mol/l, the relevant corrosion rates are definitely smaller (30 - 40 µm/a). Table 4.8 shows the results obtained at –250 mV (active range) and +500 mV (passive range) in the NaCl brine at various H_2O_2 concentrations. In the passive range, the corrosion rates in NaCl brine (0.1-8 µm/a) are comparable with those obtained in the other test brines. But in the active range, the corrosion rate depends on the brine used.

TABLE 4.7 Corrosion rates of Ti99.8-Pd at applied potentials in saturated NaCl brine containing H_2O_2

Average H_2O_2 conc. mol/l	$5 \cdot 10^{-3}$	$5 \cdot 10^{-2}$	$5 \cdot 10^{-2}$	$5 \cdot 10^{-2}$
Potential mV	Corrosion rates (25°C) µm/a	Corrosion rates (25°C) µm/a	Corrosion rates (55°C) µm/a	Corrosion rates (80°C) µm/a
-1000	2 ± 1	1 ± 1	1 ± 2	1 ± 2
-500	1 ± 1	104 ± 9	331 ± 103	143 ± 50
-400	4 ± 2	513 ± 87	539 ± 81	2159 ± 150
-350	32 ± 13	611 ± 59	2482 ± 344	4151 ± 232
-300	10 ± 6	1441 ± 15	2824 ± 311	2243 ± 167
-250	10 ± 5	792 ± 34	1979 ± 177	1323 ± 145
-200	2 ± 1	450 ± 9	1270 ± 170	1282 ± 150
-150	1 ± 1	384 ± 21	995 ± 14	948 ± 124
-100	2 ± 1	38 ± 16	271 ± 7	372 ± 99
0	1 ± 1	10 ± 8	3 ± 2	6 ± 5
500	1 ± 1	4 ± 2	8 ± 2	29 ± 10
1000	1 ± 1	1 ± 1	1 ± 1	2 ± 2

TABLE 4.8 Corrosion rates of Ti99.8-Pd at -250 mV and +500mV in saturated NaCl brine containing various H_2O_2 concentrations

Potential mV	Average H_2O_2 concentration mol/l	Corrosion rates (25°C) µm/a	Corrosion rates (55°C) µm/a	Corrosion rates (80°C) µm/a
-250	$5 \cdot 10^{-5}$	0.4 ± 0.3	0.1 ± 0.3	1.3 ± 1.3
	$5 \cdot 10^{-4}$	0.3 ± 0.3	0.7 ± 0.3	3.3 ± 1.5
	$2.5 \cdot 10^{-3}$	1 ± 1	0.4 ± 0.4	4.9 ± 2.2
	$5 \cdot 10^{-3}$	10 ± 5	0.9 ± 0.3	5.7 ± 4.4
	$2.5 \cdot 10^{-2}$	146 ± 50	19 ± 10	13.2 ± 1.5
	$5 \cdot 10^{-2}$	791 ± 50	1979 ± 150	1323 ± 147
+500	$5 \cdot 10^{-5}$	0.3 ± 0.3	0.1 ± 0.1	5.6 ± 1.8
	$5 \cdot 10^{-4}$	0.3 ± 0.3	1.8 ± 0.5	3.5 ± 1.5
	$5 \cdot 10^{-3}$	1 ± 1	0.5 ± 0.4	1.9 ± 1.9
	$5 \cdot 10^{-2}$	6 ± 2	8 ± 3	1 ± 1

At 80°C and -250 mV a corrosion rate of approximately 1400 µm/a was determined in saturated NaCl brine with an average H_2O_2 content of $5 \cdot 10^{-2}$ mol/l. At a concentration $\leq 10^{-5}$ mol/l no influence of H_2O_2 on the corrosion of Ti99.8-Pd was detected, neither in the passive range nor in the active range.

In addition to the corrosion rates, the current density j was also measured. From the corrosion rates the partial anodic current density j_+ can be calculated (Figure 4.7):

$$j_+ = \frac{w \cdot z \cdot F \cdot \rho}{M} \qquad (16)$$

The partial cathodic current density j_- is given by:

$$j_- = j - j_+ \qquad (17)$$

with

$$j = \frac{I}{A}, \qquad (18)$$

obtained from experiments.

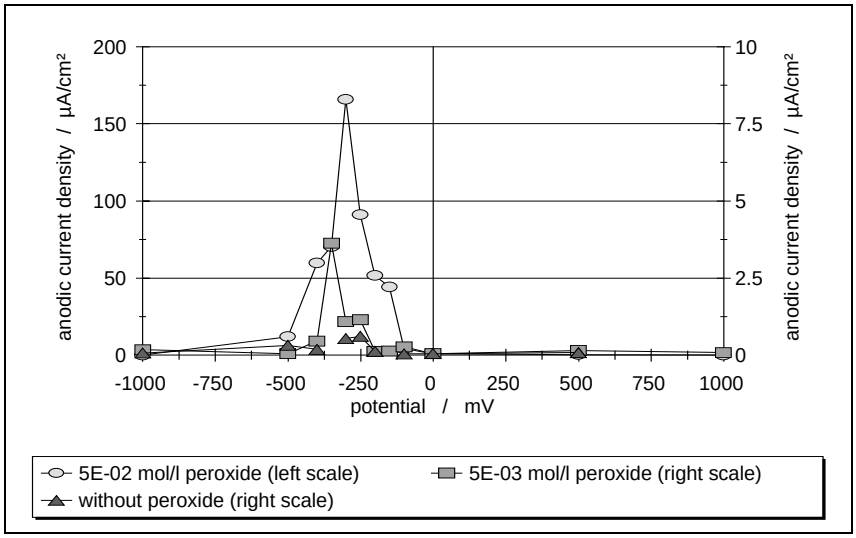

FIGURE 4.7 Dependence of the partial anodic current density on the potential at various H_2O_2 contents in saturated NaCl brine at 25°C

Figure 4.8 shows the dependence of the partial cathodic current density on the potential at various H_2O_2 contents in saturated NaCl brine at 25°C. The partial cathodic current density is more negative with increasing H_2O_2 content. This is in accordance with the model mentioned above. The typical cyclovoltammogram of a Ti99.8-Pd-electrode before starting corrosion measurements (Figure 4.9) shows the development of H_2 in the cathodic range and the formation of an oxide layer in the anodic range. In the anodic range (passive range), the corrosion rates are very low. At these potentials, the cyclovoltammogrammes obtained after performing the corrosion experiments demonstrate that the protecting oxide layer was not destroyed (see Figure 4.10). Another behaviour was obtained at -250mV (active range). In this case, very high corrosion rates were measured and the cyclovoltammograms (Figure 4.11) demonstrate that the protecting oxide layers were complete dissolved. At positive potentials, the current density increases because the oxide layer was built up again.

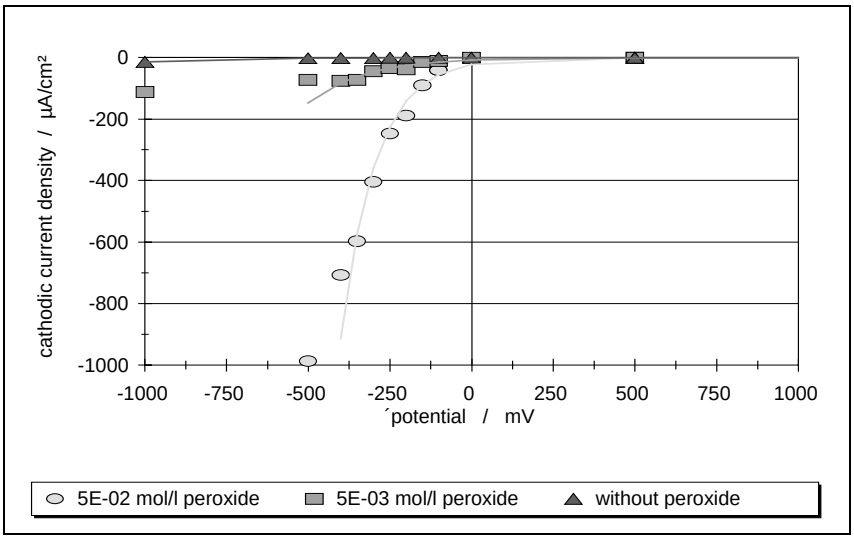

FIGURE 4.8 Dependence of the partial cathodic current density on the potential at various H_2O_2 contents in saturated NaCl brine at 25°C

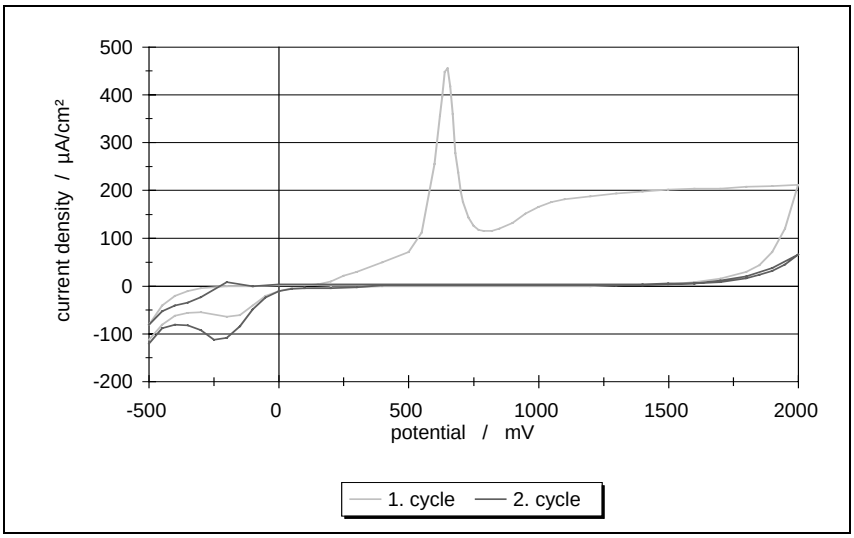

FIGURE 4.9 Cyclovoltammogram of Ti99.8-Pd at 25°C in saturated NaCl brine containing $5 \cdot 10^{-2}$ mol/l H_2O_2

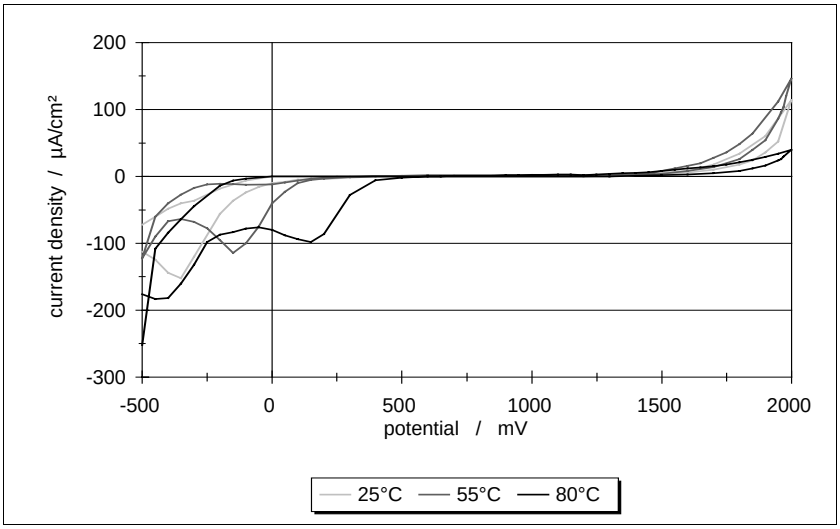

FIGURE 4.10 Cyclovoltammograms of Ti99.8-Pd at 500mV in saturated NaCl brine having a H_2O_2 concentration of $5 \cdot 10^{-2}$ mol/l

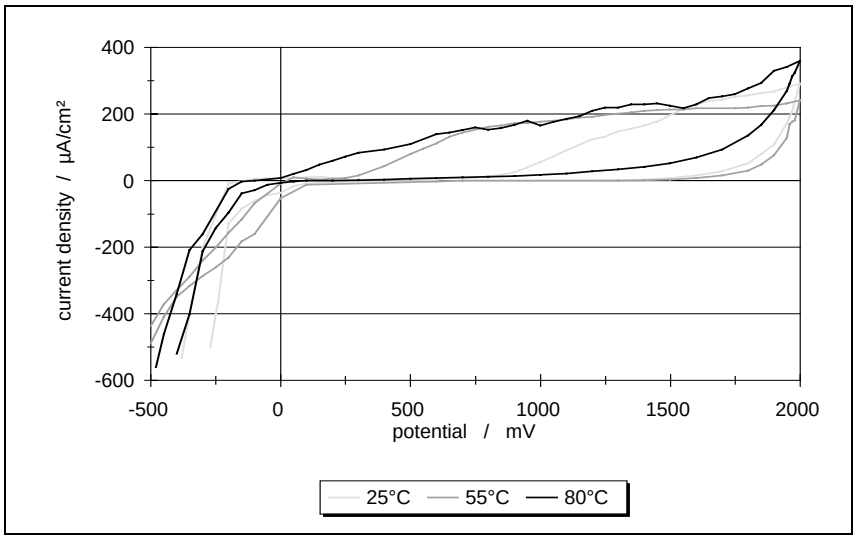

FIGURE 4.11 Cyclovoltammograms of Ti99.8-Pd at -250mV in saturated NaCl brine having a H_2O_2 concentration of $5 \cdot 10^{-2}$ mol/l

Corrosion in brine 3 and Q-brine

Referring to the results in saturated NaCl brine (model system), the questions must be answered, whether the Ti99.8-Pd has the same behaviour in disposal relevant salt brines such as brine 3 and Q-brine, and which influences are due to the brine components Mg^{2+} or SO_4^{2-}.

Potentiostatic measurements in the range from -1000 mV to +1000 mV were carried out in brine 3 and Q-brine at 25°C, 55°C and 80°C. A high average H_2O_2

concentration of $5 \cdot 10^{-2}$ mol/l was chosen in order to see differences between brine with and without H_2O_2 . The results are listed up in Tables 4.9 and 4.10.

TABLE 4.9 Corrosion rates of Ti99.8-Pd at applied potentials in brine 3 having an average H_2O_2 concentration of $5 \cdot 10^{-2}$ mol/l

Potential mV	Corrosion rates (25°C) µm/a
-1000	2 ± 1
-500	1 ± 1
-400	2 ± 1
-350	2 ± 1
-300	1 ± 1
-250	1 ± 1
-200	1 ± 2
-150	6 ± 2
-100	2 ± 1
0	6 ± 3
+500	2 ± 2
+1000	2 ± 2

TABLE 4.10 Corrosion rates of Ti99.8-Pd at applied potentials in Q-brine having an average H_2O_2 concentration of $5 \cdot 10^{-2}$ mol/l

Potential mV	Corrosion rates (25°C) µm/a
-1000	2 ± 1
-500	1 ± 1
-400	2 ± 2
-350	1 ± 1
-300	2 ± 1
-250	2 ± 1
-200	2 ± 2
-150	2 ± 1
-100	1 ± 1
0	2 ± 1
+500	2 ± 1
+1000	1 ± 1

Neither in brine 3 (Table 4.9) nor in Q-brine (Table 4.10), a marked active range was obtained. In brine 3 ($5 \cdot 10^{-2}$ mol/l H_2O_2), the maximum corrosion rate is 6 ± 3 µm/a, which is only a factor 2-3 higher than in the peroxide free brine. In Q-brine containing H_2O_2 ($5 \cdot 10^{-2}$ mol/l), the corrosion rates are very close to those without any H_2O_2 (2 ± 1 µm/a). A significant dependence of the corrosion rate on the temperature was not observed (see Tables 4.11 and 4.12).

TABLE 4.11 Corrosion rates of Ti99.8-Pd at –250 mV and +500 mV in brine 3 having various H_2O_2 concentrations

Potential mV	Average H_2O_2 concentration mol/l	Corrosion rates (25°C) µm/a	Corrosion rates (55°C) µm/a	Corrosion rates (80°C) µm/a
-250	$5 \cdot 10^{-5}$	0.4 ± 0.3	1.1 ± 1	1 ± 1
	$5 \cdot 10^{-4}$	0.3 ± 0.3	0.1 ± 0.2	0.4 ± 0.4
	$2.5 \cdot 10^{-3}$	1 ± 1		
	$5 \cdot 10^{-3}$	10 ± 5	0.2 ± 0.2	0.5 ± 0.5
	$2.5 \cdot 10^{-2}$	146 ± 50		1.5 ± 1.5
	$5 \cdot 10^{-2}$	791 ± 50	0.3 ± 0.2	2.5 ± 2
+500	$5 \cdot 10^{-5}$	2.3 ± 2	0.1 ± 0.2	1 ± 1
	$5 \cdot 10^{-4}$	1.6 ± 1.5	1.3 ± 1	0.5 ± 0.5
	$5 \cdot 10^{-3}$	1 ± 1		
	$5 \cdot 10^{-3}$	1.2 ± 1	0.7 ± 0.6	1 ± 2
	$5 \cdot 10^{-2}$	0.1 ± 0.1		
	$5 \cdot 10^{-2}$	3 ± 3	0.5 ± 0.5	0.5 ± 1

TABLE 4.12 Corrosion rates of Ti99.8-Pd at –250 mV and +500 mV in Q-brine having various H_2O_2 concentrations

Potential mV	Average H_2O_2 concentration mol/l	Corrosion rates (25°C) µm/a	Corrosion rates (55°C) µm/a	Corrosion rates (80°C) µm/a
-250	$5 \cdot 10^{-5}$	1.7 ± 1.5	1 ± 1	1 ± 1
	$5 \cdot 10^{-4}$	2.5 ± 2.5	1 ± 1	1.5 ± 2
	$2.5 \cdot 10^{-3}$	1.5 ± 2		
	$5 \cdot 10^{-3}$	0.1 ± 1	0.5 ± 1	2 ± 2
	$2.5 \cdot 10^{-2}$	0.6 ± 1		
	$5 \cdot 10^{-2}$	2.5 ± 2	0.2 ± 1	0.1 ± 1
+500	$5 \cdot 10^{-5}$	1 ± 1	0.3 ± 1	1 ± 2
	$5 \cdot 10^{-4}$	1.3 ± 1.3	2 ± 2	1 ± 1
	$5 \cdot 10^{-3}$	8.4 ± 8		
	$5 \cdot 10^{-3}$	2 ± 2	1.2 ± 2	1.5 ± 2
	$5 \cdot 10^{-2}$	10 ± 2		
	$5 \cdot 10^{-2}$	14 ± 2	1.2 ± 2	3.3 ± 3

In order to find out the reason for the high corrosion resistance of Ti99.8-Pd to corrosion, the specific conductivity of the relevant oxide layers was determined. The cyclovoltammograms recorded after performing the experiments show that in all cases the protecting oxide layers were not attacked. The course of the cyclovoltammogrammes corresponds to those represented in Figure 4.10.

4.2.3 Results in ClO^- containing brines

In order to evaluate, whether ClO^- has an influence on the corrosion behaviour of Ti99.8-Pd, potentiostatic measurements were carried out in saturated NaCl brine with a ClO^- content of $8 \cdot 10^{-2}$ mol/l in the potential range from -1000 mV to +1000 mV at 25°C. The very high ClO^- concentration was used in order to have severe test conditions.

Neither at anodic polarization nor at cathodic polarization the corrosion rates were higher than in ClO^- free brines (see Table 4.13). In the whole potential range, maximal corrosion rates of only 3 ± 1 µm/a were measured. Furthermore, the corrosion behaviour of Ti99.8-Pd is independent from temperature within the whole potential range, since ClO^- does not attack the protecting oxide layer, as can be seen from the cyclovoltammogrammes (Figure 4.12).

TABLE 4.13 Corrosion rates of Ti99.8-Pd at various applied potentials in saturated NaCl brine with a ClO^- content of 0.08 mol/l

Potential mV	Corrosion rates (25°C) µm/a	Corrosion rates (55°C) µm/a	Corrosion rates (80°C) µm/a
-1000	2 ± 1	0.02 ± 0.02	0.4 ± 0.4
-500	1 ± 2	-	0.1 ± 0.1
-400	3 ± 1	0.01 ± 0.02	0.3 ± 0.3
-300	2 ± 1	-	0.6 ± 0.6
-200	1 ± 1	0.02 ± 0.01	0.5 ± 0.3
-100	1 ± 1	0.2 ± 0.2	0.2 ± 0.2
0	1 ± 2	0.1 ± 0.1	0.2 ± 0.2
+500	1 ± 1	0.05 ± 0.04	0.3 ± 0.3
+1000	-	0.04 ± 0.04	-

-= not measured

4.3 Corrosion of Ti99.8-Pd welds

Another main point of research was the investigation of Ti99.8-Pd-welds. In order to answer the question, whether the corrosion attack is higher on welds than in the unwelded metal, measurements were carried out at rest potential in NaCl brine, brine 3 and Q-brine at 25°C, 55°C and 80°C. The average H_2O_2 concentration of the brine was between 10^{-4} mol/l and 10^{-2} mol/l. The results obtained are summarized in the Tables 4.14-4.16. They demonstrate that there are not any differences between the metal and welds in the test brines.

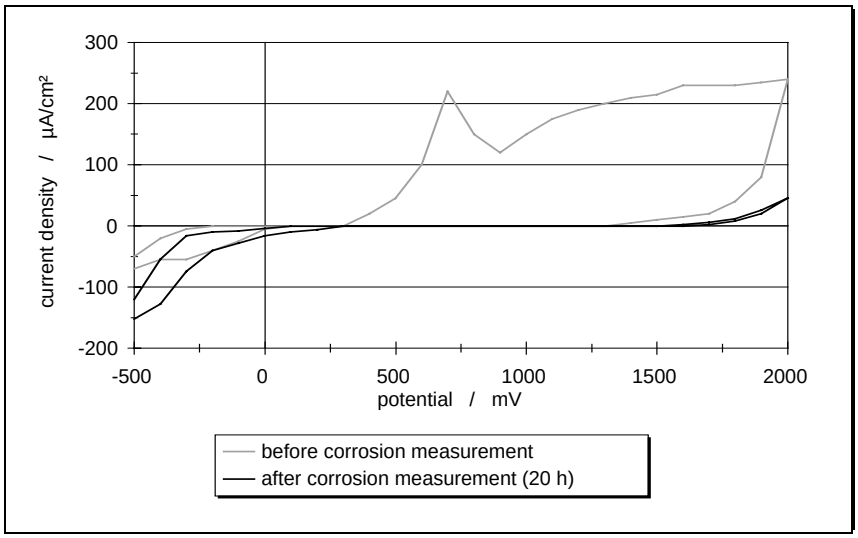

FIGURE 4.12 Cyclovoltammograms of Ti99.8-Pd at -250mV and +500 mV (25°C) in saturated NaCl brine containing 0.08 mol/l ClO^-

TABLE 4.14 Corrosion rates of Ti99.8-Pd welds in brines containing H_2O_2 at 25°C

Average H_2O_2 concentration mol/l	Corrosion rate µm/a		
	Sat. NaCl brine	*Brine 3*	*Q-brine*
0	0.6	0.5	0.3
0.0021	5.8	5.1	4.3
0.011	6.1	6.1	7
0.021	14	13	19
0.042	17	25	26

TABLE 4.15 Corrosion rates of Ti99.8-Pd welds in brines containing H_2O_2 at 55°C

Average H_2O_2 concentration mol/l	Corrosion rate µm/a		
	Sat. NaCl brine	*Brine 3*	*Q-brine*
0	1.6	0.8	1.8
0.0031	0.2	0.6	0.6
0.0061	2.0	3.9	2.1
0.0122	7.6	10	10

TABLE 4.16 Corrosion rates of Ti99.8-Pd welds in brines containing H_2O_2 at 80°C

Average H_2O_2 concentration mol/l	Corrosion rate µm/a		
	Sat. NaCl brine	*Brine 3*	*Q-brine*
0	5.4	3.9	5.3
0.003	1.0	0.7	0.9
0.0061	3.6	1.9	3.4
0.0121	8.0	4.6	6.9

4.4 Determination of the specific conductivity of the Ti99.8-Pd oxide layer

4.4.1 Theoretical background

The specific conductivity κ of the oxide layers was determined from current density-time-curves. Under potentiostatical conditions, the current density can be described by the following equation[10]:

$$j = a \cdot \frac{1}{\sqrt{t}} + \text{const.} \tag{19}$$

Under conditions, where the Ohms law is valid, the increase a is given by equation (20):

$$a = \sqrt{\frac{2 \cdot \kappa \cdot E}{\kappa_F}} \tag{20}$$

E is the potential drop in the pasive film and κ_F is a constant consisting of the molar mass of the oxide layer M, the density of the oxide layer ρ, the charge number z and the Faraday constant:

$$\kappa_F = \frac{M}{\rho \cdot z \cdot F} \tag{21}$$

Using (21) the specific conductiviy κ can be calculated from (20):

$$\kappa = \frac{a^2 \cdot \kappa_F}{2 \cdot E} = \frac{a^2 \cdot M}{2\rho \cdot z \cdot F \cdot E} \tag{22}$$

As was already explained, the corrosion corresponds to the specific conductivity of the protecting passive layers. Figure 4.13 shows the obtained specific conductivities of the Ti99.8-Pd passive layers at 25°C in saturated NaCl brine, brine 3, Q-brine and in addition in Na_2SO_4 brine, $MgCl_2$ brine and in NaCl brine containing Mg^{2+} or SO_4^{2-} ions. From Figure 4.13 it can be seen that in all brines containing Mg^{2+} ions, the specific conductivities of the protecting oxide layers are definitely lower than in saturated NaCl brine. The presence of SO_4^{2-} ions increases the specific conductivity. In brine 3 the conductivity of the passive layer is influenced by Mg^{2+} and SO_4^{2-}, but not in Q-brine. The conductivity corresponds to that one obtained in $MgCl_2$ brine. The

sulphate has not any influence at all. It can be supposed therefore that different oxide layers will be formed in the presence of Mg^{2+}. Ilmenite or spinell structures can be assumed, which might hinder the corrosive attack. Detailed investigations should be performed in this respect.

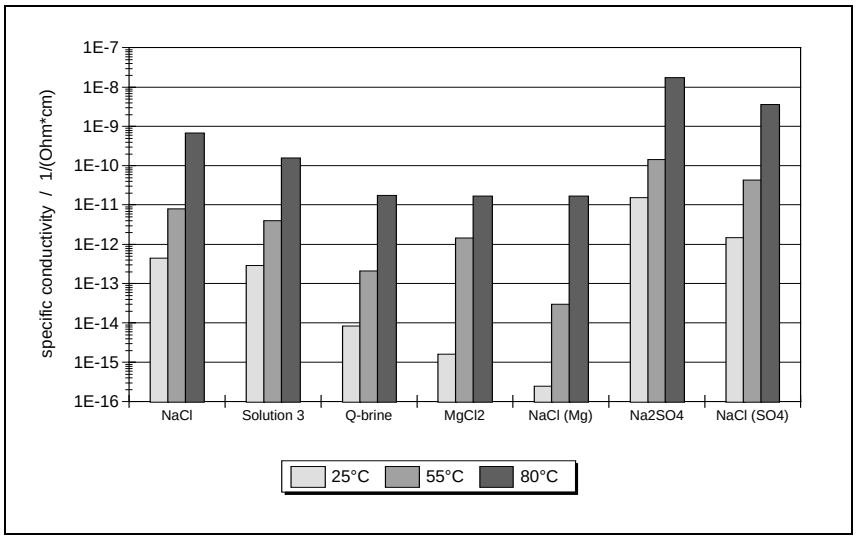

FIGURE 4.13 Specific conductivities of the Ti99.8-Pd passive layers in salt brines

5. STRESS CORROSION CRACKING STUDIES IN SALT AND GRANITIC ENVIRONMENTS

In previous Stress Corrosion Cracking (SCC) studies in $MgCl_2$-rich brine, the steels and the alloy Ti99.8-Pd were identified as promising container materials[11,12]. In the present work, the resistance of TStE355 carbon steel, AISI 316L stainless steel and Ti99.8-Pd (Grade 7 titanium alloy) to SCC was investigated in NaCl-rich brine and in bentonite buffered granitic water at different temperatures and strain rates by means of the Slow Strain Rate Technique (SSRT).

In order to be able to interpret the results obtained in the brines, additional comparative investigations were performed in argon as an inert medium. Besides specimens of the parent materials (base materials), welded specimens simulating possible container closure techniques were tested. To evaluate the resistance of the materials to SCC, metallographic and Scanning Electron Microscopic (SEM) examinations of specimens were performed in addition to the tensile experiments.

5.1 Experimental

5.1.1 Materials

The materials studied are the unalloyed fine grained carbon steel TStE355, the alpha titanium alloy Ti Gr-7 (Ti99.8-Pd, ASTM B-265) and the austenitic AISI 316L stainless steel. The chemical composition of these materials is given in Table 5.1.

Table 5.1 Chemical composition of studied materials (weight %)

Material	Composition
TStE355	0.16 C; 0.41 Si; 1.5 Mn; 0.017 P; 0.002 S; 0.036 Al; 0.006 Ni; bal. Fe
AISI 316L	0.021C; 0.31 Si; 1.3 Mn; 0.029 P; 0.002 S; 17.4 Cr; 11.5 Ni; 2.2.Mo; bal. Fe
TiGr-7	0.008 N; 0.040 C; 0.003 H; 0.04 Fe, 0.12 O; 0.15 Pd; bal. Ti

Metalographic studies carried out on the materials show a ferritic microstructure with perlite bands for the hot-rolled and annealed TStE355 carbon steel. A grain size value of 10 according to ASTM E-112 was measured. The AISI 316L stainless steel shows an austenitic structure with numerous maclas, due to the annealing process, and long ferrite bands. The TiGr-7 alloy presents an equiaxic alfa structure with a grain size of 5. Optical micrographs showing longitudinal sections of TStE355, AISI 316L and TiGr-7 microstructures are shown in Figures 5.1-5.3.

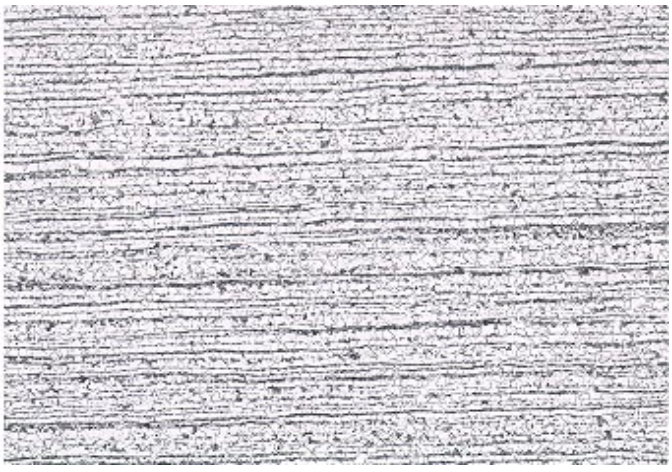

Figure 5.1 Optical micrograph showing TStE355 carbon steel microstructure (x80)

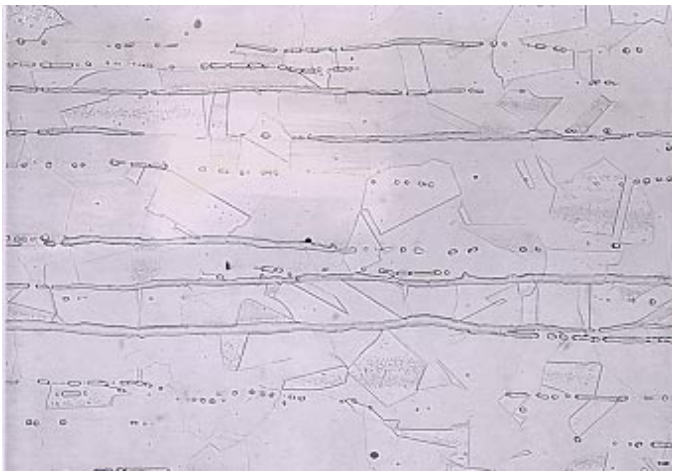

Figure 5.2 Optical micrograph showing AISI 316L stainless steel microstructure (x300)

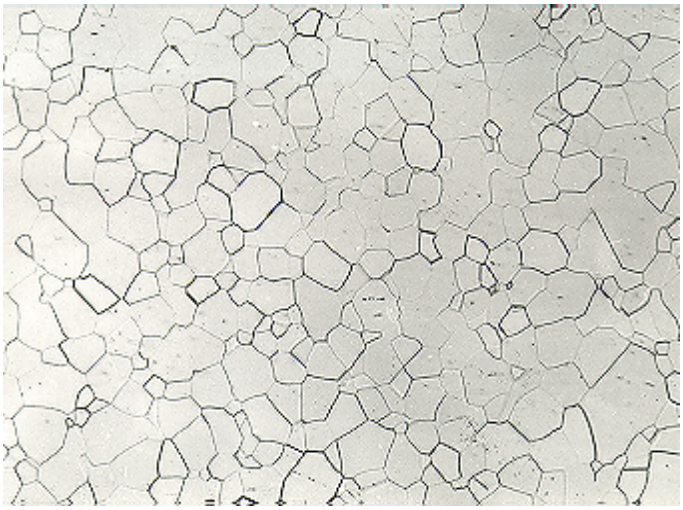

Figure 5.3 Optical micrograph showing TiGr-7 alloy microstructure (x80)

For the qualification of a suitable container closure technique, following welding procedures were examined:

-EBW (Electron Beam Welding) for the three candidate materials.
-FCAW (Flux Cored Arc Welding) for the carbon steel.
-PAW (Plasma Arc Welding) for the titanium alloy.
-GTAW (Gas Tungsten Arc Welding) for the stainless steel.

In order to characterize the weldments, metallographic specimens transversal to the welded joint have been prepared. Optical micrographs are shown in Figures 5.4-5.5. Vickers microhardnesses were measured along the welded joints. In general, it was observed a slight increase of the hardness value in the welded joint compared to that obtained for the base material.

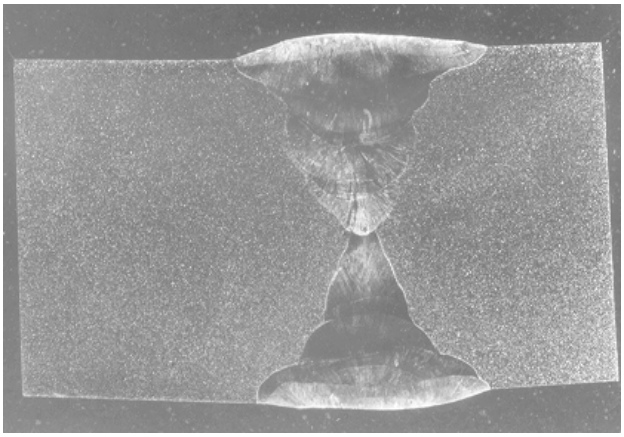

Figure 5.4 GTA welded joint of AISI 316 stainless steel (x3.3)

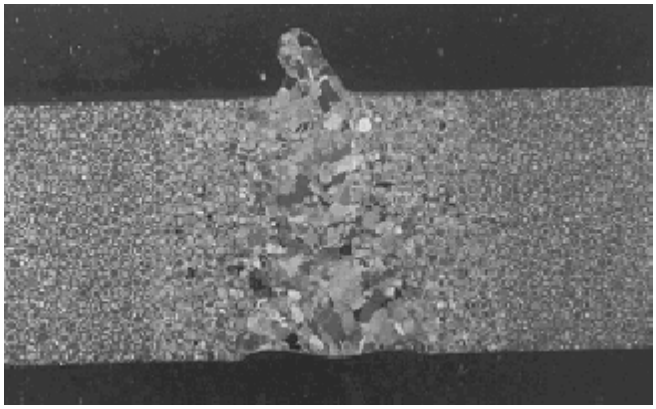

Figure 5.5 PA welded joint of TiGr-7 alloy (x3.3)

5.1.2 Test conditions and experimental setup

The susceptibility to SCC was studied by means of the slow strain rate technique. This method is considered as the best laboratory method for evaluating the resistance of materials to this corrosion phenomenon. SCC refers to cracking caused by the simultaneous presence of tensile stress and a specific corrosive medium.

The testing equipment has consisted of constant extension rate tensile testing machines of 50 KN capacity and selectable crosshead speed within the range of 0.1 to 10^{-6} mm/s. The test specimens were located in Hastelloy C-276 autoclaves and attached to a fixed frame by one end and to the pull rod by the other. The autoclaves were filled with salt brine or granitic water or argon, then they were closed, pressured and heated. Round tensile specimens of 6 mm diameter and 30 mm gauge length were machined for the steels (Figure 5.6). In the case of the titanium alloy, the test specimens had a diameter of 3.5 mm and a gauge length of 25 mm. In all cases parent specimens were taken in the transverse sense to the rolling direction. The

specimens of the welded joints were taken in the transverse sense. The materials were tested in a NaCl rich brine (25.9 wt.% NaCl, pH(25°C)=6.0) at 170°C and in a bentonite buffered granitic water at 90°C. Additional comparative investigations were also carried out in argon as an inert reference medium. The chemical composition and pH of the synthetic bentonite granitic water are given in Table 5.2.

The test conditions used in the slow strain rate tests of the materials, in both parent and welded states, are given below:

TESTING MEDIA: Salt brine and argon at 170°C:
-TStE355: Strain rates ranging from 10^{-4} to $10^{-7}s^{-1}$.
-TiGr-7: Strain rates of 10^{-6} and $10^{-7}s^{-1}$.

TESTING MEDIA: Granite and argon at 90°C:
-TStE355: Strain rates ranging from 10^{-4} to $10^{-7}s^{-1}$.
-AISI 316L: Strain rates ranging from 10^{-4} to $10^{-7}s^{-1}$.

The load supported by the specimen, the position of the actuator, as well as the time and temperature data were continuously logged during the test by means of the microprocessor that controls the machine. After each test, the elongation, reduction of area, energy, yield strength, maximum load and true stress at fracture were measured to assess the loss of ductility of the studied materials. This was complemented by metallographic and fractographic studies. Figure 5.7 shows typical load versus time curves for TStE355 carbon steel tested in argon and NaCl brine at 170°C and a strain rate of 10^{-6} s^{-1}.

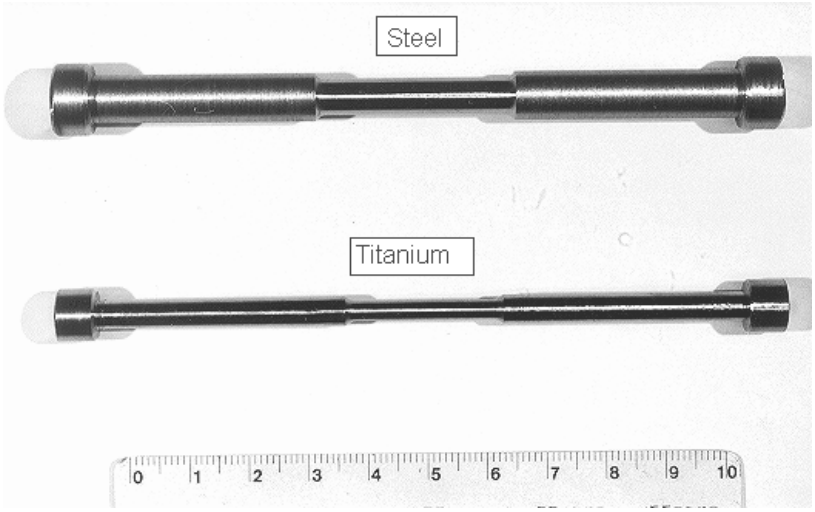

Figure 5.6 Slow strain rate test specimens of steel and titanium alloy

Table 5.2 Chemical composition (limits) of the granitic-bentonite water

Ion	Concetration (mg/l)
Cl^-	6550±250
NO_3^-	110±10
SO_4^{2-}	1500±30
HCO_3^-	27±5
SiO_2	8.3±0.5
Br^-	15±1
Ca^{2+}	135±10
K^+	20±1
Mg^{2+}	600±30
Na^+	3750±100
pH (25ºC)	7.3

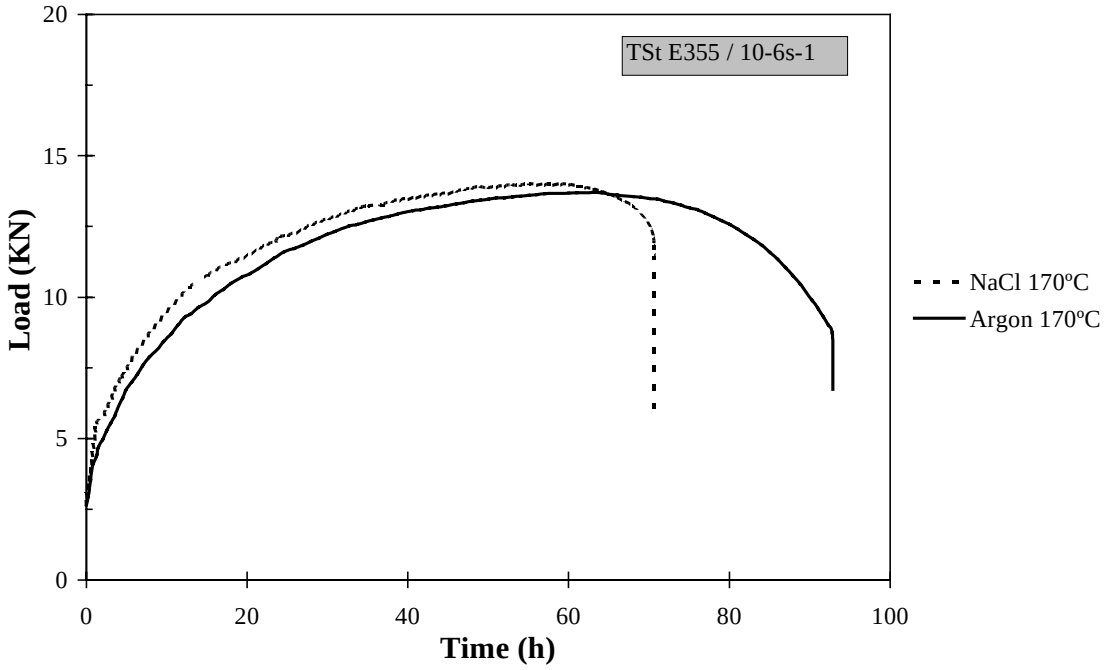

Figure 5.7 Typical load versus time curves for the TStE355 carbon steel tested in argon and NaCl brine at 170°C and a strain rate of $10^{-6}s^{-1}$

5.2 Results

5.2.1 Salt brine environment

TStE355 carbon steel

The results of the slow strain rate tests obtained for the parent material and EB and FCA welded steel specimens after testing in argon and 5M NaCl at 170°C and strain rates of 10^{-4} to $10^{-7}s^{-1}$ are given in Figure 5.8. Compared to the values in argon, there is a clear decrease of the elongation and reduction of area parameters when tested in the brine. The drop of these parameters is not significant at the highest strain rate ($10^{-4}s^{-1}$) but it is important at the other lower strain rates used in the tests. The values of the yield strength and maximum load parameters do not show important changes between the two media, for both parent and welded specimens. Figure 5.9 shows for comparison two TStE355 steel specimens tested in argon and in NaCl at 170°C and a strain rate of $10^{-7}s^{-1}$. The loss of ductility of the specimens tested in the salt brine is mainly manifested in the reduction of area in the fracture zone.

The loss of ductility which occurred by the steel when tested in the salt brine is explained by the embrittling effect of the hydrogen produced on the specimen surface during the test. Due to general corrosion, hydrogen is produced, it penetrates into the material, mainly through the highly stressed zones of the specimen, and interacts with the microstructure resulting in a deterioration of the mechanical properties.

Metallographic examinations of parent and welded specimens show secondary cracks (Figures 5.10-5.12) with a maximum crack depth of 130 µm when tested in NaCl brine at the slowest strain rate. This indicates a slight sensitivity to SCC under the test conditions applied. In all cases, the fracture of welded specimens is located in the base material.

The SEM fracture surface examinations of tested specimens show a change from a fully ductile fracture surface with dimples formation for specimens tested in argon to a more brittle fracture mode when the tests were performed in the salt brine. The brittle nature of the fracture surface becomes greater as the strain rate is slower. Figure 5.13 shows a transgranular cracking mode (TGSCC) of a TStE355 steel specimen tested in NaCl at 170°C.

Concerning the welded specimens, it was not observed any effect of the EB and FCA welding procedures in the SCC behaviour of the material.

X-Ray Diffraction (XRD) analysis on the surface of steel specimens tested in NaCl at 170°C shows that the oxide layer mainly consists of magnetite (Fe_3O_4).

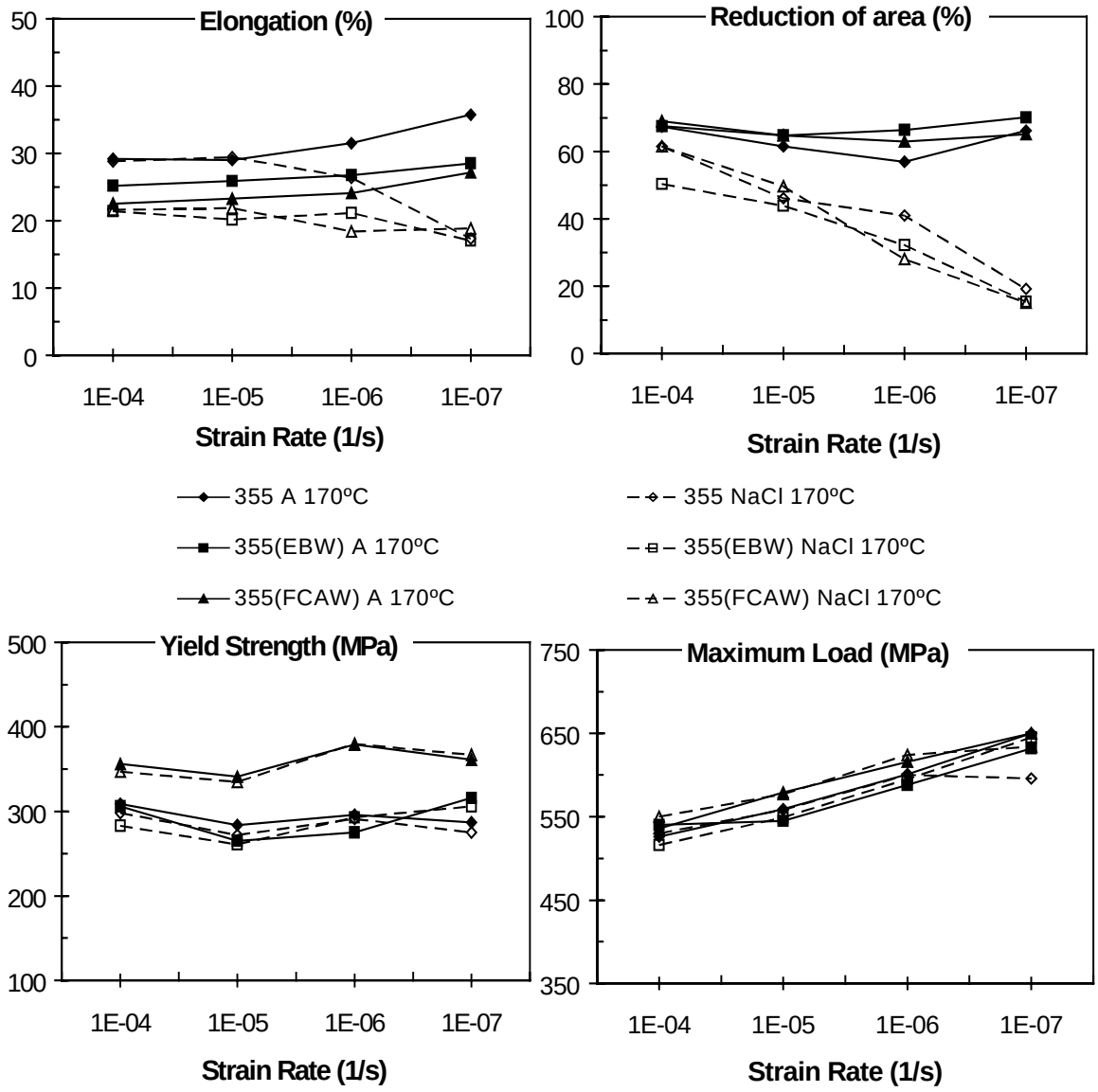

Figure 5.8 Elongation, reduction of area, yield strength and maximum load values versus strain rate for the parent and welded TStE355 steel tested at 170°C in argon and NaCl brine

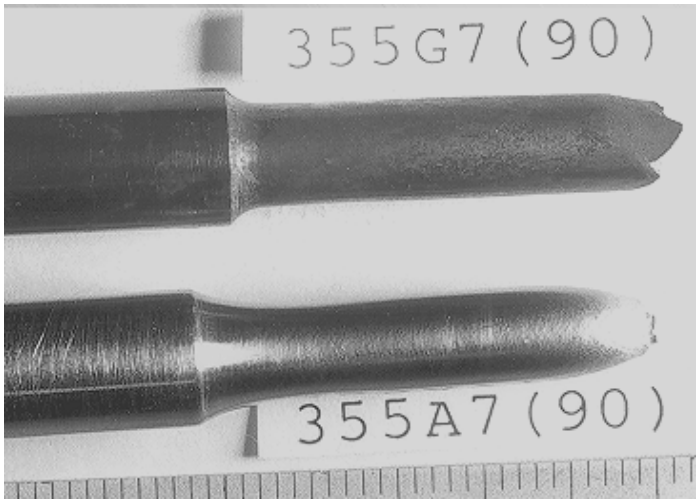

Figure 5.9 Macrographs of two TStE355 slow strain rate tensile specimens tested in argon and granitic water at 90°C at a strain rate of $10^{-7}s^{-1}$

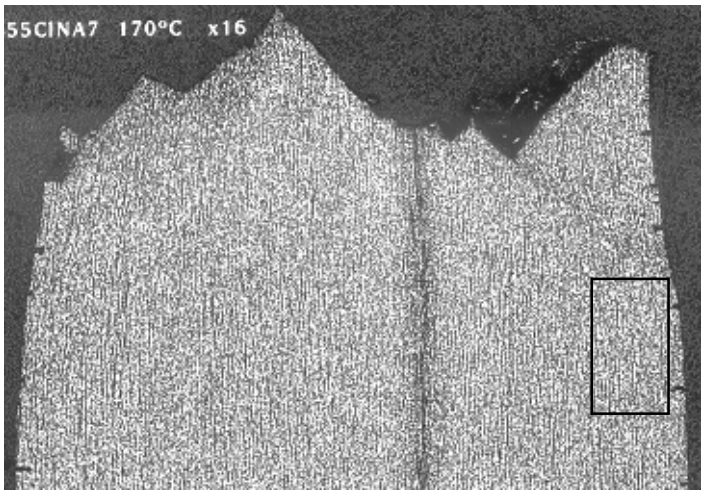

Figure 5.10 Optical micrograph of a TStE355 steel specimen tested in NaCl brine at 170°C and a strain rate of $10^{-7}s^{-1}$ (x16)

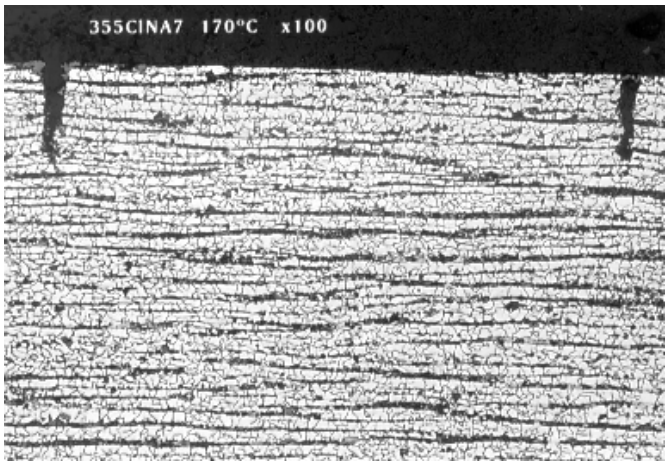

(x95)

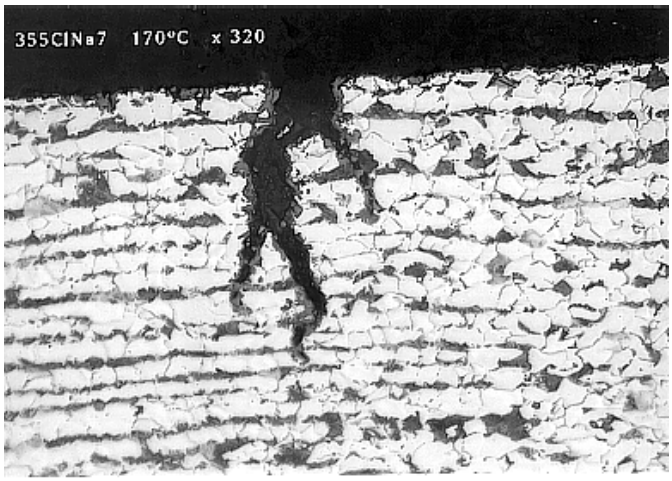

(x300)

Figures 5.11-5.12 Optical micrographs showing detailed views of the previous TStE355 steel specimen (Fig. 5.10) tested in NaCl brine at 170°C and a strain rate of $10^{-7}s^{-1}$

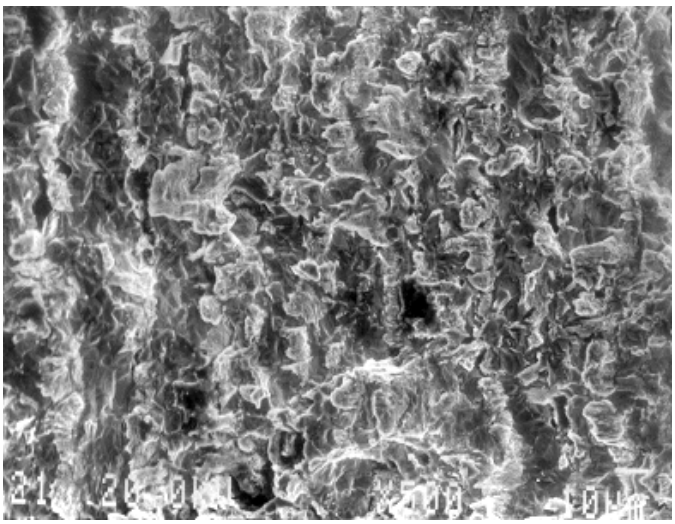

Figure 5.13 SEM micrograph of the fracture surface of a TStE355 steel specimen tested in NaCl brine at 170°C and a strain rate of $10^{-7}s^{-1}$

TiGr-7 alloy

The SSRT results obtained on TiGr-7 alloy and its EB and PA welded joints at 170°C and a strain rate of $10^{-7}s^{-1}$ are summarized in Table 5.3. These values show that after testing in the brine the mechanical values of the material, both for the parent and the welded specimens, are very close to those obtained in argon. Figure 5.14 shows two TiGr-7 alloy specimens tested in argon and NaCl brine at 170°C and a strain rate of $10^{-7}s^{-1}$.

Table 5.3 SSRT results obtained for TiGr-7 alloy in argon and NaCl brine at 170°C and a strain rate of $10^{-7}s^{-1}$

	TiGr7		TiGr7 EBW		TiGr7 PAW	
	Argon	NaCl	Argon	NaCl	Argon	NaCl
Elongation (%)	30.0	31.3	23.6	26.4	19.1	18.2
Reduction in area (%)	71.9	68.7	68.7	69.2	69.4	70.8
Yield Strength (MPa)	178	181	187	185	194	199
True Stress Fracture (MPa)	538	487	581	573	592	577
Maximum Load (MPa)	228	243	246	244	248	239
Secondary cracks	None	None	None	None	None	None
Time to fracture (h)	820	878	697	733	523	519
Fracture mode	Ductile	Ductile	Ductile	Ductile	Ductile	Ductile

No secondary cracks were observed in the metallographic examinations of the specimens after testing in the brine, indicating that under the test conditions applied the TiGr-7 alloy is not sensitive to SCC (Figure 5.15). EB and PA weldings do not affect the behaviour of the material to SCC. The fracture surface of the specimens shows a fully ductile fracture mode for tests performed in argon and in NaCl brine (Figure 5.16).

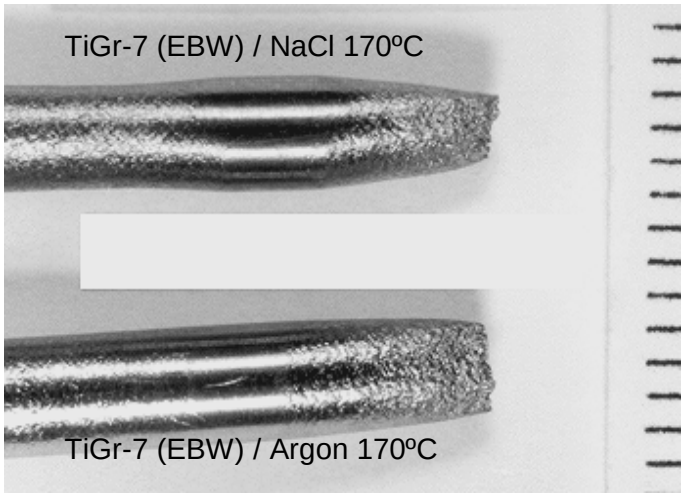

Figure 5.14 Macrographs of two TiGr-7 alloy specimens tested in argon and NaCl brine at 170°C and a strain rate of $10^{-7}s^{-1}$

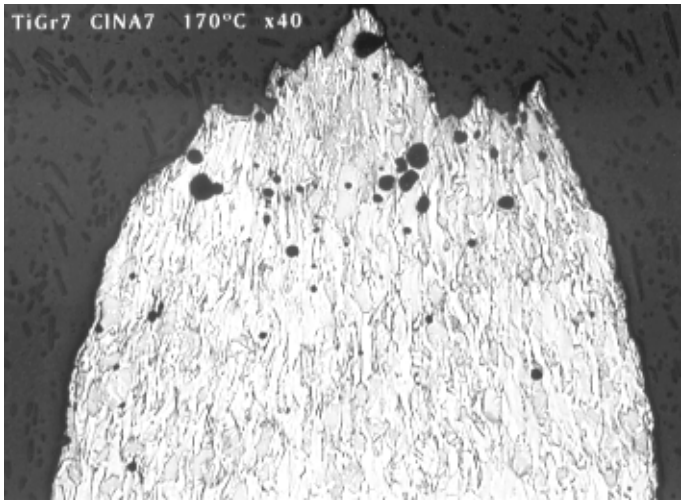

Figure 5.15 Optical micrograph of a TiGr-7 alloy specimen tested in NaCl brine at 170°C and a strain rate of $10^{-7}s^{-1}$ (x40)

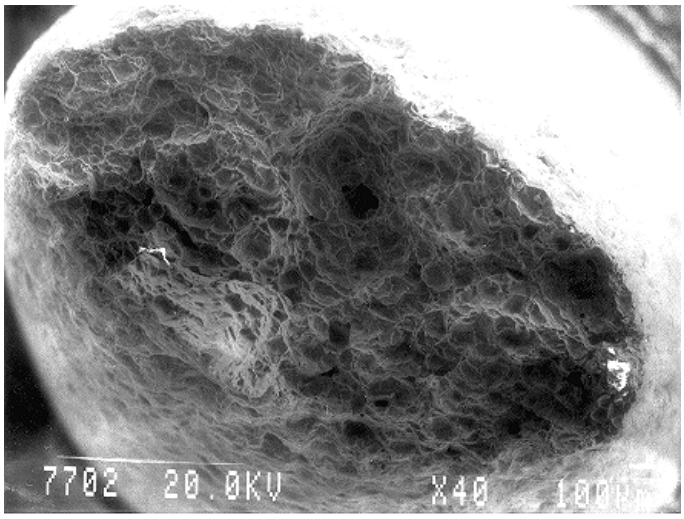

Figure 5.16 SEM micrograph of the fracture surface of a TiGr-7 alloy specimen tested in NaCl brine at 170°C and a strain rate of $10^{-7}s^{-1}$

5.2.2 Granitic water

TStE355 carbon steel

Values of elongation, reduction of area, yield strength and maximum load obtained in the slow strain rate tests on TStE355 steel in argon and granitic water at 90°C, and strain rates of 10^{-4} to $10^{-7}s^{-1}$, are given in Figure 5.17. Compared to the results in argon, the steel suffers a loss of ductility in granitic water, mainly noticed in the reduction of area and true stress at fracture. The drop of these parameters is not significant at the highest strain rate ($10^{-4}s^{-1}$) but it is important at any of the other slower strain rates used in the tests, due to the longer exposure to the corrosion medium. There are no important changes in the yield strength and maximum load parameters in granitic water. Figure 5.18 shows two steel specimens tested at the same temperature and strain rate in argon and granitic water. The loss of ductility is mainly manifested in the reduction of area parameter.

The loss of ductility observed by the carbon steel when tested in bentonite-granitic water is explained by the embrittling effect of the hydrogen produced during the slow strain rate test. In all cases, the fracture of welded specimens was located in the base metal.

In the metallographic studies carried out on the parent and welded TStE355 steel specimens, no clear signs of sensitivity to SCC in granitic water were found. Areas of localized corrosion are present on the lateral surface of TStE355 specimens when tested at the slowest strain rate of $10^{-7}s^{-1}$ (Figures 5.19-5.21). However, these areas, deeper in the case of welded specimens, have a crack length/crack width ratio relation near 1, indicating rather a localized corrosion due to the local and repetitive breaking of the oxide layer than secondary cracking. The crack length / crack width ratio parameter gives an idea of the sharpness of the crack and is useful to quantify and compare the resistance of the tested materials to SCC. It is important to mention that the term crack is used in a wide sense including both secondary cracks and localized corrosion due to the breaking of the oxide layer.

SEM examinations of the fracture surface show transgranular fracture modes for specimens tested in the granitic water (Figure 5.22), whereas a fully ductile fracture surface is observed for specimens tested in argon. X-Ray Diffraction (XRD) analysis of the corrosion products formed on the surface of steel specimens when tested in granitic water at 90°C shows that the oxide film is magnetite (Fe_3O_4).

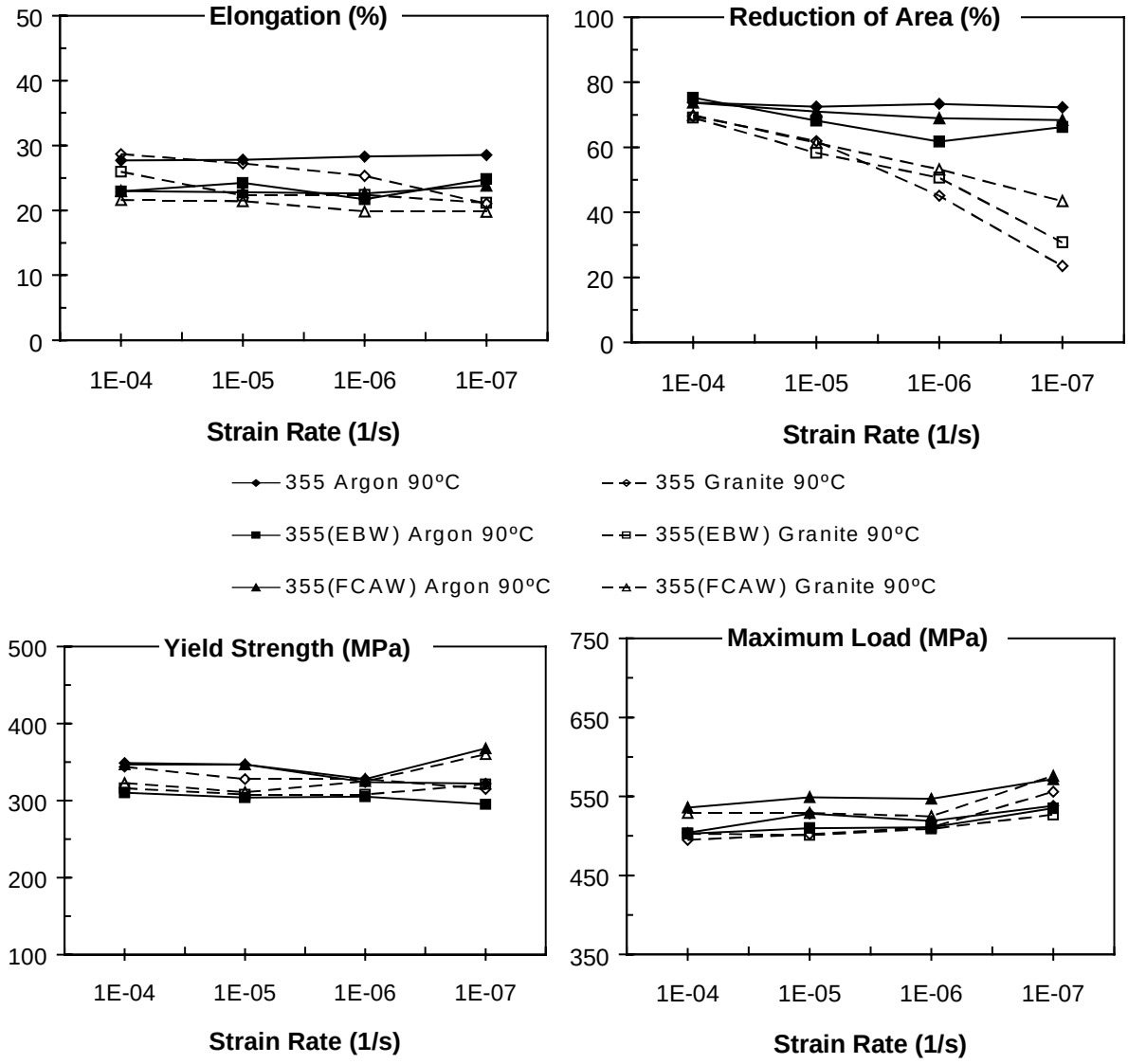

Figure 5.17 Elongation, reduction of area, yield strength and maximum load values versus strain rate for the parent and welded TStE355 steel tested at 90°C in argon and granitic water

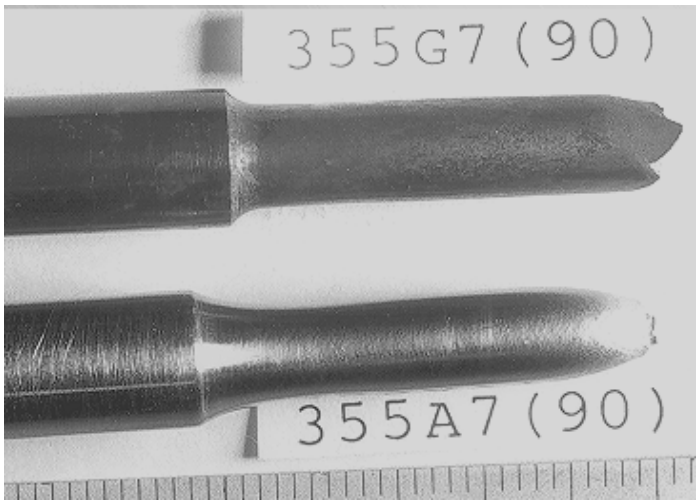

Figure 5.18 Macrographs of two TStE355 tensile specimens tested in argon and granitic water at 90°C and a strain rate of $10^{-7}s^{-1}$

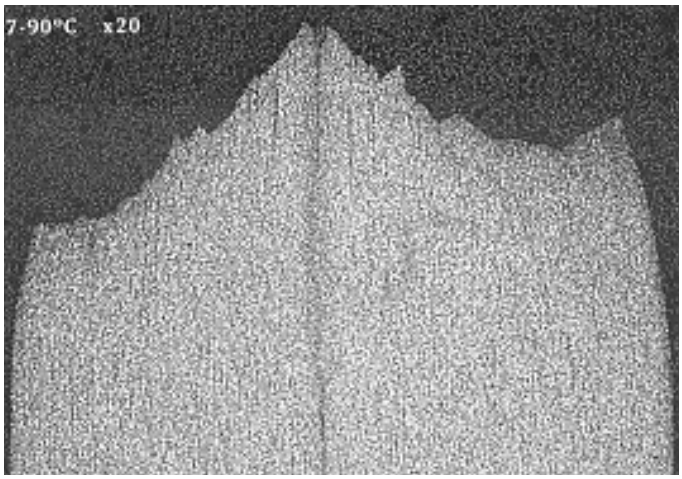

Figure 5.19 Optical micrograph of a parent TStE355 steel specimen tested at a strain rate of $10^{-7}s^{-1}$ in granitic water at 90°C (x20)

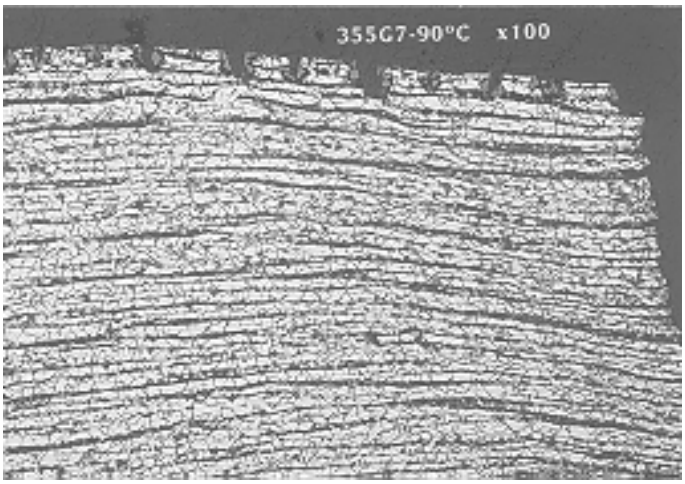

Figures 5.20 Optical micrograph of a parent TStE355 steel specimen showing a detail of the previous specimen (Figure 5.19) (90°C/granitic water/ $10^{-7}s^{-1}$) (x100)

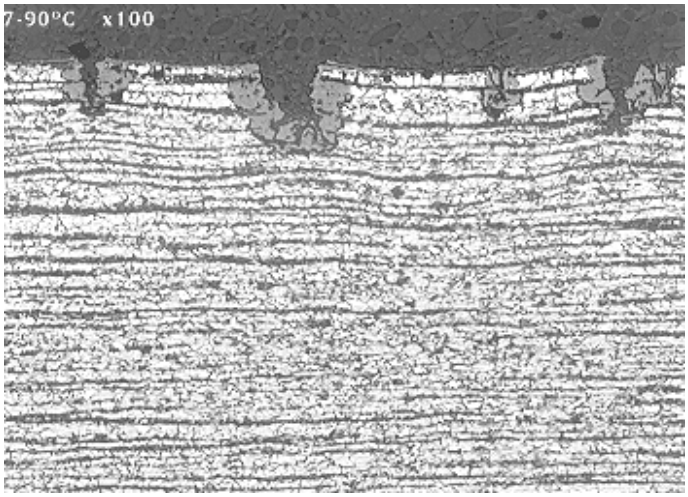

Figure 5.21 Optical micrograph of a FCA welded TStE355 steel specimen tested at a strain rate of $10^{-7}s^{-1}$ in granitic water at 90°C (x100)

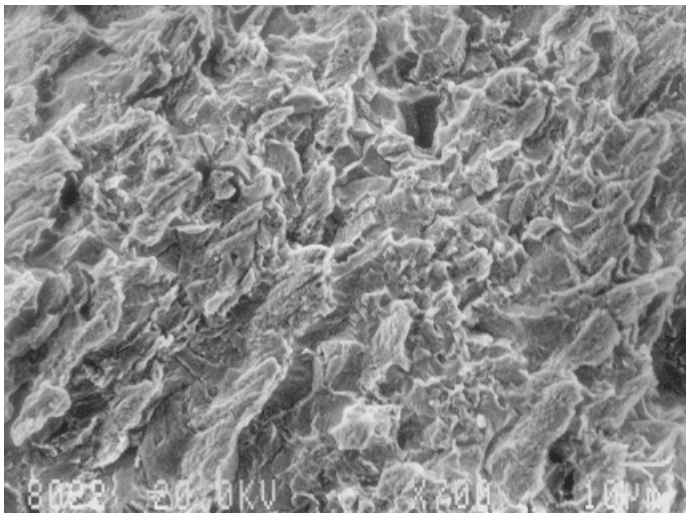

Figure 5.22 SEM micrograph of the fracture surface of a TStE355 steel specimen tested at a strain rate of $10^{-7}s^{-1}$ in granitic water at 90°C

AISI 316L Stainless steel

The results of the slow strain rate tests obtained for the parent and EB and GTA welded AISI 316 stainless steel in argon and granitic water at 90°C and strain rates of 10^{-5} to $10^{-7}s^{-1}$ are given in Figure 5.23. The values of elongation, reduction of area, maximum load and yield strength are very close to those obtained in argon, thus indicating no loss of ductility. The fracture of the welded specimens was always located in the base material.

Secondary cracks typical for stress corrosion cracking have not been observed under any of the test conditions. Several AISI 316L steel specimens tested in the granitic water at the slowest strain rate of $10^{-7}s^{-1}$ show isolated pits near the fracture zone (Figures 5.24-5.25).

The SEM examinations show a fully ductile fracture surface with dimples formation for the specimens tested in the granitic environment (Figure 5.26). EB and GTA weldings do not affect the resistance of the AISI 316 stainless steel to SCC.

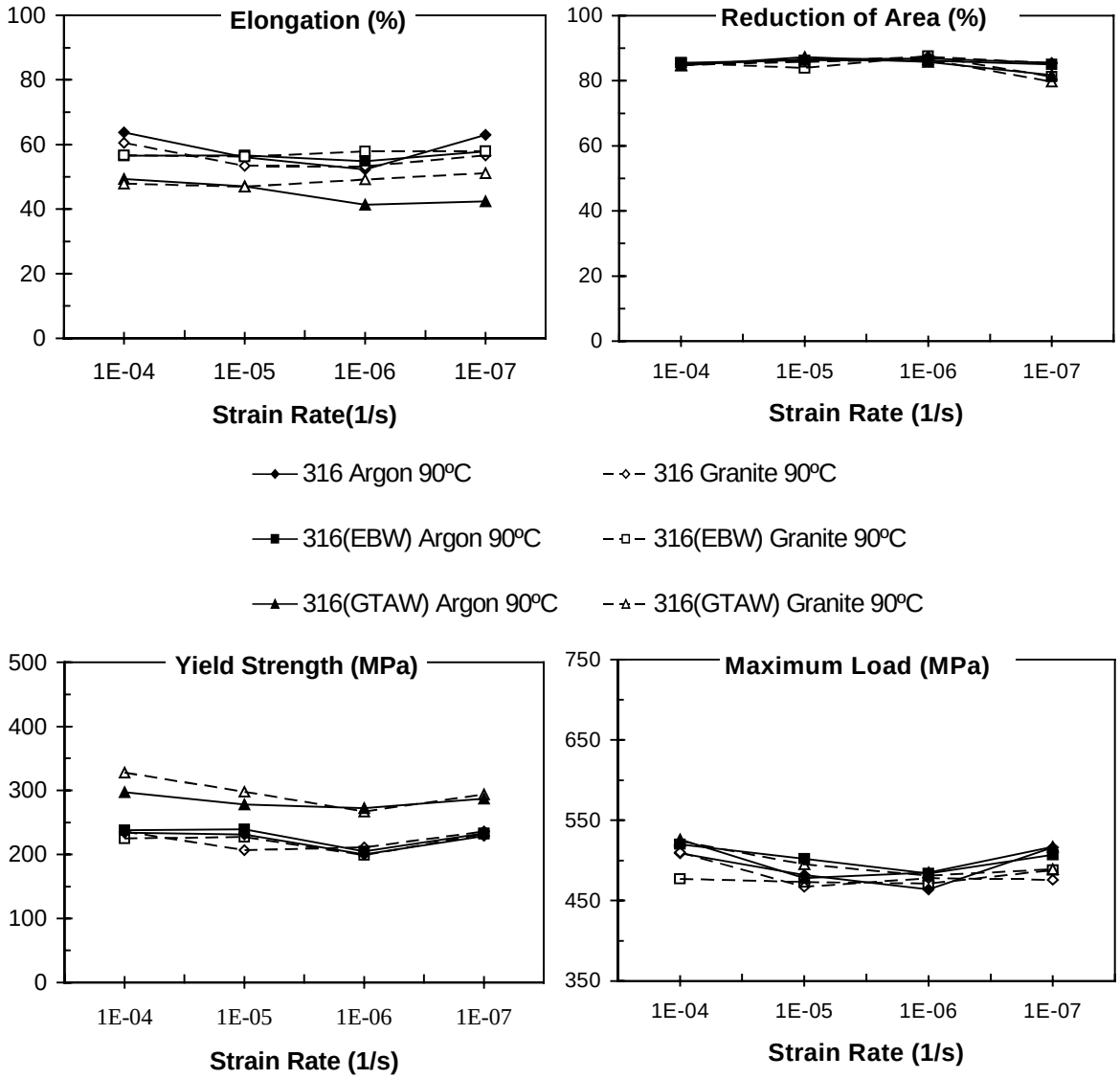

Figure 5.23 Elongation, reduction of area, yield strength and maximum load values versus strain rate for the parent and welded AISI 316L stainless steel tested at 90°C in argon and granitic water.

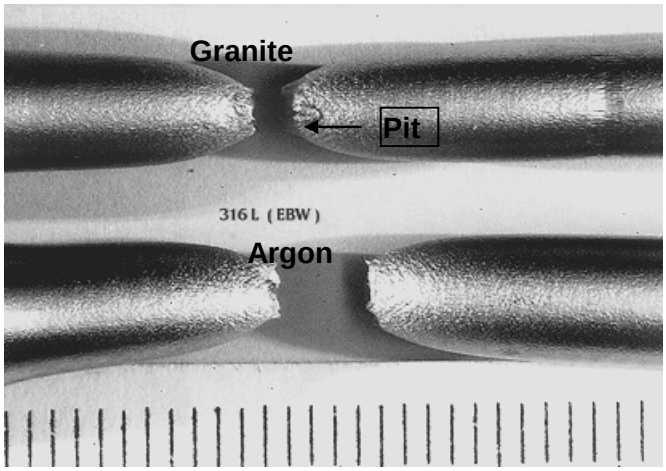

Figure 5.24 Macrographs of AISI 316L specimens tested in argon and granitic water at 90°C and $10^{-7}s^{-1}$

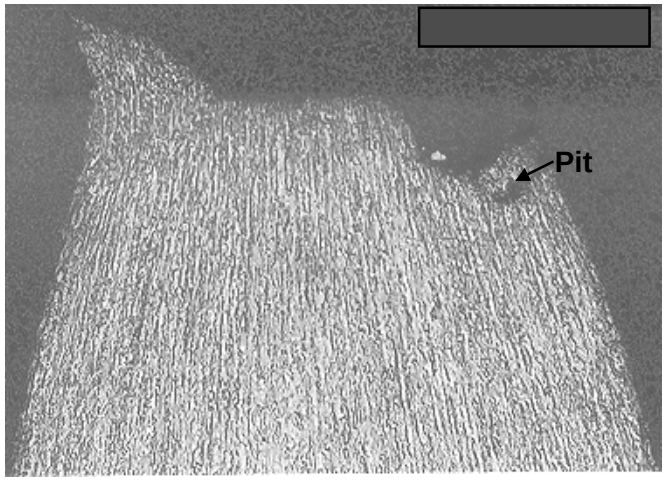

Figure 5.25 Optical micrograph of a AISI 316L steel specimen tested in granitic water at 90°C and $10^{-7}s^{-1}$ (x18)

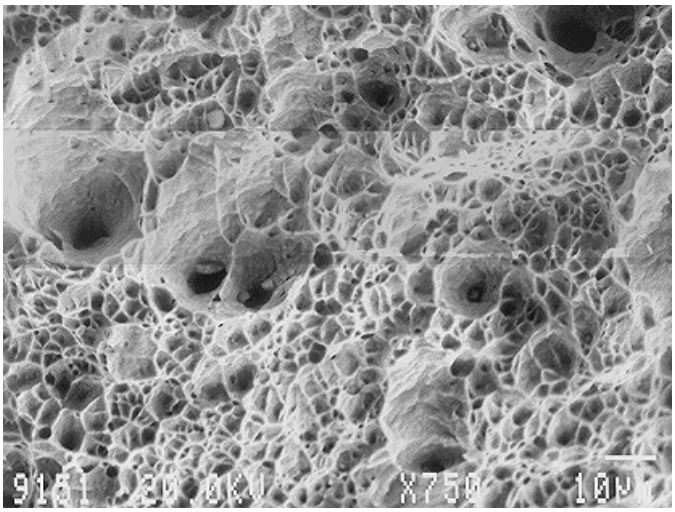

Figure 5.26 SEM micrograph of the fracture surface of a 316L steel specimen tested in granitic water at 90°C and $10^{-7}s^{-1}$ (x75)

6. ELECTROCHEMICAL CORROSION STUDIES ON CANDIDATE CONTAINER MATERIALS IN CLAY ENVIRONMENTS

In previous studies[13,14,15], the corrosion behaviour of candidate container materials (carbon steel, stainless steels, nickel- and titanium alloys) was examined under in-situ conditions in the underground laboratory HADES, located in Boom clay. However, the results of these in-situ experiments did not allow to quantify unequivocally the corrosion rate of the materials. To elucidate the questions remaining from the in-situ studies, a new laboratory programme has been setup and started[16,17]. The aim of the present laboratory studies is to investigate systematically the corrosion behaviour of preselected materials under representative disposal conditions in clay environments. The various relevant environmental parameters (content of aggressive anions, temperature) were varied according to the results of previous theoretical studies and accordind to the relevant disposal concepts.

The susceptibility of the various candidate container materials to pitting corrosion was evaluated by performing cyclic potentiodynamic polarization experiments according to ASTM Standard G61-81, and determining the following characteristic potentials from the polarization curves:

- the free corrosion potential, E_{corr}: this is the potential that the metal assumes under open circuit conditions in the studied environment,

- the critical potential for pit nucleation, E_{np}: this is the potential above which pits nucleate and develop, and

- the protection potential, E_{pp}: this is the potential below which no pitting occurs and above which pits already nucleated can grow.

6.1 Materials, Techniques, and Parameters

6.1.1 Investigated candidate container materials

The susceptibility to localized corrosion of nine candidate container materials was investigated: carbon steel TStE355, stainless steels AISI 316L, AISI 316L hMo, AISI 316Ti and AISI 309S, higher alloyed stainless steels Cronifer 1925 hMo and UHB 904L, nickel alloy Hastelloy C4, and titanium alloy Ti/0.2Pd. The chemical composition of these materials is given in Table 6.1.

TABLE 6.1 Chemical composition of the investigated candidate container materials.

	Chemical composition (wt%)										
	Fe	Cr	Ni	Mn	Mo	Si	Ti	C	S	P	Others
Carbon steel											
TStE 355	bal	0.030	0.030	1.120	0.000	0.344	0.003	0.180	0.002	0.010	Nb 0.017; N_2: 0.005
Stainless steel											
AISI 316L	bal	16.90	11.00	1.54	2.08	0.54	-	0.017	0.001	0.032	
AISI 316L hMo	bal	17.67	12.53	1.16	2.84	0.61	-	0.015	0.001	0.030	
AISI 316Ti	bal	16.80	10.70	1.08	2.05	0.40	0.3	0.044	0.009	0.028	
AISI 309S	bal	22.58	13.51	1.70	-	0.33	-	0.063	0.002	0.021	
Higher alloyed stainless steel											
UHB 904L	bal	19.70	25.00	1.48	4.47	0.19	-	0.019	0.001	0.019	Cu:1.51;N_2:0.080
Cronifer 1925hMo	45.45	20.60	24.85	0.92	6.40	0.30	-	0.005	0.002	0.018	Cu:0.86;N:0.198
Nickel alloy Hastelloy C4	0.98	15.75	67.00	0.04	15.85	0.02	<0.01	0.003	0.003	0.004	Co:0.01
Titanium alloy Ti/0.2Pd	0.04	-	-	-	-	-	bal	0.01	-	-	Pd:0.16;O_2:0.13; N_2<0.01;H_2:0.001

6.1.2 Electrochemical techniques

The susceptibility to localized corrosion of the investigated container materials was determined by conducting cyclic potentiodynamic polarization measurements. A typical polarization curve recorded in synthetic oxidizing clay water (SOC) for stainless steel AISI 316Ti is shown in Figure 6.1. From the polarization curve, a value for the corrosion potential E_{corr} under deaerated conditions as well as the characteristic potentials E_{np} and E_{pp} for pitting corrosion can be determined. When the potential shifts in the anodic direction from the corrosion potential, i.e. the open circuit potential, the stainless steel surface is protected by a passivation layer. Below the pitting potential, E_{np}, metastable pitting is possible and this is visible on the polarization curve as the occurrence of small peaks in the current density superimposed on the passivation current. Above E_{np}, pitting becomes stable and the current density rises rapidly. When the scanning direction is reversed (in our experiments, at a current density of 1 mA/cm^2) to the cathodic direction, pits continue to grow even at potentials where no new pits are initiated. The voltage where the backward scan crosses the forward scan is taken as E_{pp}. In the region cathodic to this potential, pits do not grow.

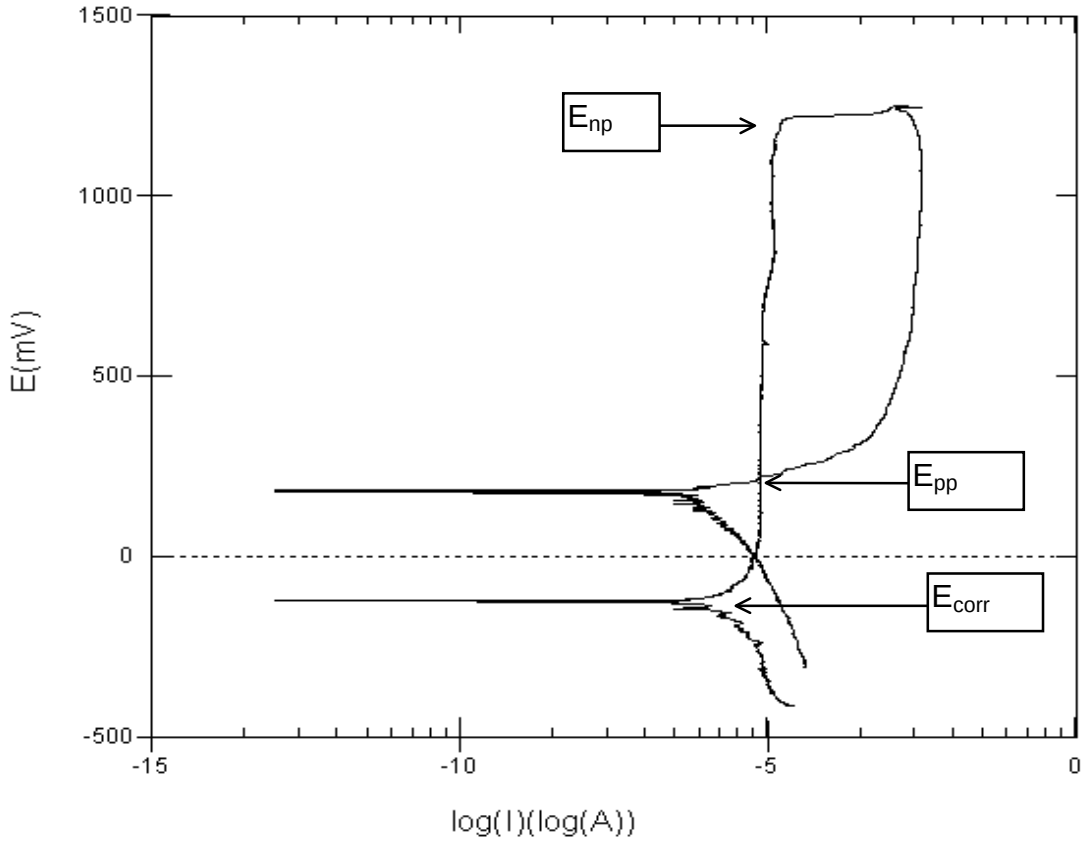

FIGURE 6.1 Polarization curve for AISI 316Ti in synthetic oxidizing clay water containing 10000 ppm Cl^- and 5400 ppm SO_4^{2-} at 90°C, with indication of E_{corr} and the critical pitting potentials E_{np} and E_{pp} (E in mV vs. NHE).

Special care was devoted to the preparation of the samples. The sample preparation can influence the polarization curves in two ways. Firstly, it is difficult to avoid crevice corrosion during a pitting experiment. The simultaneous occurrence, however, of pitting and crevice corrosion complicates the interpretation of the polarization curves. Secondly, the repeatability of results depends on the reproducibility of the surface state of the samples. The following procedure has proven to be reliable in producing samples suited for crevice-free and repeatable pitting corrosion tests:

- A circular sample with a diameter of 15.8 mm was milled from a plate.
- A stainless steel rod was stud-welded to the back of the sample for electrical contact.
- The specimen was embedded in Epoxi-Patch®, a two-compound epoxy resin that wets the steel adequately well for avoiding crevices between metal and resin. The resin was applied at 100°C after preheating the sample to the same temperature.
- After curing of the Epoxi-Patch®, sample and epoxy resin were embedded in a second, cold mounting resin, Epo-thin®, to permit automatic polishing of the specimen.

- Finally, the sample was ground and polished, finishing with 600 grit SiC paper, according to ASTM.

The electrochemical laboratory setup consisted of an EG&G model 263A potentiostat, a PC, a thermostat/cryostat bath, and a specially designed double-walled three-electrode corrosion cell. As reference electrode, a Ag/AgCl electrode with saturated KCl brine was used. This electrode allowed to perform electrochemical experiments at elevated temperatures. Two graphite rods were employed as counter electrodes. Prior to the electrochemical experiment, the electrolyte was purged with nitrogen to eliminate oxygen from the brine. The samples underwent the final polishing steps ten minutes before the start of the experiment.

6.1.3 Experimental parameters

The influence of four environmental parameters on the pitting corrosion of candidate container materials was investigated. These were: the temperature and the concentration of chloride, sulphate and thiosulphate. Two different temperatures were considered: 16°C, being the temperature of the Boom clay host rock formation at 225 metres below ground level, and 90°C, being an intermediate temperature in the near field surrounding the containers. Finally, the electrochemical experiments were performed in ten different brines, with varying concentrations of chloride, sulphate and thiosulphate.

6.2 Results

All candidate container materials were tested in synthetic oxidizing clay water (SOC) under aerobic conditions at 90°C and 16°C. The corrosion medium had the following composition in wt.%:

1.01 Mg^{2+}; 10.2 SO_4^{2-}; <15 K^+; 49.7 Cl^-; 413 Na^+; 1.62 F^-; 832 HCO_3^-/CO_3^{2-}; 5.86 Ca^{2+}.

6.2.1 Pitting corrosion in synthetic oxidizing Boom clay water (aerobic tests) at 90°C

Influence of chloride

Tests were performed in SOC containing 216 ppm sulphate and varying chloride contents: 100, 1000, and 10000 ppm Cl^-, respectively. The elevated chloride concentrations simulated conditions that might occur in developing pits or in crevices. For each alloy/brine combination, three cyclic potentiodynamic polarization measurements were performed, and from the obtained polarization curves, the values of the characteristic pitting potentials E_{np} and E_{pp} as well as a value for the corrosion potential E_{corr} were determined. An important remark has to be made here: The value for the corrosion potential derived from the polarization curves does not necessarily represent the actual value encountered in the disposal of waste containers. Indeed, from these experiments it appears that the corrosion potential is displaced in the anodic direction with time. This phenomenon was also observed by other researchers and is believed to be related to passive film thickening and changing film composition[18]. Furthermore, the value of the corrosion potential depends on the oxygen concentration in the electrolyte. As the test brines were purged with nitrogen to remove oxygen, the values of E_{corr} derived from the polarization curves are probably too low. Therefore, a more relevant value for the actual E_{corr} was determined from independent experiments where the evolution of the open circuit potential was monitored during several days. This value is only slightly

influenced by alloy and electrolyte composition for the alloys and electrolytes studied here. Of course, the obtained value can still only be used as an indication. For an exact interpretation of the polarization curves, it is important that in-situ measurements of the corrosion potential of the candidate container materials in the Boom Clay formation be made.

Figure 6.2 shows a typical polarization curve for the carbon steel TStE355 in SOC at 90°C. The corrosion behaviour is characteristic for a corrosion allowance material.This means, the current density increases exponentially with overpotential and passivation does not occur.

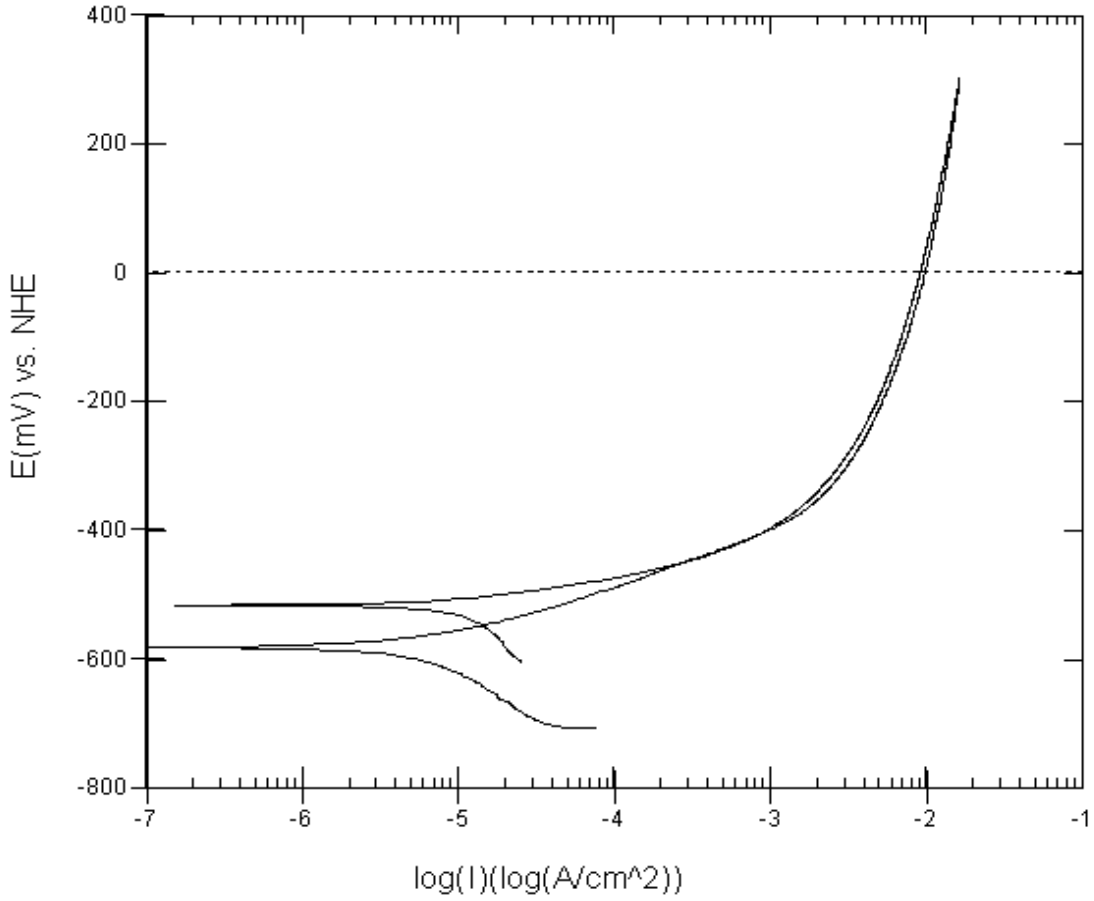

FIGURE 6.2 Polarization curve for carbon steel TStE 355 in SOC containing 1000 ppm chloride and 216 ppm sulphate at 16°C.

Among the corrosion-resistance materials, only Hastelloy C4 and Ti/0.2 Pd resist pitting completely, i.e. in all studied electrolytes with chloride concentrations up to 10000 ppm. The other alloys (stainless steels) suffer from pitting corrosion in a varying extent. Figure 6.3 shows the characteristic pitting potentials for these alloys in SOC containing 216 ppm sulphate at 90°C as a function of the chloride content. Figure 6.4 shows the evolution of the corrosion potential as a function of time in SOC containing 100 ppm chloride. After three days, E_{corr} has reached a value of approximately 300 mV (NHE). As this value is only slightly dependent on the alloy composition and chloride content of SOC, the same approximate value of 300 mV

(NHE) was used for the interpretation of all polarization curves. This potential is indicated in this report as the ‘actual corrosion potential’.

To facilitate the interpretation of the polarization curves, the actual corrosion potential in SOC was indicated as a horizontal line on the diagrams of Figure 6.3. At chloride concentrations of 100 and 1000 ppm, the pitting potentials of all investigated materials stay well above the corrosion potential. AISI 316L and Cronifer 1925 hMo do not show pitting, and consequently no pitting potentials are indicated on Fig. 6.3a and 6.3f, respectively. At 10000 ppm however, pitting problems can arise for three steels: AISI 316L, AISI 316Ti, and AISI 309S. Their pitting potentials are approximately equal to or lower than the actual corrosion potential. AISI 316L and AISI 309S seem to be the most susceptible to pitting corrosion at high chloride concentrations.

The value of E_{pp} drops under E_{corr} for the steels AISI 316L, AISI 316L hMo, AISI 316Ti, AISI 309S, UHB 904L, and Cronifer 1925 hMo at chloride concentrations of 1000 ppm and higher. The materials AISI 316L, AISI 316L hMo, AISI 316Ti, and AISI 309S have E_{pp} below E_{corr} in SOC containing 100 ppm chloride, which is close to realistic conditions. Therefore, the use of these steels in oxidizing clay water could cause long-term pitting corrosion problems

Summarizing, the alloys can be divided into four groups:

- Group I contains corrosion-allowance materials such as carbon steel TStE355. They corrode rapidly and do not passivate.

- Group II contains corrosion-resistance materials that do not show pitting under any of the tested conditions: Hastelloy C4 and Ti/0.2 Pd (Ti99.8-Pd).

- Group III contains materials with protection potentials below the actual corrosion potential at elevated chloride concentrations, but not at realistic concentrations for oxidizing clay water. These are: UHB 904L, and Cronifer 1925 hMo. They are not expected to have corrosion problems in oxidizing clay water.

- Group IV contains materials that might exhibit long-term corrosion problems in oxidizing clay water at chloride concentrations encountered in realistic conditions. These are: AISI 316L, AISI 316L hMo, AISI 316Ti, and AISI 309S.

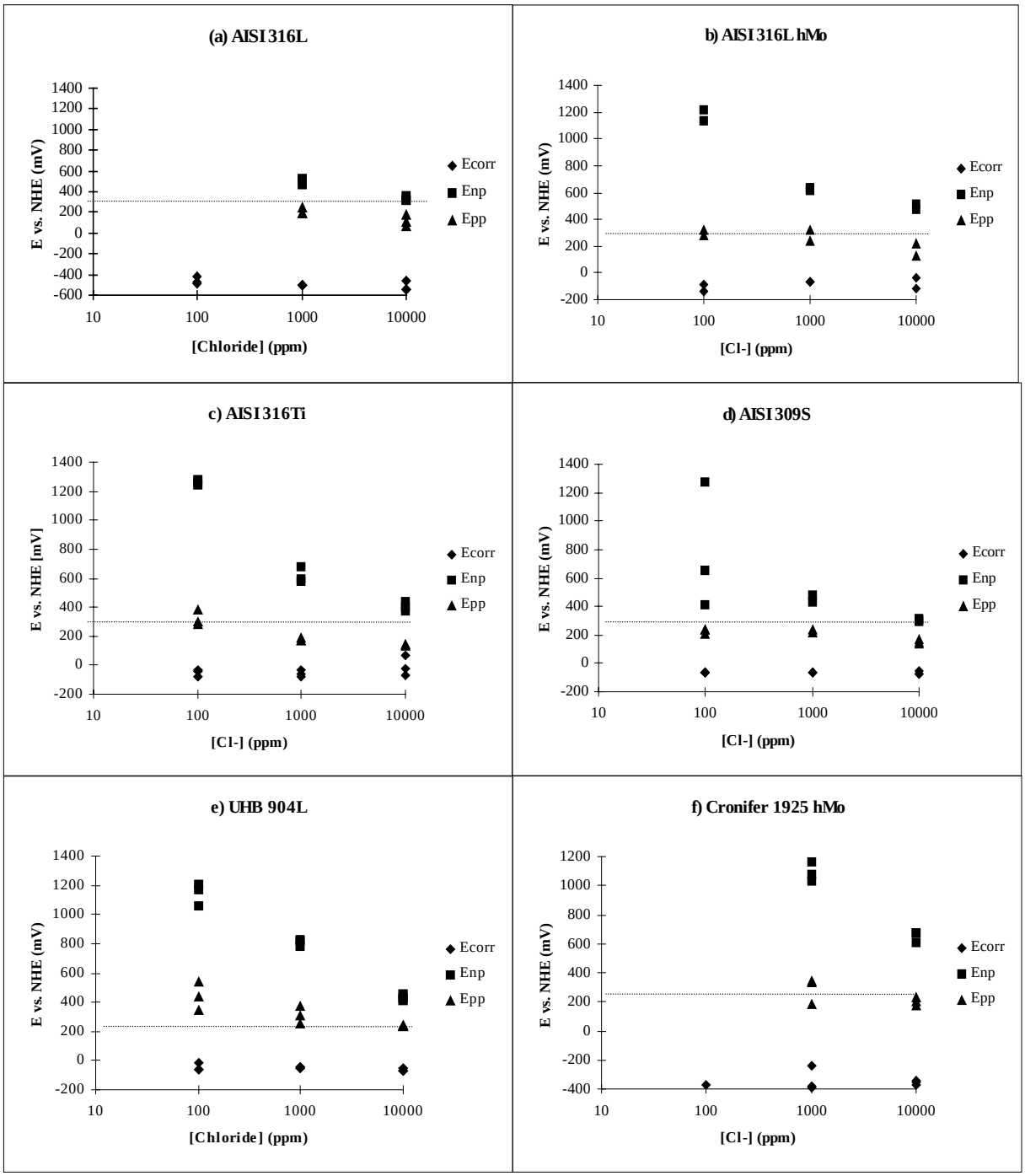

FIGURE 6.3 Influence of chloride concentration on the characteristic pitting potentials of candidate container materials in SOC containing 216 ppm chloride at 90°C

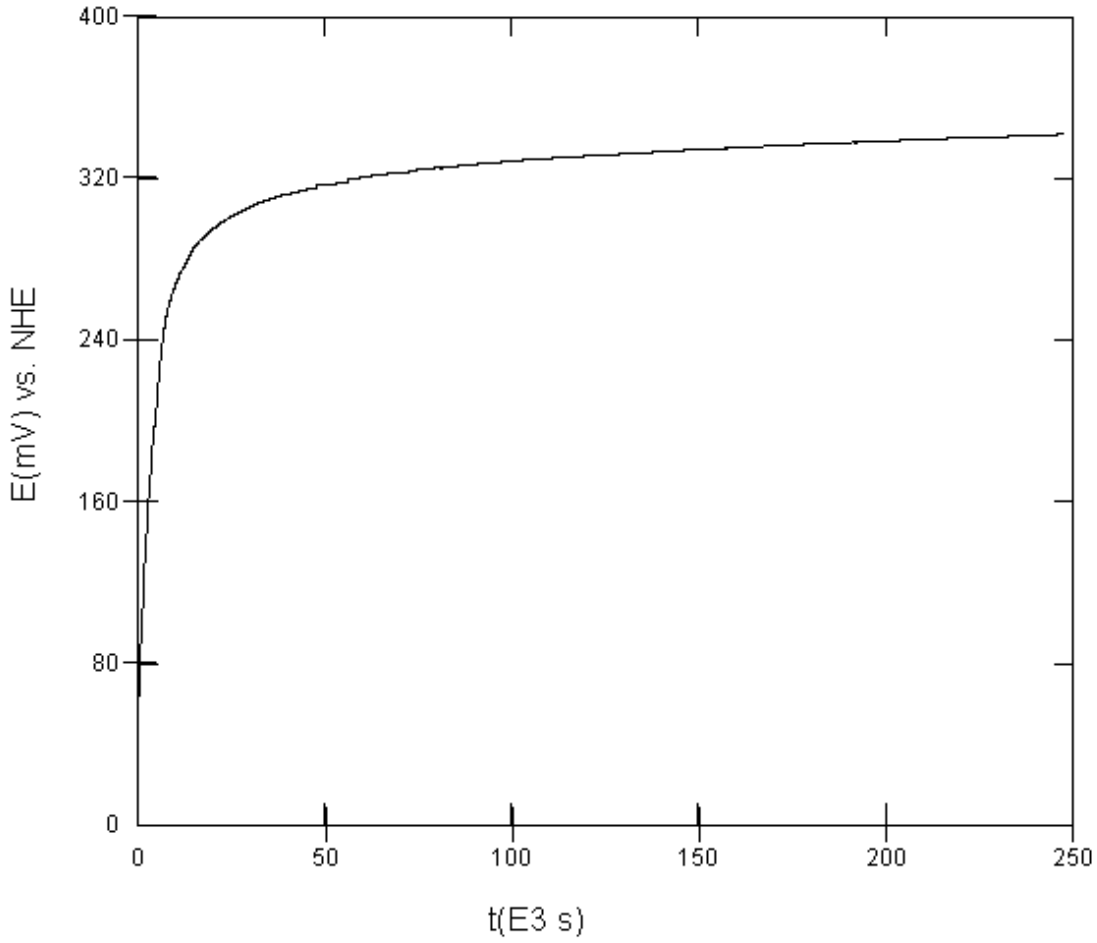

FIGURE 6.4 Evolution of the corrosion potential with time for AISI 316L hMo in SOC containing 1000 ppm chloride and 216 ppm sulphate at 90°C.

Influence of sulphate.

Figure 6.5 shows the values of the corrosion potential and the characteristic pitting potentials for AISI 316L hMo in SOC brines containing 216 ppm and 5400 ppm sulphate respectively. The latter concentration corresponds to an almost complete oxidation of the Boom clay water. The results show that an increased oxidation state of the clay water, or an increased sulphate concentration, causes an increased resistance of the alloy to pitting corrosion. This effect diminishes at higher chloride concentrations. For the other alloys the same conclusion is valid. Alternatively formulated, the critical chloride concentration for pitting corrosion of a given alloy increases with sulphate concentration, or with Boom clay water oxidation.

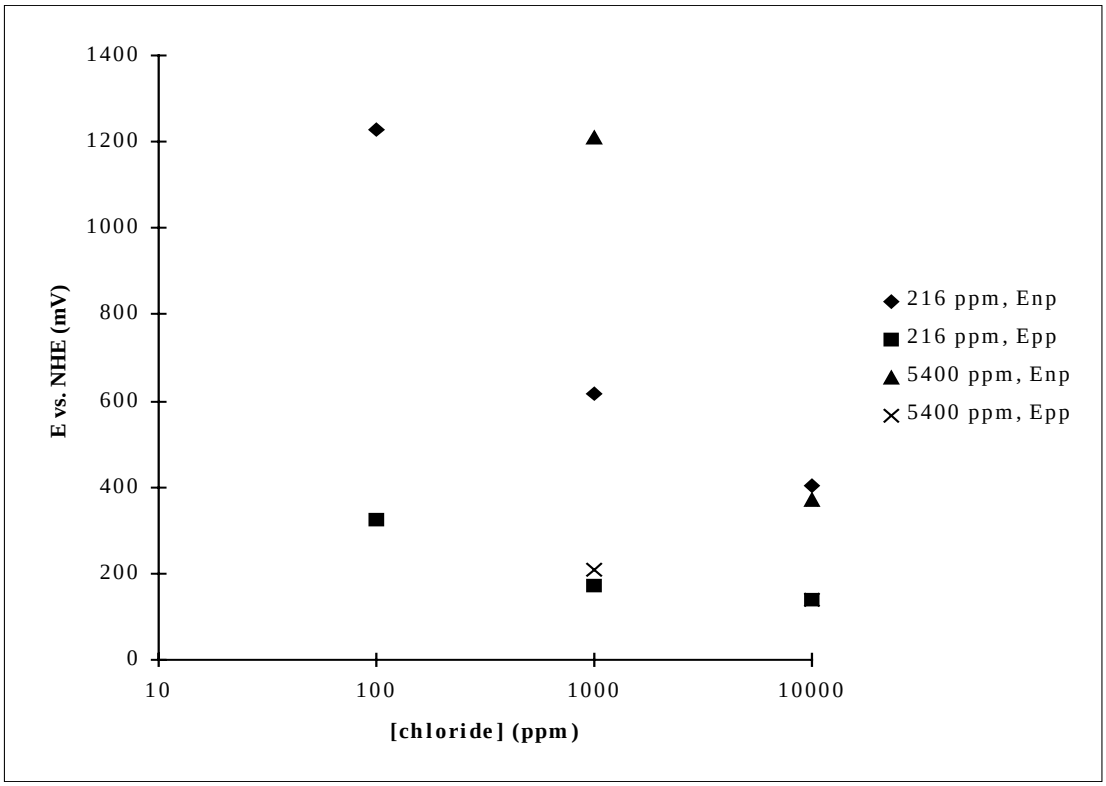

FIGURE 6.5 Influence of sulphate concentration on the characteristic pitting potentials of AISI 316L hMo in SOC at 90°C at different chloride concentrations.

Influence of thiosulphate

Thiosulphate can be present in interstitial Boom clay water as an intermediate compound in the oxidation of pyrite to sulphate, caused by oxygen ingress in the near field during the excavation works or caused by an irradiation and thermal field[19,20] as the one emitted by high-level radioactive waste. As thiosulphate is a doubly charged anion, it is enriched in pit nuclei by electromigration. Thiosulphate is reduced on the metal surface, yielding adsorbed sulphur[21] :

$$S_2O_3^{2-} + 6H^+ + 4e^- \rightarrow 2S_{ads} + 3H_2O$$

The reduction of thiosulphate to adsorbed sulphur can have serious implications on the pitting behaviour of container materials in Boom clay water. In the absence of thiosulphate anions, alloys exhibit metastable pitting at potentials cathodic to E_{np}, i.e. pits nucleate, but they repassivate after growing only a few micrometers. As adsorbed sulphur activates the surface and hinders repassivation[22], the reduction of thiosulphate at the metal surface can transform metastable pits into stable pits, thus effectively lowering the pitting potential.

As the presence of thiosulphate could induce pitting in brines that would normally not cause pitting corrosion, thiosulphate was added to the SOC brine containing 1000 ppm chloride in amounts of 2, 20, 50, and 100 ppm, respectively. In-situ measurements of the interstitial clay water chemistry reported thiosulphate concentrations up to 17 ppm under the influence of a gamma radiation field[19].

Figure 6.6 shows the values of the characteristic pitting potentials as a function of thiosulphate content in SOC containing 1000 ppm chloride and 216 ppm sulphate at 90°C, for AISI 316L, AISI 316L hMo, AISI 316Ti, AISI 309S, UHB 904L, and Cronifer 1925hMo. Hastelloy C4 and Ti/0.2 Pd did not pit in any of the tested thiosulphate containing brines.

From Figure 6.6 it is clear that E_{np} and E_{pp} decrease with thiosulphate content. The stainless steels AISI 316L hMo, AISI 316Ti, and AISI 309S are the most sensitive to the addition of thiosulphate to SOC. The effect is more pronounced for E_{pp} than for E_{np}. Again, as was the case for chloride, the corrosion potential is not dependent on thiosulphate concentration. If we accept an approximate value of 300 mV (NHE) for the actual corrosion potential, it is clear that the increase of thiosulphate does only pose direct pitting problems for AISI 309S. For this alloy, E_{np} drops below the actual corrosion potential in SOC. Again, for a complete interpretation of the results, a value of the in-situ corrosion potential is needed.

For the alloys AISI 316L, AISI 316L hMo, AISI 316Ti, and Cronifer 1925 hMo, E_{pp} drops below the actual corrosion potential. In these cases, the presence of high thiosulphate concentrations may cause long-term corrosion problems. To confirm this, measurements should be done in real clay water, and a prediction of the maximum thiosulphate concentration expected under influence of a gamma radiation field is needed.

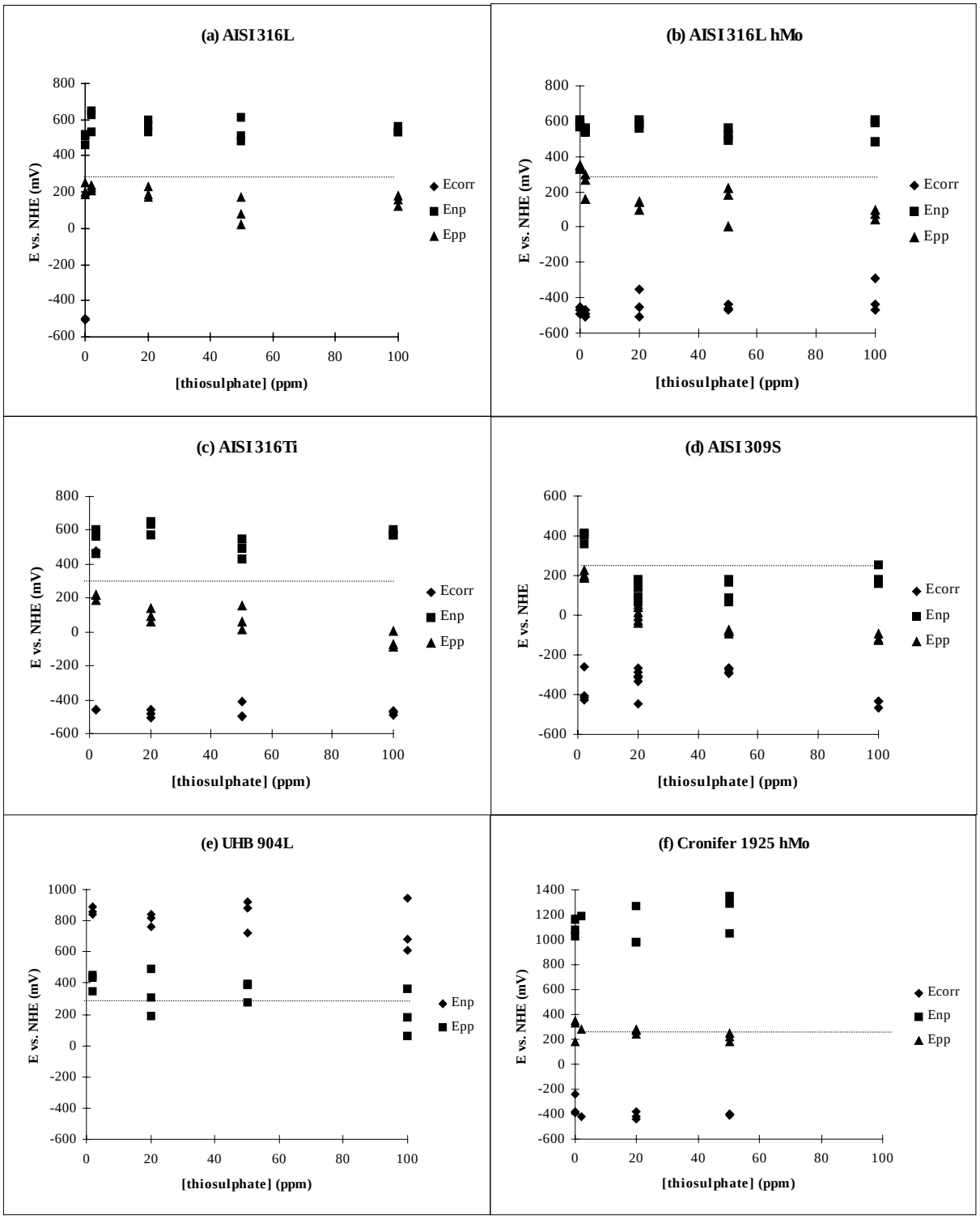

FIGURE 6.6 Influence of the thiosulphate concentration on the characteristic pitting potentials of candidate container materials in SOC containing 1000 ppm chloride and 216 ppm sulphate at 90°C

6.2.2 Pitting corrosion in synthetic oxidizing clay water (aerobic tests) at 16°C

Influence of chloride

Tests were performed at three different chloride concentrations: 100, 1000, and 10000 ppm. The higher concentrations were used to simulate conditions that might occur in developing pits or in crevices. At 16°C, the corrosion behaviour is different from that at 90°C. Whereas at 90°C, for most of the alloys and in most of the SOC brines, the characteristic pitting potentials E_{np} and E_{pp} could be determined from the polarization curves. This method is less applicable at lower temperatures. Indeed, in most cases, at 16°C, no localized corrosion occurs and hence no characteristic pitting potentials can be determined. The following alloys do not exhibit pitting corrosion in any of the investigated SOC brines: UHB 904L, Cronifer 1925 hMo, Hastelloy C4, and Ti/0.2 Pd. For the other alloys, the values of corrosion, pitting and protection potential as function of chloride content of SOC are shown in Figure 6.7.

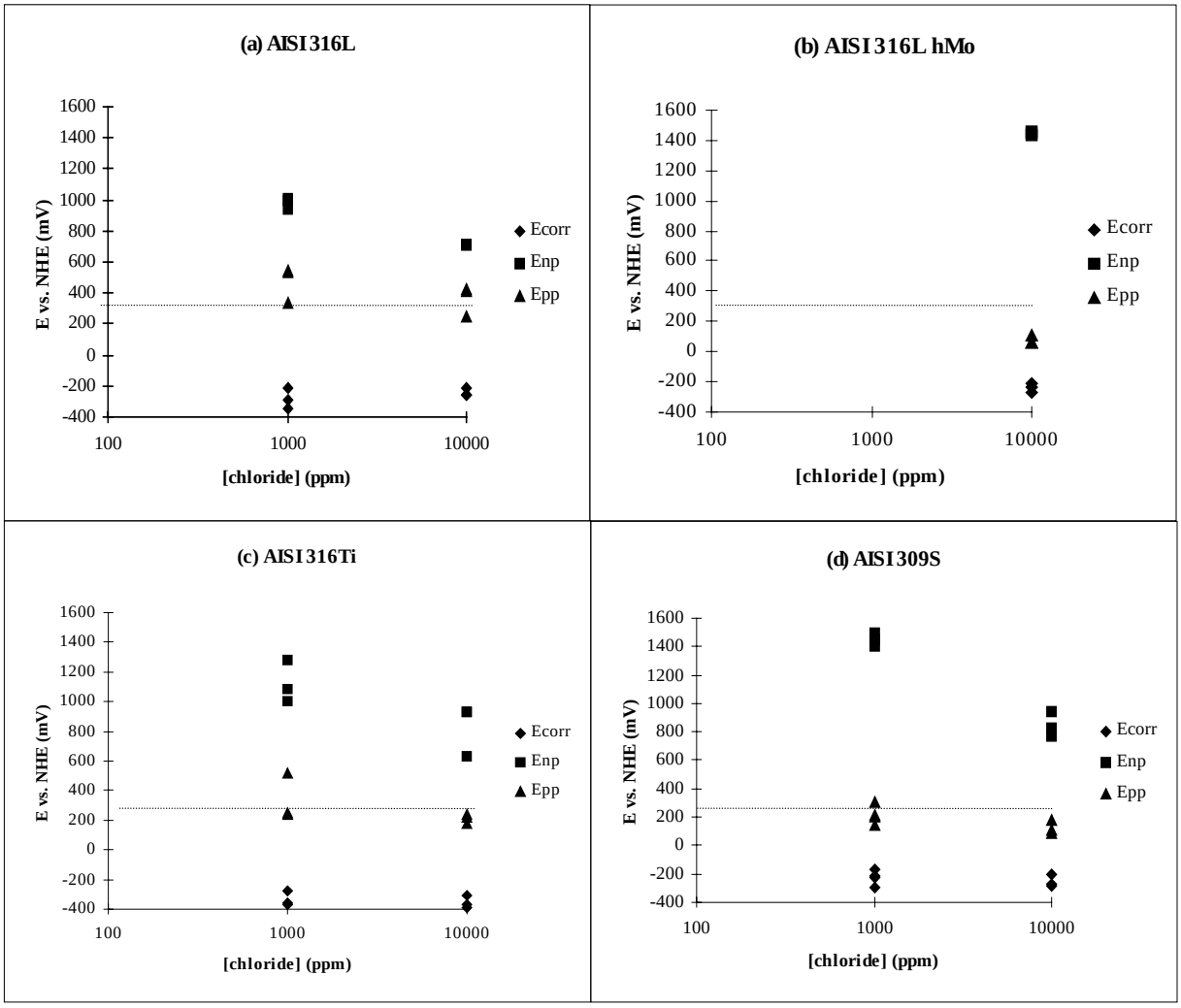

FIGURE 6.7 Influence of chloride concentration on the characteristic pitting potentials of candidate container materials in SOC containing 216 ppm sulphate at 16°C

None of the investigated alloys suffered from pitting corrosion in SOC containing 216 ppm sulphate and 100 ppm chloride at 16°C (Figure 6.7). Again, as was the case at 90°C, the value of the corrosion potential is independent of alloy composition and chloride content (for the alloys and brines that were used in this study). The pitting and protection potentials decrease with chloride content, and it can be assumed that a linear relationship between the critical pitting potentials and log [Cl^-] is obeyed, as was the case at 90°C. Again, interpretation of the polarization curves depends on the value chosen for the corrosion potential. In these experiments, it was obtained a value of around - 400 mV (vs. NHE) for E_{corr}, after purging of the brine with nitrogen to remove oxygen. The approximate value of 300 mV (NHE) was used to interpret the polarization curves. At 16°C, E_{np} remains sufficiently high for all investigated alloys, even at 10000 ppm chloride, to exclude pitting problems in oxidizing clay water at this temperature.

Influence of sulphate

In SOC with increased sulphate concentration (5400 ppm), the resistance of the candidate container materials increases. No pitting problems were encountered for the corrosion resistant alloys at 16°C in SOC brines containing 5400 ppm sulphate.

Influence of thiosulphate

In SOC containing thiosulphate, E_{np} and E_{pp} shift in the cathodic direction with increasing thiosulphate content. At 16°C, however, the value of E_{np} remains sufficiently high, even in SOC containing 100 ppm thiosulphate, to exclude pitting problems.

6.2.3 Surface analysis of pitted specimens

After the electrochemical experiments, the samples were submitted to surface analysis using SEM-EDS. The morphology of pits on the surface of AISI 316L hMo and UHB 904L was investigated in detail. Samples of the two alloys electrochemically tested in SOC containing 1000 ppm chloride at 90°C were compared. Figure 6.8a shows a typical view of a AISI 316L hMo surface at magnification 100, with two large pits with typical diameters of 30 to 40 µm and several smaller satellite pits. Analysis of the pit bottom revealed intergranular attack inside the pits. Figure 6.8b shows a typical view of a UHB 904L surface pitted under identical circumstances. Again, a central pit, with diameter 30 to 40 µm, surrounded by several smaller pits is visible. This ‘rose-like’ shape indicates subsurface growth of a large pit which is covered by a thin layer of metal.

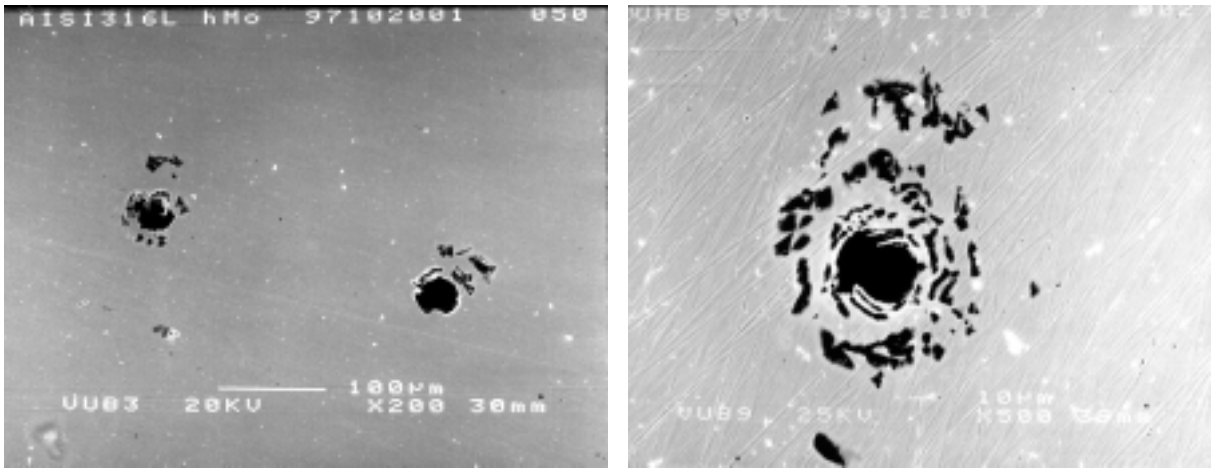

(a) **(b)**

FIGURE 6.8 SEM micrographs of container materials, pitted in SOC containing 1000 ppm chloride and 216 ppm sulphate: (a) AISI 316L hMo, (b) UHB 904L.

6.2.4 Pitting corrosion in synthetic interstitial clay water (anaerobic tests)

Due to unforeseen problems, the experiments in synthetic interstitial clay water could not be started before the end of the current programme. Therefore, the original experimental programme was adapted. Alloy AISI 309S, of importance for the French containers, was added to the materials selection. In addition, four chloride and four thiosulphate concentrations were considered for each of the investigated materials, whereas in the original planning only two chloride and two thiosulphate concentrations were foreseen. Also, the influence of sulphate on the pitting corrosion was examined. This supplementary experimental effort compensated the delay in the anaerobic tests.

7. CONCLUSIONS

7.1 Salt environment

The results obtained for the alloy Ti99.8-Pd confirm previous findings that this material is the strongest candidate for the realization of the **corrosion-resistant container concept** in rock salt. This alloy exhibits in the test brines up to 170°C an excellent resistance to general corrosion and pitting corrosion. A gamma radiation field of 10 Gy/h and species as H_2O_2, ClO^- (radiolytic products) do not accelerate the corrosion rate of this alloy. Furthermore, in the slow strain rate test in NaCl-rich brine at 170°C, Ti99.8-Pd is completely resistant to stress corrosion cracking (SCC) and it does not suffer a loss of ductility. A such corrosion-resistant container concept would consist of a thick-walled carbon steel container as mechanical support provided with a corrosion protection made of Ti99.8-Pd.

The TStE355 carbon steel continues to be considered as a promising material for the **corrosion-allowance container concept** in salt environment. The steel corrodes actively in the brines, and its general corrosion rates imply corrosion allowances acceptable for thick-walled containers. Under the test conditions applied in NaCl-rich brine environment, corrosion allowances of 1.5 mm (T=90°C) and 14 mm (T=170°C), respectively, are needed for containers with a service life of e.g. 300 years. The corresponding corrosion allowances in $MgCl_2$-rich brine are 21 mm (T=90°C) and 67 mm (T=170°C).This is in agreement with previous studies under similar experimental conditions[23].

At the realistic disposal temperature of 170°C, initial pH values of the NaCl-rich brine between 1 and 5, and of the $MgCl_2$-rich brine between 3 and 7 do not influence significantly the corrosion rate of the steel. Also chemical species such as $B(OH)_4^-$, H_2O_2, ClO^- and Fe^{3+} in concentrations of 10^{-1}-10^{-3} mol/l do not affect the corrosion rate of the steel (T=170°C). However, the Tungsten-Inert-Gas (TIG) welding and Electron Beam (EB) welding reduce significantly the resistance of the steel both to general corrosion and local corrosion. The welded material suffered from severe local corosion attacks in the welds and in the Heat Affected Zone (HAZ), and its corrosion rate was by a factor of about 3 higher than that of the unwelded material. A possible measure to improve the corrosion resistance of welds is the thermal stress relief treatment. Corresponding studies on such thermal treated welds are planned.

According to the results of the slow strain rate tests, the TStE355 steel is slightly sensitive to stress corrosion cracking (SCC) in NaCl-rich brine. Furthermore, it suffers a loss of ductility in this environment at 170°C, which is interpreted by a hydrogen embrittlement phenomenon due to the penetration of atomic hydrogen into the metal structure. However, both effects are significant only at very low strain rates. The various welding procedures studied do not affect the resistance of the steel to SCC in NaCl-rich brine.

An important question which still needs to be clarified with a view to the use of the corrosion-allowance carbon steels is namely, whether the amount of hydrogen generated by the corrosion of iron or by the radiolysis of brines can be tolerated in

the repository. Should this give rise to problems of technical safety, the carbon steel containers could be protected by the corrosion-resistant alloy Ti99.8-Pd.

7.2 Granitic environment

In the 90°C granitic test environment, the TStE355 steel appears to be resistant to stress corrosion cracking at slow strain rates of 10^{-4}-10^{-7} s^{-1}. However, a loss of ductility ("hydrogen embrittlement"), especially at very slow strain rates occurred, as in the NaCl brine.

For the stainless steel AISI 316L, neither stress corrosion cracking nor a loss of ductility is expected according to the test results.

7.3 Clay environment

At 16°C in oxidizing clay water having a realistic chloride concentration of 100 ppm, all investigated materials (Ti99.8-Pd, Hastelloy C4, stainless steels, and carbon steel TStE355) are resistant to pitting corrosion. At 90°C, among the corrosion-resistant materials only Ti99.8-Pd and Hastelloy C4 are completely resistant to pitting corrosion under all test conditions applied. In case of the stainless steels, pitting corrosion can occur in oxidizing clay environment at high chloride concentrations. Finally, the actively corroded TStE355 carbon steel is a corrosion-allowance material and corrodes readilly at the open circuit corrosion potential. By use of this steel, thick-walled containers are needed.

For a completely correct interpretation of the corrosion results obtained from the polarization curves, in-situ measurements of the corrosion potential of the container materials in the Boom clay layer are necessary.

8. RECOMMENDATIONS FOR FUTURE WORK

For the reliable selection of container materials, and the assessment of the long-term effectiveness of the containers as a barrier in repositories in rock salt, granite and clay formations, further studies are needed. They should include above all:

- Qualification of a welding technique for a corrosion resistant closing of carbon steel containers.

- Examination of the contact corrosion between carbon steel and Ti99.8-Pd.

- Determination of the retardation of radionuclides by corrosion products of carbon steel containers (Fe_3O_4, Fe_2O_3 etc.).

- Performance of electrochemical studies on the container materials under anaerobic conditions and at high temperature (about 150°C).

- Further corrosion studies under gamma radiation (effect of radiolytic products on corrosion)

- Examination of the suitability of Cu-base materials (Cu-Ni alloys) as container materials.

- Development of corrosion models in order to predict the lifetime of waste containers.

9. FINAL REMARKS

Significant improvements were achieved in the understanding of the corrosion process and the effect of essential parameters on the corrosion behaviour of container materials in rock salt, granite and clay environments. A large number of experimental data was gained which are usefull inputs for corrosion modelling. However, from these studies some questions remained open (see session 8). The solution of such special questions will be the subject of future investigations.

Regarding the project performance, the participation of scientists from different countries was an important benefit to achieve the objectives. The cooperation between the scientists helped to broaden the body of knowledge within the various countries.

ACKNOWLEDGEMENTS

The authors gratefully acknowledge B.Fiehn (FZK.INE), F.Druyts (SCK.CEN), V.Madina (INASMET), and Dr.C.Nehm (FU Berlin) for their contributions to this report. The European Commission, and the national authorities and institutions of the authors are also gratefully acknowledged for the funding of this project.

10. REFERENCES

[1] G.P.Marsh, G.Pinard-Legry, E.Smailos et al., “HLW Container Corrosion and Design,” Proc. of the Second European Community Conf. and Radioactive Waste Management and Disposal, Luxembourg, April 22-26, 1985, p.314, R.A. Simon (Ed.), Cambridge University Press, EUR 13389 (1986).

[2] E.Smailos, W.Schwarzkopf, R.Köster and K.H.Grünthaler,”Advanced Corrosion Studies on Selected Packaging Materials for Disposal of HLW Canisters in Rock Salt,” Proc. of the Symposium on Waste Management 1998, Tucson, Arizona, USA, February 28-March 3, 1998, Vol.2, pp. 985-994, Arizona Board of Regents (1988).

[3] E.Smailos, I.Azkarate, J.A.Gago, P.Van Iseghem, B.Kursten, T.McMenamin, ”Corrosion Studies on Metallic HLW Container Materials,” Proc. of the 4th European Conf. on Management and Disposal of Radioactive Waste, Luxembourg, 25-29 March 1996, pp. 209-223, T.McMenamin (Ed.), EUR 17543 (1997).

[4] E.Smailos, W.Schwarzkopf and R.Storch,”Corrosion Studies on Packaging Materials for High-Level Waste Disposal in a Rock-Salt Repository,” Proc. of the 12th Scandinavian Corrosion Congress and Eurocorr ’92, Espoo, Finland, June 1992, pp. 327-338 (1992).

[5] E.Smailos, B.Fiehn, J.A.Gago and I.Azkarate,”Corrosion Studies on Selected Packaging Materials for Disposal of Heat-Generating Radioactive Waste in Rock-Salt Formations,” EUR 17108 (1997).

[6] R.E.Westerman, J.H.Haberman et.al.,”Corrosion and Environmental Characterization of Iron-Base Nuclear Waste Package Structural Barrier Materials,” PNL Report No. 5426 (1986).

[7] E.Smailos, D.Schild and K.Gompper,”Corrosion of Ti99.8-Pd under Gamma Irradiation in $MgCl_2$-Rich Brine,” in Materials Research Society Symposium Proceedings, Vol. 506, pp. 477-484 (1998).

[8] G.Marx und C.Nehm, unpublished report (1995).

[9] A.Henglein, W.Schnabel und J.Wendenburg, ”Einführung in die Strahlenchemie”, Verlag Chemie, Weinheim (1969).

[10] D.Wegen, Dissertation, FU Berlin (1991).

[11] V.Madina, I.Azkarate and J.A.Gago,”Stress Corrosion Cracking Studies on Candidate Materials for HLW Disposal,” Proc. of the European Corrosion Congress “EUROCORR ‘97”, Trondheim, Norway, 22-25 September, 1997, Vol. I, pp. 737-742 (1997).

[12] V.Madina, I.Azkarate, A.Martínez-Esparza and J.A.Gago,"Crevice Corrosion and Hydrogen Assisted Stress Cracking of Titanium Alloys for HLW Disposal," Proc. of "EUROCORR '98", Session Nuclear Corrosion and Environmental Sensitive Fracture, Utrecht, Netherlands, 28 September-1 October 1998.

[13] B. Kursten, P. Van Iseghem, "In Situ Corrosion Studies on Candidate Container Materials for the Underground Disposal of High-Level Radioactive Waste in Boom Clay," EUROCORR '98, 28 Sept.-1 Oct. 1998, Utrecht, The Netherlands.

[14] B. Kursten, B. Cornélis, S. Labat, P. Van Iseghem, "Completion of the corrosion programme in Boom clay - in situ experiments," EUR 17105 (1997).

[15] B. Kursten, P. Van Iseghem, "In Situ Corrosion Studies on Candidate Container Materials for the Underground Disposal of High-Level Radioactive Waste in Boom Clay," Corrosion 99, paper 99473, 25-29 April 1999, San Antonio, Texas, USA.

[16] F. Druyts, B. Kursten, P. Van Iseghem, "Electrochemical Study of the Pitting Corrosion of Stainless Steel Candidate Overpack Materials for the Disposal of High-Level Radioactive Waste in Boom Clay," Materials Science Forum, 289-292 (1998), pp. 1083-1089.

[17] F. Druyts, B. Kursten, "Influence of Chloride Ions on the Pitting Corrosion of Candidate HLW Overpack Materials in Synthetic Oxidized Boom Clay Water," Corrosion '99, paper 99472, 25-29 April 1999, San Antonio, Texas, USA.

[18] J-H Wang, C.C. Su, Z. Szklarska-Smialowska, "Effects of Cl^- Concentration and Temperature on Pitting of AISI 304 Stainless Steel," Corrosion 44 (1988) 10, pp. 732-737.

[19] V.P. Evangelou, "Pyrite Oxidation and its Control," pp. 137-171, CRC Press (1995).

[20] L. Noynaert, G. Volckaert, P. De Cannière, et al., "The CERBERUS Project, a Demonstration Test to Study the Near Field Effects of a HLW-Canister in an Argillaceous Formation," Final Report, SCK-CEN, R-3166, 1997.

[21] R.C. Newman, W.P. Wong, H. Ezuber, A. Garner, "Pitting of Stainless Steels by Thiosulfate Ions," Corrosion 45 (1989) 4, pp. 282-287.

[22] P. Marcus, "Sulfur-Assisted Corrosion Mechanisms," in Corrosion Mechanisms in Theory and Practice, eds. P. Marcus, J. Oudar, Publ. Marcel Dekker, 1995.

[23] E.Smailos,"Corrosion of High-Level Waste Packaging Materials in Disposal Relevant Brines," Nuclear Technology, Vol. 104, pp. 343-350 (1993).